HABILITATIONSSCHRIFT

zur Erlangung der venia legendi
vorgelegt am Fachbereich Physik
der
Johann Wolfgang Goethe-Universität
Frankfurt am Main
von
Dipl.-Ing. Dr. techn. Dominik J. SCHWARZ

The Cosmological QCD Transition

Dominik J. SCHWARZ

Institut für Theoretische Physik
Robert-Mayer-Straße 10
Postfach 11 19 32
D-60054 Frankfurt am Main

Frankfurt am Main im Februar 1999

To Petra and Max

Zusammenfassung

Der kosmologische QCD-Phasenübergang

Die moderne Kosmologie beschreibt das frühe Universum als extrem heissen, rasch expandierenden Feuerball (ursprünglich spöttisch 'Big Bang' genannt). Dabei ist das Universum anfänglich beliebig heiß und dicht. Durch die Expansion kühlt das Universum ab, wobei die Materie verschiedene Zustände durchläuft. Das Standardmodell der Kosmologie ist gut fundiert und steht auf drei Beinen: Hubble-Expansion (Friedmann 1922, Hubble 1929), 2.7K-Hintergrundstrahlung (Gamov 1946, Penzias & Wilson 1965) und primordiale Nukleosynthese (Gamow 1946, Alpher & Herman 1950). Die beobachtete Hubble-Expansion testet das Modell heute (das Universum ist in etwa 15 Milliarden Jahre alt), die 2.7 K Hintergrundstrahlung vermißt das Universum im Alter von 300 000 Jahren, und mithilfe der primordialen Nukleosynthese verstehen wir die ersten 3 Minuten. Das Standardmodell der Teilchenphysik erlaubt uns eine weitere Extrapolation, noch näher an den 'Big Bang'. So folgt aus der Theorie der starken Wechselwirkungen, der Quantenchromodynamik (QCD), daß das Universum in den ersten 10^{-5} s hauptsächlich aus Quarks und Gluonen besteht. Im QCD-Phasenübergang kondensieren diese dann zu Hadronen, die in der Form von Protonen und Neutronen, später dann in Kernen gebunden, bis heute überleben.

Die fundamentalen Teilchen der Quantenchromodynamik sind Quarks und Gluonen, die jeweils Farbladung tragen. Die typische Energieskala der QCD liegt im Bereich von 100 MeV. Unterhalb dieser Skala sind die Kräfte zwischen Farbladungen stark, das heißt es kommen ausschließlich gebundene Zustände in Form von Hadronen vor (confinement). Weit oberhalb von 100 MeV ist die QCD asymptotisch frei, Farbladungen können frei propagieren (deconfinement). Dieser störungstheoretisch zugängliche Teil der Theorie ist durch Experimente an Beschleunigern gut abgesichert. Im Niederenergiebereich stimmen numerische Berechnungen (Gitter-QCD) von Hadronmassen mit den experimentellen Daten überein. Im frühen Universum (Big Bang), in Schwerionenstößen (Little Bang), sowie im Inneren von sehr kompakten Sternen (z.B. Neutronensterne) sind die kollektiven Eigenschaften der QCD von entscheidender Bedeutung. Diese Systeme werden im thermischen Gleichgewicht durch die Temperatur und durch chemische Potentiale zu den erhaltenen Quantenzahlen charakterisiert. Bei Temperaturen unter der QCD-Skala liegt ein Gas von Hadronen vor. Bei größeren Temperaturen erwartet man ein Quark-Gluon-Plasma. Dessen Existenz ist bis heute experimentell nicht nachgewiesen, aber durch Gitter-QCD bestätigt. Die Ordnung des Phasenübergangs ist auch am Gitter ungewiß. Es gibt verschiedene Methoden, Quarks auf das Gitter zu setzen. Für Wilson-Quarks findet man einen Phasenübergang erster Ordnung (Iwasaki et al. 1996), für 'staggered'

Quarks ist der Übergang kontinuierlich (crossover) (Brown et al. 1990). Die Übergangstemperatur liegt bei ungefähr 150 MeV (Bernard et al. 1996).

Der kosmologische QCD-Phasenübergang könnte demnach erster Ordnung sein. Die Hadronphase entsteht durch Nukleation von Blasen. Diese Blasen wachsen für kurze Zeit sehr schnell, bis ungefähr 1% des Universums mit der neuen Phase ausgefüllt ist. Dann stellt sich ein Gleichgewichtszustand zwischen Hadronengas und Quark-Gluon-Plasma bei der kritischen Temperatur ein. Die Abkühlung aufgrund der Expansion des Universums wird für etwa 10^{-6} s unterbrochen, da die durch die Kondensation von Hadronen freigesetzte latente Wärme das Universum heizt (Koexistenz der Phasen). Witten (1984) und Applegate & Hogan (1985) haben vorgeschlagen, daß der QCD-Phasenübergang dramatische beobachtbare Konsequenzen haben könnte. So zeigte Witten, daß der Grundzustand von Materie 'seltsame' Quarkmaterie (up, down and strange quarks) sein könnte. Im QCD-Phasenübergang könnten Baryonen Klumpen, sogenannte 'quark nuggets', bilden, die zur gesuchten dunklen Materie beitragen würden. (Man weiß heute, daß mindestens 90% der Materie im Universum dunkel, d.h. nicht mit Licht wechselwirkend, ist.) Applegate & Hogan haben erkannt, daß derselbe Mechanismus ohne Annahme der Stabilität von 'quark nuggets' zu großen Inhomogenitäten in der Verteilung von Baryonen führt, die, falls der typische Blasenabstand bei der Nukleation am Beginn des QCD-Phasenübergangs groß genug ist, bis zur primordialen Nukleosynthese überleben könnten. Das würde die Vorhersagen für die beobachteten Häufigkeiten von leichten Elementen (Deuterium, Helium-3, Helium-4, Lithium-7) ändern. Genauere Analysen haben jedoch gezeigt, daß der typische Abstand der Blasen zu klein ist, um Quarkklumpen zu bilden oder, die primordiale Nukleosynthese zu modifizieren (Ignatius et al. 1994; Schwarz 1998a).

Gemeinsam mit Schmid und Widerin (ETH-Zürich) habe ich Effekte auf Längenskalen untersucht, die viel größer als der typische Blasenabstand sind (Schmid, Schwarz, & Widerin 1996; 1997; 1999]. Falls der kosmologische QCD-Phasenübergang erster Ordnung ist, verschwindet die Schallgeschwindigkeit während der Koexistenz von Hadronengas und Quark-Gluon-Plasma. Dies führt dazu, daß alle Druckgradienten — die rückstellenden Kräfte — verschwinden. Dadurch wächst die Amplitude von primordialen akustischen Störungen (Dichte-, Geschwindigkeits- und Druckfluktuationen) linear mit der Wellenzahl. Das führt zu einer enormen Verstärkung von Inhomogenitäten in der Strahlungsflüssigkeit (Photonen, Leptonen und QCD-Materie). Kalte dunkle Materie in der Form von Axionen oder primordialen schwarzen Löchern, um nur zwei Kandidaten zu nennen, spürt die Massekonzentrationen in der Strahlungsflüssigkeit und wird von diesen angezogen. Wolken kalter dunkler Materie bilden sich, die kurz nach dem Übergang vom strahlungs- zum materiedominierten Universum von der Hubble-

Expansion entkoppeln. Somit könnten diese Wolken die ersten Objekte im Universum darstellen. Ihre Massen lägen im Bereich von $10^{-20}M_\odot$ bis $10^{-10}M_\odot$ (Schmid, Schwarz, & Widerin, 1999). Solche Objekte könnte man als Gravitationslinsen (femto-lensing; dabei dient ein γ-ray burst als Lichtquelle) finden, und sie würden die erwarteten Zählraten in Experimenten die nach dunkler Materie Ausschau halten, ändern. Insbesondere ist dies für die Axionsuche interessant. Die QCD induzierten Inhomogenitäten in der Strahlungsflüssigkeit führen zu keinen beobachtbaren Effekten, da die Inhomogenitäten durch die Entkopplung der Neutrinos bei 1 MeV ausgeschmiert werden (collisional damping).

Schwach wechselwirkende kalte dunkle Materie, wie schwere Neutrinos oder das leichteste supersymmetrische Teilchen, verhält sich während des QCD-Phasenübergangs nicht wie kalte Materie, sondern ist eng an die Strahlungsflüssigkeit gekoppelt (Schmid, Schwarz, & Widerin 1999; Hofmann & Schwarz, in Vorbereitung).

Durch die Beobachtung der Anisotropien der kosmischen 2.7K-Hintergrundstrahlung (COBE Satellit, Smoot et al. 1992) wissen wir, daß es primordiale Dichtefluktuationen gibt und ihr Spektrum nahezu skaleninvariant ist. Solche Fluktuationen müssen auch schon zur Zeit des QCD-Phasenübergangs bestanden haben. Die einzige Theorie, die gegenwärtig diese Fluktuationen überzeugend erklären kann, ist die Theorie der Inflation (Guth 1980, Linde 1982, Albrecht & Steinhardt 1982, Linde 1983). Dabei nimmt man an, daß das sehr frühe Universum exponentiell schnell expandiert (Inflation) und dadurch Quantenfluktuationen zu makroskopischen Dichtefluktuationen aufgeblasen werden (Chibisov & Mukhanov 1981, Starobinsky 1982, Guth & Pi 1982, Hawking 1982). In einer Arbeit mit Martin (Observatoire de Paris) habe ich gezeigt, daß diese Fluktuationen nur auf Skalen, die kleiner als der Hubbleradius ($\equiv c/$Expansionsrate) sind, von mikroskopischen Ereignissen, wie dem QCD-Phaseniübergang, beeinflußt werden können (Martin & Schwarz 1998).

Bisher wurde im QCD-Phasenübergang die Nukleation von Blasen in homogenen Medien untersucht. Aus der Existenz primordialer Dichtestörungen folgt, daß die Strahlungsflüssigkeit inhomogen verteilt ist. Mit Ignatius (Universität Helsinki) habe ich begonnen, die Nukleation von Blasen in inhomogenen Medien zu studieren. Wir haben herausgefunden, daß der typische Blasenabstand um ein bis zwei Größenordnungen über den Vorhersagen aus homogener Nukleation liegt, wodurch inhomogene Nukleosynthese wieder interessant werden könnte (Ignatius & Schwarz, in Vorbereitung). In der vorliegenden Arbeit werden erste Resultate dazu vorgestellt.

Neben Dichtestörungen werden in der Inflation auch Gravitationswellen erzeugt (Starobinskii 1979). Der QCD-Übergang modifiziert das Spektrum dieser Wellen, unabhängig von der Ordnung des Übergangs (Schwarz 1998b).

Diese Habilitationsschrift ist wie folgt gegliedert: Kapitel 1 führt die wichtigsten Konzepte ein und liefert einen detaillierten Überblick über die möglicherweise beobachtbaren Effekte des kosmologischen QCD-Phasenübergangs. In Kapitel 2 werden die Eigenschaften von Materie bei Temperaturen in der Nähe der QCD-Skala diskutiert. Verschiedene Szenarien für die Nukleation von Blasen werden in Kapitel 3 untersucht. Die daraus folgenden Baryoninhomogenitäten und die Anfangsbedingungen der Nukleosynthese werden in Kapitel 4 beleuchtet. In Kapitel 5 wende ich mich den Effekten auf großen Skalen zu. Die Verstärkung von Inhomogenitäten in einem QCD-Phasenübergang erster Ordnung wird ausführlich analysiert. Die Modifikationen des Gravitationswellenspektrums werden in Kapitel 6 behandelt, und in Kapitel 7 werden offene Fragen angesprochen. Zwei Anhänge erklären einige Grundlagen des strahlungsdominierten Universums (Anhang A) und der Theorie der kosmologischen Störungen (Anhang B) dar.

Mein Ziel ist aufzuzeigen, daß das Studium des kosmologischen QCD-Phasenübergangs wichtige Erkenntnisse über die Entstehung unseres Universums und der Natur der starken Wechselwirkungen liefert. Kosmologische Überlegungen und Beobachtungen sind komplementär zu Ergebnissen der Gitter-QCD und zu Schwerionenexperimenten. So kann aus der guten Übereinstimmung der homogenen Nukleosynthese mit den beobachteten Elementhäufigkeiten geschlossen werden, daß die typischen Blasenabstände im QCD-Phasenübergang nicht zu groß sein dürfen. Dies bedeutet, daß die Oberflächenspannung der Blasen klein sein muß, was wiederum in guter Übereinstimmung mit Resultaten der Gitter-QCD ist.

Albrecht, A. & Steinhardt, P. J. (1983) Phys. Rev. Lett. **48**, 1220.
Alpher, R. A. & Herman, R. C. (1950) Rev. Mod. Phys. **22**, 153.
Applegate, J. H. & Hogan, C. J. (1985) Phys. Rev. D **31**, 3037.
Bernard, C. & al. (1996) Phys. Rev. D **54**, 4585.
Brown, F. R. & al. (1990) Phys. Rev. Lett. **20**, 2491.
Friedmann, A. (1922) Z. Phys. **10**, 377.
Gamov, G. (1946) Phys. Rev. **70**, 572.
Guth, A. (1981) Phys. Rev. D **23**, 347.
Guth, A. & Pi, Y.-S. (1982) Phys. Rev. Lett. **49**, 1110.
Hawking, S. (1982) Phys. Lett. B **115**, 295.
Hubble, E. P. (1929) Proc. Nat. Acad. Sci. **15**, 168.
Ignatius, J. & al. (1994) Phys. Rev. D **50**, 3738.
Iwasaki, Y. & al. (1996) Z. Phys. C **71**, 343.
Linde, A. D. (1982) Phys. Lett. B **108**, 389.
Linde, A. D. (1983) Phys. Lett. B **129**, 177.
Martin, J. & Schwarz, D. J. (1998) Phys. Rev. D **57**, 3302.
Mukhanov, V. & Chibisov, G. (1981) Pis'ma Zh. Eksp. Teor. Fiz. **33**, 549 [JETP

Lett. **33**, 532].
Penzias, A. A. & Wilson, R. W. (1965) Astrophys. J. **142**, 419.
Schmid, C., Schwarz, D. J., & Widerin, P. (1996) Hel. Phys. Acta **69**, 198.
Schmid, C., Schwarz, D. J., & Widerin, P. (1997) Phys. Rev. Lett. **78**, 791.
Schmid, C., Schwarz, D. J., & Widerin, P. (1999) Phys. Rev. D **59**, 043517.
Schwarz, D. J. (1998a) Nucl. Phys. A **642**, 336c.
Schwarz, D. J. (1998b) Mod. Phys. Lett. A **34**, 2771.
Smoot, G. F. & al. (1992) Astrophys. J. **396**, L1.
Starobinskii, A. A. (1979) Pis'ma Zh. Eksp. Teor. Fiz. **30**, 719 [JETP Lett. **30**, 682].
Starobinsky, A. (1982) Phys. Lett. B **117**, 175.
Witten, E. (1984) Phys. Rev. D **30**, 272.

Abstract

The cosmological QCD transition might produce observable effects. I discuss the baryon number inhomogeneities arising from the bubble scale in a first order transition, which might give rise to inhomogeneous nucleosynthesis. During a first order transition the sound speed vanishes at scales above the bubble scale. This leads to the amplification of primordial inhomogeneities. In the further evolution of the Universe these large inhomogeneities produce clumps of cold dark matter on very small scales. The primordial spectrum of gravitational waves is modified independently of the order of the transition.

Acknowledgement

This habilitation thesis was made possible by the support and love of my wife Petra and the everyday demonstration of the second law of thermodynamics by my son Max.

I thank Janne Ignatius, Christoph Schmid, and Peter Widerin for enjoyable research and collaboration on the cosmological QCD transition. Thanks to Juan Garcia-Bellido, Stefan Hofmann, and Jerome Martin for collaboration on related cosmological issues.

I profitted by discussions and comments that I received from R. Brandenberger, R. Caldwell, B. J. Carr, A. Chamseddine, L. Czernai, J. Ellis, T. Gajdosik, W. Greiner, U. Heller, M. Hanauske, M. Hofmann, P. Jetzer, K. Kajantie, F. Karsch, W. Kegel, A. Linde, J. Madsen, H. Markum, V. Mukhanov, H. Nachbagauer, M. Nagasawa, A. Rebhan, P. Sikivie, N. Straumann, F. Weber, and E. Zabrodin. I thank Stefan Hofmann for reading the manuscript.

Let me thank my teachers at the Technische Universität Wien, especially W. Kummer, A. Rebhan, and M. Schweda.

I am very grateful to Walter Greiner, who encouraged me to undertake the effort to write this thesis. I thank him and the Institut für theoretische Physik der J. W. Goethe Universität Frankfurt for their hospitality and enthusiasm.

Parts of this research were done at ETH-Zürich, supported by the Schweizer Nationalfonds. My work in Frankfurt was supported by the Alexander von Humboldt-Stiftung.

Contents

Chapter 1

Introduction

One of the most spectacular epochs in the early Universe is the QCD (quantum chromodynamics) epoch. QCD describes the strong interactions between quarks and gluons and is well tested in the perturbative regime, i.e. at high energies and momenta. At low energies quarks and gluons are confined into hadrons. The scale of QCD is $\Lambda_{\rm QCD} = \mathcal{O}(100\ \mathrm{MeV})$. At temperatures $T \sim \Lambda_{\rm QCD}$ a transition between a quark-gluon plasma (QGP) and a hadron gas (HG) happens [1]. When the cosmological QCD transition took place the Universe was $\sim 10^{-5}$ s young. The first studies of the cosmological QCD transition date back to the early 80's [2]. It was realized that a first-order QCD transition proceeds via bubble nucleation [3, 4] with small supercooling [5, 6]. The bubbles were shown to grow most probably by weak deflagration [7, 8]. Most of the following work has been based on this scenario of a first-order QCD transition with homogeneous bubble nucleation and bubble grow by weak deflagration. A detailed discussion of this scenario has been given by Kajantie and Kurki-Suonio [9].

Based on this scenario a separation of cosmic phases has been suggested by Witten [5], which may give rise to large inhomogeneities in the distribution of baryons in the Universe. Originally it was hoped that the mean bubble nucleation distance is a reasonable fraction of the size of the Universe, the Hubble scale. From recent lattice QCD results for the latent heat and surface tension in the quenched approximation (no dynamical quark flavors) [10] a tiny mean bubble nucleation distance follows [11, 12, 13].

The mean bubble nucleation distance might be larger for other bubble nucleation scenarios. Nucleation at impurities has been investigated by Christiansen and Madsen [13]. Another possibility is that the nucleation of bubbles is determined by preexisting inhomogeneities of temperature (e.g. generated during inflation). The latter issue is currently under investigation by Ignatius and myself [14].

Apart from the question 'What happened at the cosmological QCD transition?', the cosmological QCD transition is of interest for two further reasons: Firstly, the QCD epoch sets the initial conditions for one of the pillars of standard cosmology — big bang nucleosynthesis (BBN). The QCD transition and baryon transport thereafter determine the distribution of protons and neutrons at the beginning of nucleosynthesis. It was first recognized by Applegate and Hogan [6] that an inhomogeneous distribution of baryons due to a first-order QCD transition could change the primordial abundances of the light elements. This issue has attracted a lot of interest [15, 16, 17] because inhomogeneous BBN might allow a higher baryon to photon ratio than homogeneous BBN [18]. Moreover, inhomogeneous BBN might allow the primordial production of heavy elements like ^{12}C [19].

Secondly, the QCD transition might generate relics which might be observable today. Most of these relics are only formed if the QCD transition is first-order and if the latent heat is much larger than that found from quenched QCD in lattice calculations. Strange quark nuggets as dark matter and gravitational waves from colliding bubbles have been suggested by Witten [5]. Hogan [20] and more recently Cheng and Olinto [21] argued that magnetic fields might be generated. Today, these relics appear to be unlikely, because the typical scale for bubble nucleation is very small.

Recently, Schmid, Widerin and myself [22, 23, 24] showed that a first-order QCD transition might lead to the formation of small cold dark matter (CDM) clumps. We showed that the sound speed vanishes during a first-order QCD transition and thus the restoring forces vanish. This leads to large amplifications of primordial density fluctuations in the radiation fluid and in cold dark matter.

It was speculated from various reasons that black holes could form during the QCD transition [25, 26, 27]. From the present day perspective these scenarios seem to be highly unlikely.

Independently from the order of the transition a primordial background of gravitational waves is modified by the QCD transition, as I showed in [28].

A speculative but interesting idea was put forward by Brandenberger, Halperin, and Zhitnitsky [29]: They speculated that a separation of baryons and anti-baryons due to the non-perturbative QCD vacuum might be possible during the QCD epoch. This would effectively give a new baryogenesis scenario and a new candidate for dark matter (B-shells).

Reviews on the cosmological QCD transition may be found in Refs. [30, 31, 32, 33].

This work is organized as follows: In the remaining sections of the introduction a brief overview on the physics and history of the various effects from the QCD transition is given. Moreover, I try to introduce enough material such that any other chapter can be read independently.

In chapter 2 I discuss the environment of the cosmological QCD transition. The following chapters deal with a first-order scenario. First (chapter 3) three different bubble nucleation scenarios are investigated. Then the resulting isothermal baryon fluctuations and inhomogeneous BBN are discussed (chapter 4). In chapter 5 I review the effects of the QCD transition on primordial density perturbations. The scenario of a smooth QCD crossover is discussed in chapter 6. Some conclusions and open problems are presented in chapter 7. Short introductions of the Friedmann model and the theory of linear cosmological perturbations are provided in appendix A and B respectively.

1.1 Scales

The QCD transition is expected to happen at $T_\star \sim \Lambda_{\mathrm{QCD}}$. From recent lattice QCD calculations for quenched QCD the transition temperature is $T_\star \approx 260$ MeV [34]. For two-flavor QCD $T_\star \approx 140$ MeV was found [35], almost independent of the quark mass. For the most interesting case of two light quark-flavors and one massive strange quark no values for the transition temperature have been obtained so far. In the following all numbers refer to a transition temperature of $T_\star = 150$ MeV.

1.1.1 The Hubble scale

The cosmological scale, the Hubble scale, is set by the expansion rate of the universe H. It is determined from the Friedmann equation [1]

$$H^2 = \frac{8\pi G}{3}\rho \ , \tag{1.1}$$

where ρ denotes the total energy density of the universe. During the radiation dominated epoch $\rho \sim T^4$ from the Stefan-Boltzmann law. For a collisionless, ultra-relativistic gas

$$\rho = \frac{\pi^2}{30} g T^4 \qquad \text{and} \qquad p = \frac{\rho}{3} \ . \tag{1.2}$$

$g \equiv g_{\mathrm{bosons}} + 7/8 g_{\mathrm{fermions}}$ is the effective number of helicity degrees of freedom. The mean energy of a particle at temperature T is $\sim 3T$. It is a good approximation for our purpose to treat all particles with $m \ll 3T$ as they were massless, all other particles are neglected in the total energy density ρ. Above the QCD transition $g_{\mathrm{quarks}} = 12 \times N_f$ (number of quark-flavors) and $g_{\mathrm{gluons}} = 8$, below the QCD transition $g_{\mathrm{pions}} = 3$. At the QCD epoch

[1] In the radiation dominated universe the spatial curvature can be neglected.

there are the photons, three flavors of neutrinos, and electrons and muons. Counting all up we find for the QCD epoch

$$g(T > T_\star) = 51.25(61.75) \ , \tag{1.3}$$

without (with) strange quark, and

$$g(T < T_\star) = 17.25 \ . \tag{1.4}$$

At the QCD transition the Hubble radius is about 10 km:

$$R_{\mathrm{H}} \equiv cH^{-1} \approx \left(\frac{51.25}{g}\right)^{\frac{1}{2}} \left(\frac{150 \text{ MeV}}{T_\star}\right)^2 9.0 \text{ km} \ . \tag{1.5}$$

Today this corresponds to scales of 1 pc or 3 light-years. The Hubble time at the QCD transition is $t_{\mathrm{H}} \equiv H^{-1} \sim 10^{-5}$ s. This is extremely long in comparison with the relaxation time scale of the strong interactions, which is about 1 fm$/c \sim 10^{-23}$ s. Thus, the transition is very close to an equilibrium process.

The mass inside a Hubble volume is $\sim 1 M_\odot$:

$$M_{\mathrm{H}} \equiv \frac{4\pi}{3} R_{\mathrm{H}}^3 \rho \approx \left(\frac{51.25}{g}\right)^{\frac{1}{2}} \left(\frac{150 \text{ MeV}}{T_\star}\right)^2 3.1 M_\odot \ . \tag{1.6}$$

This mass is redshifted $\propto 1/a$ as the Universe expands, a is the scale factor of the Friedmann-Robertson-Walker metric, because it is made up of radiation. An invariant mass is the mass of cold dark matter in a comoving volume, $M_{\mathrm{CDM}} \equiv (a/a_{\mathrm{equality}})M(a)$. At the QCD transition $a/a_{\mathrm{equality}} \sim 10^{-8}$ and thus

$$M_{\mathrm{H}}^{\mathrm{CDM}} \sim 10^{-8} M_\odot \ . \tag{1.7}$$

Another figure of interest is the baryon number inside the a Hubble volume at the QCD transition, $B_{\mathrm{H}} \equiv (4\pi/3) R_{\mathrm{H}}^3 n_{\mathrm{B}}$. The baryon number density n_{B} follows from the ratio of baryons to photons at BBN, $\eta \equiv (n_{\mathrm{B}}/n_\gamma)_{\mathrm{BBN}}$, and the conservation of baryon number and entropy, $n_{\mathrm{B}}/s =$ constant:

$$n_{\mathrm{B}}(T_\star) = \eta \left(\frac{n_\gamma}{s}\right)_{\mathrm{BBN}} s(T_\star) \ , \tag{1.8}$$

Finally, the baryon number inside a Hubble volume reads:

$$B_{\mathrm{H}} \approx \left(\frac{51.25}{g}\right)^{\frac{1}{2}} \left(\frac{150 \text{ MeV}}{T_\star}\right)^3 \frac{\eta}{10^{-10}} 4.9 \times 10^{47} \ . \tag{1.9}$$

From standard BBN $\eta = (1.5 \text{ to } 6.3) \times 10^{-10}$ [18]. Thus, at most $B_{\mathrm{H}} \sim 10^{48}$.

1.1.2 The bubble scale

The typical duration for a first-order QCD transition is $0.1 t_{\mathrm{H}}$ (see section 2.1.2). If the cosmological QCD transition is of first order, it proceeds via bubble nucleation (see chapter 3). From the small values of surface tension and latent heat found in recent lattice QCD calculations [10] the amount of supercooling is found to be small [12]. The temperature as a function of the scale factor is shown in Fig. 1.1.2 for the small supercooling scenario. Hadronic bubbles nucleate during a short period of supercooling, $\Delta t_{\mathrm{sc}} \sim 10^{-3} t_{\mathrm{H}}$. The typical bubble nucleation distance is

$$d_{\mathrm{nucl}} \sim 1 \text{ cm } \sim 10^{-6} R_{\mathrm{H}} \tag{1.10}$$

for homogeneous nucleation [13]. The hadronic bubbles grow very fast, within $10^{-6} t_{\mathrm{H}}$, until the released latent heat has reheated the universe to $T_\star$. By that time, just a little fraction of volume has gone through the transition. For the remaining 99% of the transition the HG and the QGP coexist at the pressure $p_{\mathrm{HG}}(T_\star) = p_{\mathrm{QGP}}(T_\star)$. During this time the hadronic bubbles grow slowly and the released latent heat keeps the temperature constant until the transition is completed. The energy density decreases continuously from $\rho_{\mathrm{QGP}}(T_\star)$ at the beginning of the transition to $\rho_{\mathrm{HG}}(T_\star)$ when the transition is completed.

1.2 The order of the cosmological QCD transition

The order of the QCD phase transition and (for a first-order transition) the magnitude of the latent heat are still a subject of debate. Below I first introduce the bag model, because it gives a simple parametrization for the pressure $p(T)$ and it is useful to introduce some notation. Then I sum up the knowledge obtained from lattice QCD (order of the transition, latent heat, surface tension).

1.2.1 The bag model

The MIT bag model [36] represents the short-distance dynamics by an collisionless gas of massless quarks and gluons [in the following I call that an Stefan-Boltzmann (SB) gas for brevity] and the long-distance confinement effects by a constant negative contribution to the pressure, the bag constant B,

$$p_{\mathrm{QGP}}(T) = p_{\mathrm{QGP}}^{\mathrm{SB}}(T) - B \ , \tag{1.11}$$

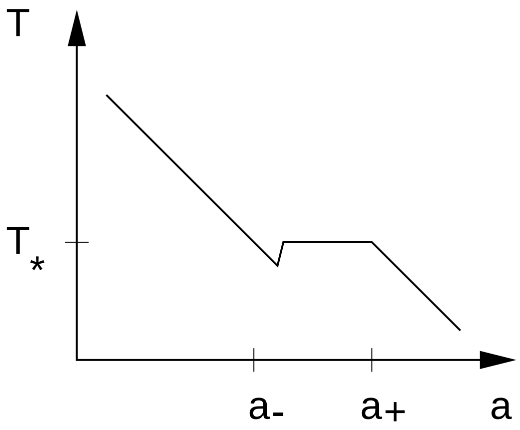

Figure 1.1: Qualitative behavior of the temperature T as a function of the scale factor a during a first-order QCD transition with small supercooling. Above the critical temperature $T_\star$ the Universe (filled with a quark-gluon plasma) cools due to its expansion ($a < a_-$). After a tiny period of supercooling (in the figure the amount of supercooling and its duration are exaggerated) bubbles of the new phase (hadron gas) nucleate. Almost in an instant these bubbles release enough energy (latent heat) to reheat the Universe to the critical temperature. During the rest of the transition both phases coexist in pressure and temperature equilibrium ($a_- < a < a_+$). Therefore the temperature is constant. After reheating the bubble growth is governed by the expansion of the Universe. The transition is completed when no quark-gluon plasma is left over. For $a > a_+$ the temperature decreases again due to the expansion of the Universe.

with $p_{\rm QGP}^{\rm SB}(T) = (\pi^2/90) g_{\rm QGP} T^4$. The low temperature phase is a hadron gas (HG). It may be modeled as a SB gas of massless pions,

$$p_{\rm HG} = \frac{\pi^2}{90} g_{\rm HG} T^4, \tag{1.12}$$

because the contribution of pions is small anyway, $g_{\rm HG}/g_{\rm QGP} = 3/37$.

At the phase transition the quark-gluon phase and the hadron phase are in pressure equilibrium,

$$p_{\rm QGP}(T_\star) = p_{\rm HG}(T_\star) \equiv p_\star \ . \tag{1.13}$$

This condition gives, together with (1.11) and (1.12), the relation between $T_\star$ and B:

$$B = \frac{\pi^2}{90}(g_{\rm QGP} - g_{\rm HG}) T_\star^4 \ . \tag{1.14}$$

Let me take $T_\star$ from lattice QCD calculations with two flavors, which give $T_\star = 140$ to 160 MeV [37, 35]. This corresponds to a range of bag constants $B^{1/4} = 195$ to 245) MeV. This range is in agreement with fits to the light-hadron masses, which yield $B^{1/4} = 145$ to 245 MeV (a compilation of various bag model light-hadron fits can be found in [38]).

The QCD transition is first order in the bag model, because the entropy density $s \equiv \mathrm{d}p/\mathrm{d}T$ makes a jump. The latent heat per unit volume

$$l \equiv T_\star \Delta s \tag{1.15}$$

measures the amount of 'internal' energy that is released during the phase transition. In the bag model the latent heat is

$$l = \frac{2\pi^2}{45} \Delta g T_\star^4 = 4B, \tag{1.16}$$

where $\Delta g \equiv g_{\mathrm{QGP}} - g_{\mathrm{HG}}$.

Besides the latent heat, the surface tension is the crucial parameter for the nucleation of bubbles (see chapter 3). The surface tension

$$\sigma \equiv \left(\frac{\mathrm{d}W}{\mathrm{d}A} \right)_V \tag{1.17}$$

is the work $\mathrm{d}W$ that has to be done per area $\mathrm{d}A$ to change the phase interface at fixed volume. The absence of surface excitations in hadronic spectra suggests that $\sigma^{1/3} \ll B^{1/4}$ [38] in the bag model. This implies $\sigma \ll 2.7 T_\star^3$ for two quark flavors. A self-consistent calculation of the surface tension within the MIT bag model shows that the surface tension vanishes for massless quarks and gluons if no interactions besides the bag constant (i.e. $\alpha_s = 0$) are taken into account [38]. This can be cured by introducing short-range interactions [38] or by including the strange quark with mass $m_s = 100$ to 300 MeV [39].

1.2.2 Lattice QCD results

In quenched QCD the phase transition is of first order [34]. The latent heat was determined to be $l \approx 1.4 T_\star^4$ [10]. It is useful to take the ratio R_L of the latent heat to the value $T_\star \Delta s^{\mathrm{SB}}$, where Δs^{SB} is the difference in entropy between two Stefan-Boltzmann gases,

$$R_L \equiv \frac{l}{(T_\star \Delta s)^{\mathrm{SB}}} = \begin{cases} 1 & \text{bag model} \\ 0.2 & \text{quenched lattice QCD} \end{cases} . \tag{1.18}$$

For two light quarks it is likely that the transition is a crossover [35, 40]. This is in agreement with theoretical considerations [41], which predict a second-order phase transition in the massless quark limit.

For three light flavors and for the physical relevant case of two light and one heavy flavor the phase transition is likely to be of first order [42]. This result was obtained using the Wilson quark action, whereas results with staggered quarks [43] indicate a crossover for the physical quark masses. For four quark flavors the transition is first order [44].

Since the latent heat for lattice QCD is known for quenched QCD only, I decided to use the latent heat ratio $R_L = 0.2$ from quenched QCD as an indication for the physical case.

For the surface tension rather small values are found form lattice QCD. Refs. [10] found that $\sigma \approx 0.015 T_\star^3$ for quenched lattice QCD. There are no values for unquenched QCD available yet. However, an upper bound was obtained for the case of four-flavor lattice QCD in Ref. [45], i.e., $\sigma < 0.1 T_\star^3$.

1.3 Effects from a first-order QCD transition

Let me now briefly summarize the effects that have been suggested to emerge from the cosmological QCD transition. There are two kinds of effects: The effects that have been found in the mid 80's and early 90's stem from the bubble scale and thus they affect scales $\lambda \leq d_{\mathrm{nucl}}$. The formation of quark nuggets, the generation of isothermal baryon fluctuations, the generation of magnetic fields and gravitational waves belong to the effects from the bubble scale.

In the recent years it was found that there is another class of possible consequences from the QCD transition which are connected to the Hubble scale and therefore affect scales $\lambda \leq R_{\mathrm{H}}$. Among these effects are the amplification of inhomogeneities and later formation of cold dark matter clumps, the modification of primordial gravitational waves, and the enhanced probability of black hole formation during the QCD transition.

1.3.1 Quark nuggets

In the mid 80s interest in the cosmological QCD transition arose, because it was realized that a strong first order QCD phase transition could lead to important observable signatures. Most interest was based on a separation of cosmic phase as suggested by Witten [5]. If the cosmological QCD transition is first-order, bubbles of hadron gas are nucleated and grow until they merge and fill up the whole universe. Towards the end of the of this coexistence of the QGP and HG phases, shrinking quark droplets remain. These droplets are expected to be baryon enriched compared to the hadron phase, because in equilibrium baryons are suppressed by the Boltzmann factor in the HG and baryon diffusion across the phase boundary might be inefficient.

In 1971 Bodmer [46] suggested the possibility that strange quark matter might be the ground state of bulk matter, instead of ^{56}Fe. Later Witten [5] discovered this idea again. Further strange quark matter was studied by Farhi and Jaffe [38]. The idea of strange quark matter is based on the observation that the Pauli principle allows to pack more quarks into a fixed volume in phase space if three instead of two flavors are available. Thus the energy per baryon would be lower in strange quark matter than in nuclei. However, the strange quark is heavy compared to up and down quarks and this mass counteracts the advantage from the Pauli principle. No strange quark matter has been found experimentally so far, see [47]. The issue of stability of strange quark matter has not been settled yet, for a recent review see [48].

Witten [5] pointed out that a separation of phases during the coexistence of the hadronic and the quark phase could gather a large number of baryons in strange quark nuggets [5]. These quark nuggets could contribute to the dark matter today [5] or affect BBN [49]. At the end of the transition the baryon number in the quark droplets could exceed the baryon number in the hadron phase by several orders of magnitude, $n_{\rm B}^{\rm QGP}$ could be close to nuclear density [50]. However, it was realized that the quark nuggets, while cooling, lose baryons. The quark nuggets evaporate as long as the temperature is above ~ 50 MeV [51]. Quark nuggets may survive this evaporation if they contain much more than $\sim 10^{44}$ baryons initially [52]. This number should be compared with the number of baryons inside a Hubble volume at the QCD transition, which is 10^{48} (see section 1.1.1). Thus, the mean bubble nucleation distance should be $> 3 \times 10^{-2} R_{\rm H} \sim 300$ m in order to collect enough baryons. This seems impossible from recent lattice QCD calculations of latent heat and surface tension [10].

In [50, 52] a chromoelectric flux tube model was used to estimate the penetration rate of baryons through the interface. A quark that tries to penetrate the interface creates a flux tube, which most probably breaks up into a quark anti-quark pair. By this mechanism mesons evaporate easily. On the other hand baryons are formed rarely, because a diquark anti-diquark pair has to be produced in the break up of the flux tube. One could easily think of mechanisms that would increase the evaporation rate of baryons [53]. If a significant fraction of diquarks was formed in the quark phase, these diquarks could penetrate the interface by creating a flux tube, which eventually breaks creating a quark anti-quark pair. The quark would leave together with the diquark and form a baryon, whereas the anti-diquark would remain in the quark phase. Such a mechanism would increase the evaporation rate.

Thus, independently from the existence (stability) of strange quark matter it seems highly unlikely that strange quark nuggets could survive from in the cosmological QCD transition below temperatures of ~ 50 MeV.

1.3.2 Inhomogeneous nucleosynthesis

Applegate and Hogan [6] found that a strong first order QCD phase transition induces inhomogeneous nucleosynthesis. It is extremely important to understand the initial conditions for BBN, because many of our ideas about the early universe rely on the validity of the standard (homogeneous) BBN scenario. The standard BBN scenario is in good agreement with observations [18]. In inhomogeneous nucleosynthesis [15] large isothermal fluctuations of the baryon number (the remnants of the quark droplets at the end of the QCD transition) could lead to different yields of light elements. As a minimal requirement for an inhomogeneous scenario of nucleosynthesis the mean bubble nucleation distance has to be larger than the proton diffusion length, which corresponds to ~ 3 m [16] at the QCD transition. This is two orders of magnitude above recent estimates of the typical nucleation distance [13].

On the other hand the observed cosmic abundances of light elements do not favor inhomogeneous nucleosynthesis, except a small region in parameter space corresponding to an inhomogeneity scale of ~ 40 m [16].

However, interesting inhomogeneity scales for BBN might follow if the bubble nucleation is not homogeneous. Heterogeneous nucleation in the presence of impurities or nucleation in the inhomogeneous Universe could increase the baryon inhomogeneity scale to interesting values (see chapter 3).

Although, dramatically different values for η than in the standard BBN are excluded both from precision measurements and from calculations of inhomogeneous BBN, it might be possible to alter the abundance of heavy elements ($A > 7$) dramatically in various inhomogeneous scenarios [19]. More on inhomogeneous BBN will be discussed in chapter 4.

1.3.3 Cold dark matter clumps

Scales λ that are of the order of the Hubble radius R_{H} are not sensitive to details of the bubbles. Together with Schmid and Widerin I found in Refs. [22, 23, 24] that the evolution of cosmological density perturbations is strongly affected by a first-order QCD transition for subhorizon scales, $\lambda < R_{\mathrm{H}}$. Cosmological perturbations on all scales are predicted by inflation [54, 55, 56, 57, 58] and have been observed in the temperature fluctuations of the cosmic microwave background radiation by the COBE satellite [59, 60].

In the radiation dominated universe subhorizon density perturbations perform acoustic oscillations. The restoring force is provided by pressure gradients. The pressure gradients, hence the isentropic sound speed $c_s = (\partial p/\partial \rho)_S^{1/2}$ (on scales much larger than the bubble separation scale) drops to zero at a first order QCD transition [23], because both phases coexist at the pressure $p_\star$ only (a is the scale factor of the universe):

$$c_s^2 \equiv \left(\frac{\partial p}{\partial \rho}\right)_S = \frac{\mathrm{d}p_\star/\mathrm{d}a}{\mathrm{d}\rho(a)/\mathrm{d}a} = 0 \ . \tag{1.19}$$

It stays zero during the entire transition and suddenly rises back to the radiation value $c_s = 1/\sqrt{3}$ after the transition. A significant decrease in the effective sound speed c_s during the cosmological QCD transition was pointed out by Jedamzik [27] independently.

As the sound speed drops to zero, the restoring force for acoustic oscillations vanishes and density perturbations for subhorizon modes fall freely. The fluid velocity stays constant during this free fall. Perturbations of shorter wavelengths have higher velocities at the beginning of the transition, and thus grow proportional to wavenumber k during the phase transition. The primordial Harrison-Zel'dovich spectrum [61] of density perturbations is amplified on subhorizon scales. The spectrum of density perturbations on superhorizon scales, $\lambda > R_{\mathrm{H}}$, is unaffected. At $T \sim 1$ MeV the neutrinos decouple from the radiation fluid. During this decoupling the large peaks in the radiation spectrum are wiped out by collisional damping [62].

Today the universe is dominated by dark matter, most likely cold dark matter (CDM). If CDM is kinetically decoupled from the radiation fluid at the QCD transition, the density perturbations in CDM do not suffer from the neutrino damping. This is the case for primordial black holes or axions, but not for supersymmetric dark matter and heavy neutrinos. At the time of the QCD transition the energy density of CDM is small, i.e. $\rho^{\mathrm{CDM}}(T_\star) \sim 10^{-8}\rho^{\mathrm{RAD}}(T_\star)$. CDM falls into the potential wells provided by the dominant radiation fluid. Thus, the CDM spectrum is amplified on subhorizon scales. The peaks in the CDM spectrum go nonlinear shortly after radiation-matter equality. This leads to the formation of CDM clumps with mass $< 10^{-10} M_\odot$. Especially the clumping of axions has important implications for axion searches with strong magnetic fields [63]. If the QCD transition is strong enough, these clumps could be detected by gravitational femtolensing [64].

1.3.4 Other effects

Generation of magnetic fields Hogan [20] argued that magnetic fields might be generated in violent processes at the bubble scale. Later on field lines should reconnect to yield large scale magnetic fields which could play an important role in structure formation after the recombination of matter. Recently, Cheng and Olinto [21] suggested that such magnetic fields might be generated by currents on the bubble surfaces.

If the shrinking QGP droplets are baryon enriched, there is a positive net charge on the inner side of the surface of the bubble walls, which is compensated by a negative net charge of electrons outside the bubble. This is due to the different Debye screening lengths of electrons and baryons. Thus surface currents on the bubble surfaces are possible which could give rise to magnetic fields. The typical scale at their creation would be the bubble scale.

Subhorizon ($\lambda < R_{\rm H}$) fields are damped during neutrino and photon decoupling [65]. In the most optimistic scenario magnetic fields of the order of 10^{-20} Gauß at the 10 Mpc scale today would be possible [66].

Generation of gravitational waves A measure for the energy density in gravitational waves is the fractional energy density per logarithmic frequency interval,

$$\Omega_{\rm g}(f) \equiv \frac{1}{\rho_{\rm c}} \frac{{\rm d}\rho_{\rm g}}{{\rm d}\ln f} \ , \tag{1.20}$$

f is the frequency of the gravitational wave under consideration.

The generation of gravitational waves from violent bubble collisions during a strongly first-order QCD transition has been suggested by Witten [5]. The production of gravitational waves would be possible if detonation bubbles collide, i.e. the bubble walls move faster than the sound speed. A more quantitative analysis for the collision of vacuum bubbles (all latent heat goes into the kinetic energy of the bubble walls) has been performed by Kosovsky et al. [67]. However, neither in the bag model nor from lattice QCD a bubble nucleation scenario with detonation waves (almost vacuum bubbles) is likely. In the opposite, the most likely scenario are weakly deflagrating bubbles [12]. The generation of gravitational waves under these circumstances has been investigated by Hogan [68] and Kamionkowski et al. [69]. An estimate in [68] yields

$$\Omega_{\rm g} \sim 10^{-5} (d_{\rm nucl} H)^3 c_s^6 \ , \tag{1.21}$$

for $f \sim H$ at the time of the QCD transition, which is $f \sim 10^{-7}$ Hz today. These gravitational waves are induced by the large inhomogeneities in energy density due to the coexistence of the QGP and the HG during a period $\sim H^{-1}$. The most optimistic scenarios allow $\Omega_{\rm g} \sim 10^{-13}$, however scenarios based on recent lattice QCD results give $\Omega_{\rm g} \sim 10^{-23}$, which is completely out of reach of any presently known technique for the detection of gravitational waves. The calculations in [69] result in a different dependence on $d_{\rm nucl} H$, however, $\Omega_{\rm g}$ is as small as from [68].

Formation of black holes Crawford and Schramm [25] suggested that long range forces during the QCD transition lead to the formation of planetary mass black holes. However, there is no evidence that there are such large correlations lengths at the QCD transition (km instead of fm!). Hall and Hsu [26] argued that collapsing bubbles might collapse to black holes. The mass of these objects would at most be $\rho V_{\rm bubble}$ which, if the typical bubble scale is 1 cm is $< 10^{-18} M_\odot$. Since the supercooling in the cosmological QCD transition is tiny, such a violent collapse of the walls of the shrinking quark droplets is impossible. Moreover, black holes of these masses could not survive until today, they would have evaporated long ago [70].

The vanishing of the sound speed during the coexistence phase also leads to interesting gravitational effects, as pointed out by Jedamzik

Chapter 2

The early universe at the QCD scale

In this chapter I discuss the thermodynamic properties of matter around the QCD scale. The dominant matter component can be described as a single, adiabatically expanding radiation fluid. Its equation of state, its expansion, and the behavior of the sound speed are discussed in section 2.1. Baryons are tightly coupled and thus belong to the radiation fluid. The evolution of the baryon chemical potential is described in section 2.2. The last section (2.3) of this chapter deals with the properties of cold dark matter (CDM) at the QCD scale. Not all CDM candidates behave as CDM up to the QCD scale. Especially neutralinos and heavy neutrinos belong to the radiation fluid. Axions and primordial black holes are kinetically decoupled at the QCD scale. These CDM candidates are modeled by a pressureless fluid, which couples to the radiation fluid via gravity only.

2.1 The radiation fluid

The expansion of the Universe is very slow compared to the strong, electromagnetic, and weak interactions around $T_\star$. To be more explicit, the rate of the weak interactions is $\Gamma_{\mathrm{w}} \sim G_{\mathrm{F}}^2 T_\star^5 \approx 10^{-14}$ GeV, the rate of the electromagnetic interactions is $\Gamma_{\mathrm{em}} \sim \alpha^2 T_\star \approx 10^{-5}$ GeV, and the rate of the strong interactions is $\Gamma_{\mathrm{s}} \sim \alpha_{\mathrm{s}}^2(T_\star) T_\star \approx 10^{-1}$ GeV. These rates have to be compared to the Hubble rate $H \sim T_\star^2/m_{\mathrm{Pl}} \approx 10^{-21}$ GeV. Thus, leptons, photons, and the QGP/HG are in thermal and chemical equilibrium at cosmological time scales. All components have the same temperature locally, i.e. smeared over scales $\lambda \sim 10^{-7} R_{\mathrm{H}}$. At scales $\lambda > 10^{-7} R_{\mathrm{H}}$ strongly, weakly, and electromagnetically interacting matter makes up a single perfect (i.e. dissipationless) radiation fluid.

There are no conserved quantum numbers for the radiation fluid, apart from the lepton numbers and the baryon number. However, the corresponding chemical potentials are negligible small ate the QCD epoch. For the baryon chemical potential this is shown in section 2.2. All lepton chemical potentials are assumed to vanish exactly, a discussion of that issue can be found in Ref. [80]. In this situation all thermodynamic quantities follow from the free energy. The free energy density is $f(T) = -p(T)$ from homogeneity. The entropy density is given by the Maxwell relation for the free energy,

$$s = \frac{dp}{dT} \ , \tag{2.1}$$

and the energy density $\rho(T)$ follows from the second law of thermodynamics for reversible processes,

$$\rho = T\frac{dp}{dT} - p \ . \tag{2.2}$$

2.1.1 The equation of state

The behavior of $\rho(T)$ and $p(T)$ near the QCD transition must be given by nonperturbative methods, by lattice QCD. In figure 2.1 lattice QCD data are shown for $\rho(T)$ and $p(T)$ divided by ρ of the corresponding Stefan-Boltzmann (SB) gas. The lattice results for two systems are plotted, quenched QCD (no quarks) [34], and two-flavor QCD [40]. For quenched QCD the lattice continuum limit is shown. For two flavor QCD the data with six time steps ($N_t = 6$, $a \approx 0.2$ fm) and a quark mass $am_q = 0.0125$ is shown. This corresponds to a physical mass $m_q \sim 14$ MeV, a bit heavier than the physical masses of the up and down quarks. On the horizontal axis we plot $(T/T_\star)$. Unfortunately $\rho(T)$ and $p(T)$ for three quarks (u,d,s) with physical masses is not available yet. For $T/T_\star = 4$ energy density and pressure for quenched QCD are still 10% resp. 15% below the SB gas value. It is remarkable that $\rho/\rho_{\rm SB}$ and $p/\rho_{\rm SB}$ versus $T/T_\star$ is quite similar for quenched QCD and two-flavor QCD. Moreover, the temperature dependence of the rescaled pressure for four-flavor QCD [44] is quite similar to quenched QCD.

At temperatures below $T_\star$ quarks and gluons are confined to hadrons, mostly pions. At present the hot pion phase is not seen in the two-flavor lattice QCD, since the pion comes out too heavy ($0.3 < m_\pi/m_\rho < 0.7$ from [35], whereas the physical ratio is 0.18). The lattice QCD results for $s/s^{\rm SB}_{\rm QGP}$ are shown in Fig. 2.2.

In the bag model (see section 1.2.1) the pressure was given in Eqs. (1.11) and (1.12) and thus from (2.1) and (2.2) the energy density and entropy density read:

$$\rho_{\rm QGP} \ = \ \rho^{\rm SB}_{\rm QGP} + B \tag{2.3}$$

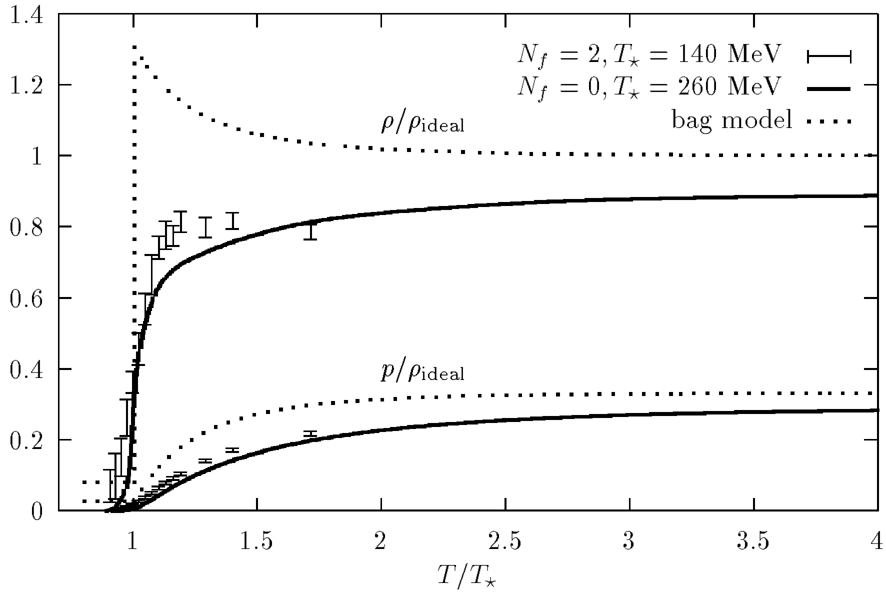

Figure 2.1: The energy density and the pressure of hot QCD, both relative to the energy density of a Stefan-Boltzmann (ideal) gas of quarks and gluons, are plotted as functions of $T/T_\star$. The lattice QCD data for $N_f = 0$ [34] and $N_f = 2$ QCD [35] are compared with the predictions of the bag model.

$$s_{\mathrm{QGP}} = s^{\mathrm{SB}}_{\mathrm{QGP}} , \tag{2.4}$$

with $\rho^{\mathrm{SB}} = (\pi^2/30)gT^4$ and $s^{\mathrm{SB}} = (2\pi^2/45)gT^3$ for massless particles. The bag results for $\rho/\rho^{\mathrm{SB}}_{\mathrm{QGP}}$, $p/\rho^{\mathrm{SB}}_{\mathrm{QGP}}$, $s/s^{\mathrm{SB}}_{\mathrm{QGP}}$ are shown in Fig. 2.1 and Fig. 2.2. Note that s/T^3 is a simple step function in the bag model.

In [23, 24] we used an analytic representation of the lattice QCD data. We decided to fit the entropy density (Fig. 2.2) and to derive the other thermodynamic quantities with Eqs. (2.2) and (2.1). Below $T_\star$ we consider again a SB gas of the three pions. We fit the shape of the lattice QCD data by

$$\frac{s^{\mathrm{fit}}}{(2\pi^2/45)T^3} = g_{\mathrm{HG}} + \Delta g\theta(T - T_\star)\left[R_L + (1 - R_L)\left(1 - \frac{T_\star}{T}\right)^\gamma\right] . \tag{2.5}$$

A good fit for the large scale properties of the radiation fluid is obtained for $\gamma \in (0.3, 0.4)$. We fix $\gamma = 1/3$. The fit is plotted in Fig. 2.2.

Note that this fit is very useful for the effective sound speed on scales much larger than the bubble scale, but it is inappropriate during the short period of supercooling (see section 2.1.3).

Finally, there is the possibility that the QCD transition could be a smooth crossover. Such a crossover has been modeled by a simple interpolation

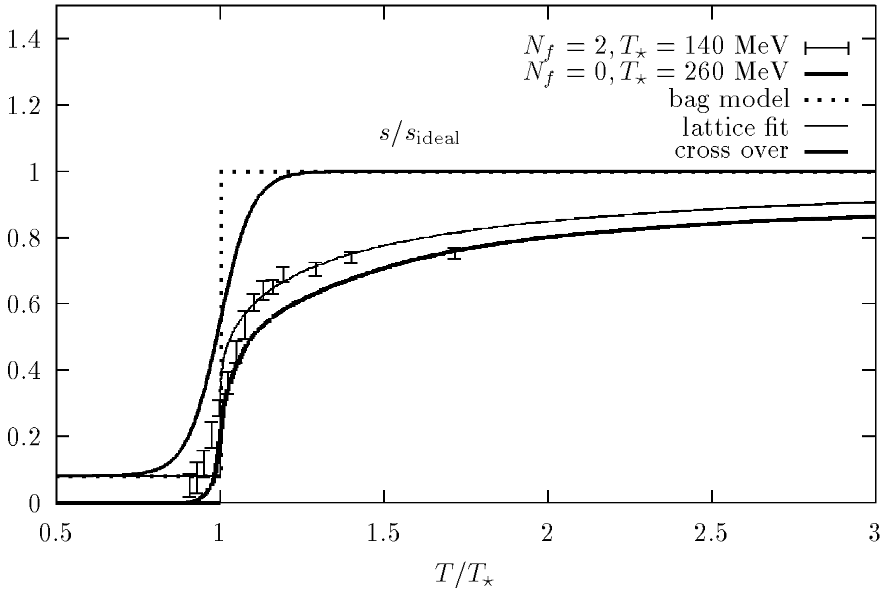

Figure 2.2: The entropy density of hot QCD relative to the entropy density of a Stefan-Boltzmann (ideal) gas of quarks and gluons is shown for the same lattice QCD results as in Fig. 2.1. Also plotted is the entropy density for a fit to the lattice QCD data, for the bag model, and for a smooth crossover.

between the SB values of the entropy density with a tanh. It was first given in Ref. [78]. The entropy density is written as

$$\frac{s^{\rm crossover}}{s^{\rm SB}_{\rm QGP}} = 1 - \frac{1}{2}\frac{\Delta g}{g_{\rm QGP}}\left[1 - \tanh\left(\frac{T - T_\star}{\Delta T}\right)\right] \ . \tag{2.6}$$

In Fig. 2.2 $\Delta T/T_\star = 0.1$. This gives the shape of the initial rise of the lattice data, but it necessarily fails to give the slow rise at higher temperatures from $s/s^{\rm SB}_{\rm QGP} \approx 0.6$ to 1.

2.1.2 The adiabatic expansion

Let me now discuss the evolution of the temperature and the other thermodynamic variables as a function of the scale factor a.

Entropy is conserved, apart from the very short stage of reheating ($\sim 10^{-6} t_{\rm H}$) after the first bubbles have been nucleated. This allows us to calculate $T = T(a)$ from $\mathrm{d}(s(T)a^3) = 0$, i.e.

$$\frac{\mathrm{d}T}{\mathrm{d}\ln a} = -\frac{3s}{\mathrm{d}s/\mathrm{d}T} \ , \tag{2.7}$$

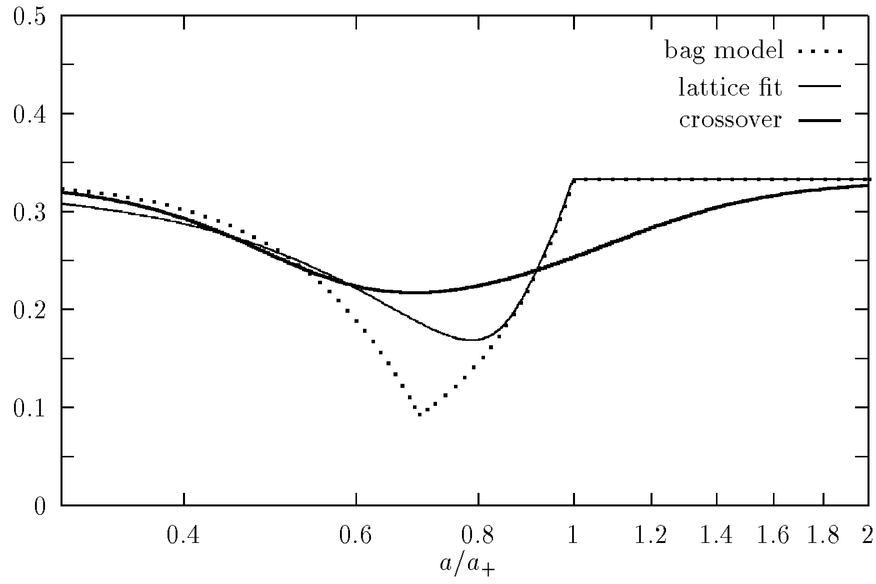

Figure 2.3: The behavior of $w = p/\rho$ during the QCD transition as a function of the scale factor a. Although the pressure is reduced, it stays positive throughout the transition.

except for $T = T_\star$ in the case of a first-order phase transition. In the bag model $T \propto 1/a$ for $T \neq T_\star$.

The expansion while the QGP and HG coexist in a first-order QCD transition is determined by entropy conservation,

$$a_+ = \left(\frac{s_-}{s_+}\right)^{\frac{1}{3}} a_- \ , \tag{2.8}$$

where the index $-(+)$ denotes the value of a quantity at the beginning (end) of the coexistence epoch. In the bag model the Universe expands by a factor of $a_+/a_- \approx 1.4$ until all QGP has been converted into the HG, whereas for the lattice QCD fit (2.5) the Universe expands by a factor of $a_+/a_- \approx 1.1$. The growth of the scale factor is related to a lapse in cosmic time by $\mathrm{d}\ln a = \mathrm{d}t$. In terms of the Hubble time the transition lasts $0.3t_\mathrm{H}$, resp. $0.1t_\mathrm{H}$ for the bag model resp. lattice QCD fit (2.5).

During a first-order QCD transition, i.e. $T = T_\star$, the pressure $p(T_\star) \equiv p_\star$ is constant. For any first-order QCD phase transition the energy density $\rho(a)$ is obtained from the first law of thermodynamics $d\rho = -3(\rho + p_\star)da/a$. The result for $a_- < a < a_+$ is:

$$\rho(a) \quad = \quad (\rho(a_-) + p_\star)\left(\frac{a_-}{a}\right)^3 - p_\star \ , \tag{2.9}$$

$$w(a) \quad = \quad \left[\left(\frac{\rho(a_-)}{p_\star} + 1 \right) \left(\frac{a_-}{a} \right)^3 - 1 \right]^{-1} , \tag{2.10}$$

where $w \equiv p/\rho$. For the lattice QCD fit (2.5) and for the bag model $p_\star = \rho(a_+)/3$.

In the models of a first-order QCD transition considered here the evolution after the transition ($a_+ < a$) is approximated to be purely radiation dominated, i. e., $w(a) = \frac{1}{3}$. The evolution of w is shown in Fig. 2.3.

2.1.3 The sound speed

The sound speed relates pressure gradients to density gradients, i.e. $\nabla p = c_s^2 \nabla \rho$. This relation is essential for the evolution of density fluctuations, which is elaborated in chapter 5. During the short period of supercooling the relation between temperature and time strongly depends on c_s^2. This is important for the correct estimate of the mean bubble nucleation distance in chapter 3.

When analyzing cosmological perturbations (chapter 5) I shall consider wavelengths $\lambda > 10^{-4} R_{\mathrm{H}}$, for which neutrinos are tightly coupled, $\Gamma_\nu / k \gg 1$. For these wavelengths the radiation fluid behaves as a perfect (i.e. dissipationless) fluid, entropy in a comoving volume is conserved, one has a reversible process. On the other hand, below the neutrino diffusion scale, $\lambda < 10^{-4} R_H$, acoustic oscillations are damped away before the QCD transition (see section 5.3).

The isentropic sound speed (for wavelengths λ much larger than the bubble separation), given by

$$c_s^2 \equiv \left(\frac{\partial p}{\partial \rho} \right)_s = \frac{\mathrm{d}p/da}{\mathrm{d}\rho/da} , \tag{2.11}$$

must be zero during a first-order phase transition for a fluid with negligible chemical potential (i.e. no relevant conserved quantum number), because $p(a) = p_\star =$ constant. The behavior of $c_s^2(a)$ is shown in Fig. 2.4 for the lattice QCD fit (2.5) and for the bag model. In the bag model $c_s^2 = 1/3$ before and after the transition. Since there are no lattice data for the HG equation of state (the pions are too heavy) the lattice fit in Fig. 2.4 follows the bag model for $T < T_\star$. For a crossover the sound speed decreases below $1\sqrt{3}$ at $T_\star$, but does not drop to zero.[1] In the figure the equation of state (2.6) with $\Delta T / T_\star = 0.1$ has been used to illustrate the sound speed in a QCD crossover.

[1] A small drop of the sound speed has been found by Dixit and Lodenquai [79] in a bag model taking interactions and masses into account. However, they missed that the sound speed drops to zero in a cosmological first-order QCD transition.

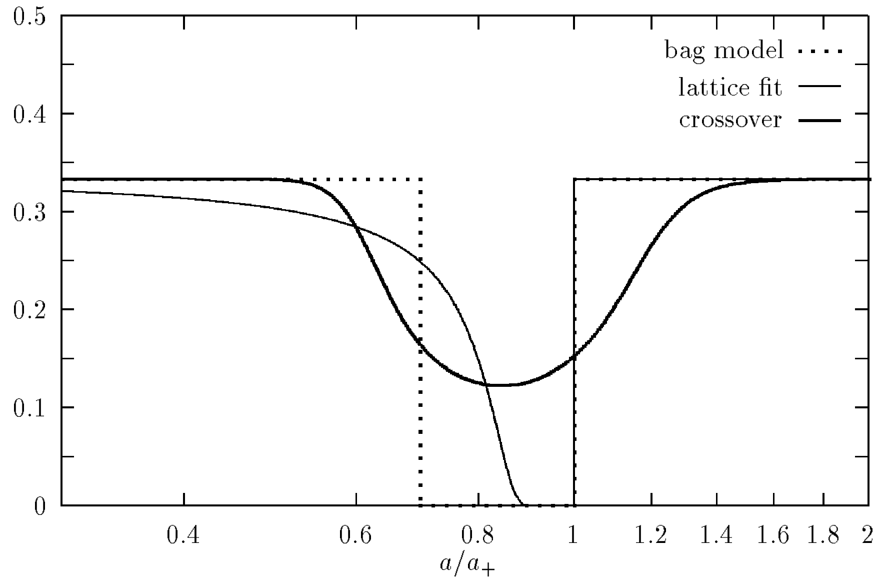

Figure 2.4: The behavior of the sound speed $c_s^2 = (\partial p/\partial \rho)_s$ during the QCD transition as a function of a. During a first-order transition (lattice fit and bag model) the sound speed vanishes.

The isentropic condition applies during the part of the phase transition after the initial supercooling, bubble nucleation, and sudden reheating to $T_\star$. During the adiabatic part of the transition, which takes about 99% of the transition time, the fluid is extremely close to thermal equilibrium, because the time to reach equilibrium is very much shorter than a Hubble time, i.e. the fluid makes a reversible transformation. This can be seen as follows: Across the bubble walls local pressure equilibrium is established immediately, $p_{\rm QGP} = p_{\rm HG}$ locally. Local temperature equilibrium, $T_{\rm QGP} = T_{\rm HG}$ is established by neutrinos, which have a mean free path of $10^{-7} R_{\rm H}$, enormously larger than the bubble wall thickness, and a collision time much shorter than the Hubble time. This local pressure and temperature equilibrium can only be satisfied if $p = p_\star$ and $T = T_\star$ at the bubble walls. Over distance scales of the order of the bubble separation (~ 1 cm) pressure (and therefore also temperature) is equalized with the velocity of sound, and thereby the released latent heat is distributed. This pressure equalization is very fast compared to the Hubble expansion velocity $v_{\rm H} \approx 10^{-6} c$ at the 1 cm scale.

From Eq. (2.2) and Eq. (2.1) the sound speed may be evaluated as

$$c_s^2 = (\mathrm{d}\ln s/\mathrm{d}\ln T)^{-1} \ . \tag{2.12}$$

The relation between temperature and time during the adiabatic expansion depends on the sound speed. From Eqs. (2.7) and (2.12) we find

$$\mathrm{d}\ln T = -3c_s^2 H \mathrm{d}t \ . \tag{2.13}$$

This relation holds during the short period of supercooling before the first bubbles have been nucleated. An estimate of c_s^2 in the QGP at $T_\star$ has been obtained from lattice QCD.

A strong decrease in the sound speed, already above $T_\star$, has been observed in lattice QCD for $N_f = 0$ [34] and for $N_f = 2$ [35]. In both cases $3c_s^2(T_\star) \approx 0.1$ when approaching the critical temperature from above (in the QGP). Note that this implies that the sound speed relevant for bubble nucleation is of order 0.3 instead of $1/\sqrt{3} \approx 0.6$.

The lattice QCD fit (2.5) does not correctly reproduce the behavior of the supercooled phase, but it nicely models the effective sound speed that is relevant for pressure perturbations on scales $\lambda > 10^{-4} R_{\mathrm{H}}$. Inserting (2.5) into (2.12), we obtain

$$c_s^2 \propto \left(1 - \frac{T_\star}{T}\right)^{1-\gamma} \ . \tag{2.14}$$

For an analytic discussion of the behavior of acoustic modes during the phase transition it is important to know c_s^2 as a function of conformal time $\eta \equiv \int a^{-1}(t)\mathrm{d}t$. In the radiation dominated regime $a \propto \eta$. Up to small corrections, this holds true during the transition. From Eq. (2.7) we find $(\eta_- - \eta)/\eta_- \propto (1 - T_\star/T)^\gamma$, which implies

$$c_s^2 = C^2 \left[(\eta_- - \eta)/\eta_-\right]^{\frac{1-\gamma}{\gamma}} \ , \tag{2.15}$$

with $C^2 = \{3^{1-\gamma}[g_+ + \Delta g R_L]/[\Delta g(1 - R_L)]\}^{1/\gamma}/\gamma$. For $\gamma = 1/3$ the sound speed goes to zero linearly in conformal time.

2.2 Baryons

The baryons are tightly coupled to the radiation fluid at the QCD scale. Their energy density is negligible compared to the energy density of the relativistic particles (photons, leptons, quarks/pions), thus they are dragged with the radiation fluid. Below I argue that the baryon chemical potential is negligible at the QCD scale.

At high temperatures ($T > T_\star$) the baryon number density may be defined as $n_{\mathrm{B}} \equiv \frac{1}{3}\sum(n_q - n_{\bar{q}})$, where n_q ($n_{\bar{q}}$) is the number density of a specific quark (anti-quark) flavor, and the sum is taken over all quark flavors. At $T < 1$ GeV only the u, d, and s quarks contribute significantly. At low temperatures ($T < T_\star$) the baryon number density is defined as $n_{\mathrm{B}} \equiv \sum(n_b - n_{\bar{b}})$, now the summation is taken over all baryon species. Practically the nucleons contribute to the baryon number of the universe only.

Below the electroweak transition ($T_{\rm ew} \sim 300$ GeV) the baryon number, B, in a comoving volume is conserved. On the other hand entropy, S, is conserved. As a consequence the ratio of baryon number density and entropy density, s, is constant. From the abundances of primordial ^{4}He and D [produced in big bang nucleosynthesis (BBN)] we know the ratio $n_{\rm B}/n_\gamma = (1.5 \text{ to } 6.3) \times 10^{-10}$ [18]. Taking into account the three massless neutrinos along with the photons that contribute to the entropy density, one finds

$$\frac{n_{\rm B}}{s} = (2 \text{ to } 8) \times 10^{-11} \ . \tag{2.16}$$

Due to this very small ratio the number of quarks equals the number of anti-quarks in the very early universe.

Let me now turn to the baryon chemical potential. At high temperatures the quark chemical potentials, $\mu_{\rm q}$, are equal, because weak interactions keep them in chemical equilibrium (e.g. u + e $\leftrightarrow$ d or s + $\nu_{\rm e}$), and the chemical potentials for the leptons are assumed to vanish (see [80] for a discussion of lepton chemical potentials). Thus, the chemical potential for a baryon is defined by $\mu_{\rm B} \equiv 3\mu_{\rm q}$. For an anti-baryon the chemical potential is $-\mu_{\rm B}$. The baryon number density of a SB Fermi gas of three quark flavors reads $n_{\rm B} \approx T^2\mu_{\rm B}/3$ at high temperature T. From Eq. (2.16) one finds that

$$\frac{\mu_{\rm B}}{T} \sim 10^{-9} \qquad \text{at } T > T_\star \ . \tag{2.17}$$

At low temperatures ($T < T_\star$) $\mu_{\rm B} = \mu_{\rm p} = \mu_{\rm n}$, neglecting the mass difference between the proton and the neutron. The ratio of baryon number density and entropy now reads

$$\frac{n_{\rm B}}{s} \approx 0.05 \left(\frac{m_{\rm p}}{T}\right)^{\frac{3}{2}} \exp\left(-\frac{m_{\rm p}}{T}\right) \sinh\left(\frac{\mu_{\rm B}}{T}\right) \ . \tag{2.18}$$

Since this ratio is constant, the behavior of $\mu_{\rm B}/T$ is given by Eq. (2.18), e.g. at $m_{\rm p}/T \approx 20$ one finds $\mu_{\rm B}/T \approx 10^{-2}$. All anti-baryons are annihilated when the ratio

$$\frac{n_{\rm b} - n_{\bar{\rm b}}}{n_{\rm b} + n_{\bar{\rm b}}} \approx \tanh\left(\frac{\mu_{\rm B}}{T}\right) \tag{2.19}$$

goes to unity. This happens when $\mu_{\rm B}/T \sim 1$, which corresponds to $T_{\rm ann} \approx m_{\rm p}/25 \approx 40$ MeV. Below this temperature the baryon chemical potential is $\mu_{\rm B}(T \ll T_{\rm ann}) \approx m_{\rm p}$. To add one proton to the universe one proton rest mass should be invested.

2.3 Cold dark matter at the QCD scale

Below, I discuss the properties of the most prominent CDM candidates at temperatures of the QCD scale. The text follows closely our presentation in [24]. I show that weakly interacting massive particles, like the lightest supersymmetric particle or a heavy neutrino, are kinetically tightly coupled to the radiation fluid at the QCD transition and belong to the radiation fluid. Two CDM candidates that are kinetically decoupled from the radiation fluid and have $p = 0$ at the QCD epoch are the axion and primordial black holes [24]. From the first law of thermodynamics the energy density of a pressureless gas goes as $\rho \propto 1/V_{\rm comoving}$. CDM that is kinetically decoupled does not influence the radiation fluid via gravity, because $\rho_{\rm CDM} \approx 10^{-8} \rho_{\rm RAD}$ at the QCD scale.

2.3.1 Neutralinos and heavy neutrinos

Let me start the discussion with the lightest supersymmetric particle [81], which is one of the most popular CDM candidates nowadays. In the minimal supersymmetric standard model [82] the lightest supersymmetric particle is the neutralino (when it is assumed to be stable). The neutralino is a mixture of the bino, neutral wino, and the two neutral higgsinos. Constraints from LEP 2 and cosmology, together with the assumption of universality at the GUT scale, show that its mass is $m_\chi > 42$ GeV [83]. It is essential to distinguish between the chemical freeze-out and the kinetic decoupling of neutralinos. The chemical freeze-out determines the amount of neutralinos today and happens when the annihilation rate of neutralinos drops below the Hubble rate, $\Gamma_{\rm ann}/H < 1$. Soon after the neutralinos become nonrelativistic the rate for neutralino annihilation, $\Gamma_{\rm ann} = \langle v\sigma_{\rm ann}\rangle n_\chi$, is suppressed by the Boltzmann factor in the number density of the neutralinos, $n_\chi \sim (m_\chi T)^{3/2} \exp(-m_\chi/T)$. The freeze-out temperature of the neutralino [81] is $T_f \sim m_\chi/20 > 2$ GeV, and neutralinos are chemically decoupled at the QCD transition.

Kinetic decoupling, in contrast, is determined by the elastic scattering between neutralinos and the dominant radiation fluid. The interaction rate for elastic scattering is $\Gamma_{\rm el} = \tau_{\rm coll}^{-1} = \langle v\sigma_{\rm el}\rangle n$, where $n \sim T^3$ is the number density of relativistic particles, e.g. electrons or neutrinos. The relevant diagrams for elastic neutralino lepton scattering are shown in figure 2.3.1. If the neutralino is a pure gaugino there is no contribution from Z_0 exchange. An order of magnitude estimate shows that $< \sigma_{\rm el} v > \sim G_{\rm F}^2 T^2$ [84, 85], similar to elastic neutron neutrino scattering [86].

One has to distinguish between the regime of perfect kinetic coupling, i.e. neutralinos tightly coupled to the radiation fluid, an intermediate regime where the neutralinos scatter elastically but the number of collisions is not

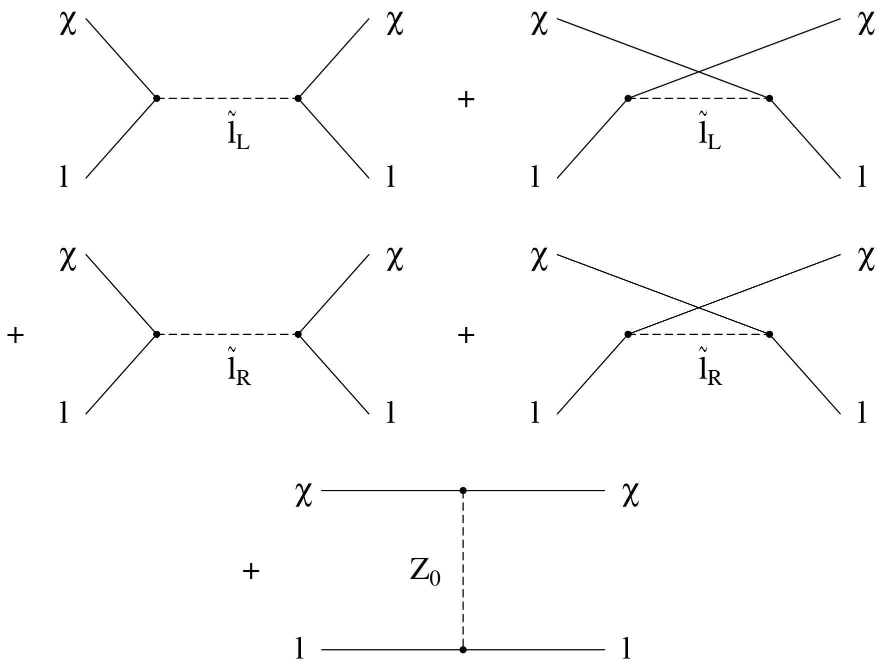

Figure 2.5: Feynman diagrams contributing to elastic neutralino-lepton scattering. χ is the neutralino, l is a lepton, and $\tilde{l}_{L,R}$ denote the corresponding left- and right-handed sleptons.

sufficient to drag them along dissipationless, and the regime of kinetic decoupling, $\Gamma_{\mathrm{el}}/H < 1$, which is roughly at $T \leq 1$ MeV, since the neutralino interacts weakly.

Let us estimate the regime where the neutralinos belong to the perfect radiation fluid. Perfectness of a fluid (dissipationless) refers to an external time scale, here ω^{-1} of an acoustic oscillation or the Hubble time. A fluid behaves as a perfect fluid, if $\omega\tau_{\mathrm{relax}} \ll 1$, i.e. the external time scale is larger than the relevant relaxation time, the fluid is continually in local thermal equilibrium, and no entropy production occurs. For the coupling of neutralinos to the radiation fluid the relaxation time is given by $\tau_{\mathrm{relax}} = N\tau_{\mathrm{coll}}$, where N is the number of collisions needed to completely change the momentum of the neutralino due to collisions with the radiation fluid. The momentum transfer at a collision of a lepton with the neutralino is of order $p_{\mathrm{l}} \sim T$. The kinetic energy of the neutralino is given by equipartition, $p_\chi^2/2m_\chi \sim T$, hence its momentum is $p_\chi \sim \sqrt{m_\chi T}$. The fractional change of the neutralino momentum from one collision at the QCD transition is $\delta p_\chi/p_\chi \sim \sqrt{T/m_\chi} \ll 1$. After N collisions the total rms change of momentum is $(\delta p_\chi/p_\chi)_{\mathrm{rms}} \sim \sqrt{NT/m_\chi}$. Local thermal equilibrium is obtained if the bulk motion of the neutralinos is governed by the leptons, i.e. the fractional change of the neutralino momentum is of order 1. The number of collisions needed to completely change direction is $N \sim m_\chi/T \approx 330$ for $m_\chi = 50$ GeV and $T = T_\star$. The collision time is given by the weak interactions rate $\Gamma_{\mathrm{w}} = \tau_{\mathrm{coll}}^{-1} \sim G_{\mathrm{F}}^2 T_\star^5$, and the relaxation time is given by

$$\tau_{\mathrm{relax}} = N\tau_{\mathrm{coll}} \sim N \times 10^{-7} t_{\mathrm{H}}, \tag{2.20}$$

with $N \sim m_\chi/T$. If the relaxation time is compared with the frequency of the acoustic oscillations, one finds that the condition for a perfect fluid, $\omega\tau_{\mathrm{relax}} \ll 1$, at the QCD transition is satisfied for scales $\lambda > \lambda_{\mathrm{dec}}(T_\star) \approx 10^{-4} R_{\mathrm{H}}$ ($m_\chi = 50$ GeV). Hence the neutralinos on these scales are part of the radiation fluid at the QCD transition. Below this scale, the neutralinos cannot follow the acoustic oscillations. On the other hand on the Hubble scale the perfect kinetic coupling of neutralinos to the radiation fluid stops when the required relaxation time becomes more than a Hubble time, $\tau_{\mathrm{relax}} > t_{\mathrm{H}}$. This gives a temperature of $T_\chi^{\mathrm{dec}} \sim 10$ MeV. Down to this temperature neutralinos on the Hubble scale belong to the radiation fluid.

Another CDM candidate is a heavy neutrino with $m_Z/2 < m_\nu < 1$ TeV [87], where only the upper mass bound gives cosmologically relevant CDM. Again, the kinetic decoupling of these neutrinos happens way below $T_\star$. Therefore the neutralino or a heavy neutrino would be tightly coupled to the radiation fluid during the QCD transition.

2.3.2 Axions

The axion has been introduced to solve the strong CP problem and it is a popular CDM candidate [88]. Direct searches in the laboratory, constraints from astrophysics and from cosmology allow the axion mass to be 10^{-5} – 10^{-2} eV. Axions could be the dominant matter today if their mass is small, i.e. $m_{\rm a} \sim 10^{-5}$ eV, which corresponds to a breaking of the Peccei-Quinn (PQ) symmetry at the scale $f_{\rm PQ} \sim 10^{12}$ GeV. These axions could be produced coherently due to a initial misalignment of the axion field and by the decay of axionic strings.

The initially misaligned axion field starts to oscillate coherently when the axion mass has grown to $m_{\rm a}(T_1) \sim 3H(T_1)$, where $T_1 \sim 1$ GeV [89]. Below $T_1 \sim 1$ GeV the oscillating axion field evolves as CDM. This can be seen as follows: The energy density of a scalar field is $\rho = \dot\varphi^2/2 + V(\varphi)$ and the pressure is $p = \dot\varphi^2/2 - V(\varphi)$. For time scales large compared to the period of the coherent oscillations $\tau_{\rm a} \sim m_{\rm a}^{-1} \sim 10^{-6} t_{\rm H}$ the virial theorem can be applied to give $\langle p_{\rm a}\rangle = 0$. Thus, a coherently oscillating scalar field, like the axion field below T_1, can be modeled by a pressureless fluid.

The axion field is inhomogeneous on scales larger $R_{\rm H}(T_1)$, if, as usually assumed, the reheating temperature after inflation lies above $f_{\rm PQ}$. This leads to inhomogeneities with $\delta\rho_{\rm a}/\rho_{\rm a} = \mathcal{O}(1)$ in the axion density. These inhomogeneities evolve into axion miniclusters of typical mass $M_{\rm mc} \sim 10^{-12} M_\odot$ and typical radius $R_{\rm mc} \sim 10^8$ m $\sim 0.1 R_\odot \sim 10^{-3}$ AU [90]. If the reheating temperature was below the PQ scale, the axion field at T_1 was homogeneous on superhorizon scales, apart from small, quantum-induced fluctuations of the axion field during inflation.

To summarize, the axion is a CDM candidate that is kinetically decoupled from the radiation fluid at the QCD scale.

2.3.3 Primordial black holes

A further possibility for CDM that decoupled kinetically long before the QCD transition is primordial black holes (PBH) [91, 92] produced before the QCD transition and therefore with masses $M_{\rm BH} \ll 1 M_\odot$. In order to survive until today PBH should have $M_{\rm BH} > 10^{15}$g $\approx 10^{-18} M_\odot$. PBH in the range from $10^{-18} M_\odot$ to $10^{-16} M_\odot$ would radiate too strongly to be compatible with γ-ray observations [70]. The production of PBHs arises naturally from hybrid inflationary scenarios [93, 94].

When these black holes are formed they are comoving with the radiation fluid, but their velocity is redshifted and soon becomes completely negligible. PBH should not overclose the Universe, thus just a tiny fraction of energy in a comoving volume is allowed to collapse to black holes. This fraction is given by $f \sim a_{\rm PBH}/a_{\rm eq}$, where $a_{\rm PBH}$ is the scale factor at PBH formation and $a_{\rm eq}$ at matter-radiation equality. Their density at the QCD epoch is

$$n_{\rm PBH}(T_\star) \sim 10^{-8} \left(\frac{150\ {\rm MeV}}{T_\star}\right) \left(\frac{T_{\rm PBH}}{T_\star}\right)^2 \frac{1}{R_{\rm H}^3} \tag{2.21}$$

at most, where $T_{\rm PBH}$ is the temperature at which PBH form with mass

$$m_{\rm PBH} \sim \left(\frac{T_\star}{T_{\rm PBH}}\right)^2 M_\odot\ . \tag{2.22}$$

In every Hubble volume PBH make up a pressureless gas if $n_{\rm PBH}(T_\star) \gg 1/R_{\rm H}^3$, thus $T_{\rm PBH} > 10^4 T_\star \sim 1$ TeV. This corresponds to PBH with $m_{\rm PBH} < 10^{-8} M_\odot$. PBH smaller than this mass are a kinetically decoupled fluid at the QCD horizon scale.

Chapter 3

A first-order QCD transition

In a first-order QCD transition the quark-gluon plasma supercools before the first bubbles of hadron gas are formed. In a homogeneous Universe without 'dirt' the bubbles nucleate due to thermal fluctuations (homogeneous nucleation). This scenario is discussed in section 3.1. The mean nucleation distance depends on various unknown quantities such as the latent heat and the surface tension.

If cosmic 'dirt' in the form of defects (like strings) or black holes is present at the QCD epoch, this 'dirt' may trigger the formation of the first hadronic bubbles (like the nucleation of vapor bubbles in a pot of boiling water). This heterogeneous nucleation scenario is discussed in section 3.2. The mean nucleation distance now depends on the mean 'dirt' separation scale additionally to the parameters of homogeneous nucleation.

There is a broad range in parameter space, where the magnitude of primordial temperature fluctuations is of the same order or larger than the typical supercooling in the homogeneous nucleation scenario. In this case, which I call inhomogeneous nucleation, the mean nucleation distance results from the scale and amplitude of the temperature fluctuations (section 3.3).

3.1 Homogeneous bubble nucleation

The probability to nucleate a bubble by a thermal fluctuation is proportional to $\exp(\Delta S)$, where ΔS is the change in entropy by creating a hadronic bubble. The second law relates ΔS to the minimal work done in this process, which is the change in the free energy because the volume and temperature are fixed [95]. The change in free energy of the system by creating a spherical bubble with radius R is

$$\Delta F = \frac{4\pi}{3}(p_{\mathrm{QGP}} - p_{\mathrm{HG}})R^3 + 4\pi\sigma R^2 \ , \tag{3.1}$$

where σ is the surface tension. Bubbles can grow if they are created with radii greater than the critical bubble radius $R_{\rm crit}$. Smaller bubbles disappear again, because the free energy gained from the bulk of the bubble is more than compensated by the surface energy in the bubble wall. $R_{\rm crit}$ is determined from the maximum value of $\Delta F(R)$, it reads

$$R_{\rm crit}(T) = \frac{2\sigma}{p_{\rm HG}(T) - p_{\rm QGP}(T)} \ . \tag{3.2}$$

At $T_\star$ the critical bubble size diverges, and no bubble can be formed. Finally, the probability to form a hadronic bubble with critical radius per unit volume and unit time is given by

$$I(T) = I_0(T) \exp\left(-\frac{\Delta F_{\rm crit}}{T}\right) \ , \tag{3.3}$$

with $\Delta F_{\rm crit} = 16\pi\sigma^3/[3(p_{\rm HG} - p_{\rm QGP})^2]$. For dimensional reasons the prefactor $I_0 \sim C T_\star^4$; $C = \mathcal{O}(1)$. A more detailed calculation of I_0 within the bag model has been provided in [96]. It was shown in Ref. [13] that the temperature dependence of the prefactor I_0 can be neglected for the calculation of the supercooling temperature $T_{\rm sc}$ in the cosmological QCD transition. I will show below that the numerical prefactor C is irrelevant in the cosmological QCD transition.

For small supercooling $\Delta \equiv 1 - T/T_\star \ll 1$ we may evaluate $(p_{\rm HG} - p_{\rm QGP})(T)$ by using the second law of thermodynamics, i.e. $p_{\rm HG} - p_{\rm QGP} \approx l\Delta$, and thus

$$I(\Delta) \approx I_0(T_\star) \exp\left(-A/\Delta^2\right) , \tag{3.4}$$

with $A \equiv 16\pi\sigma^3/(3l^2T_\star)$ and $I_0(T_\star) \approx T_\star^4$. Note that this result does not depend on the details of the QCD equation of state. For the values of $l = 1.4T_\star^4$ and $\sigma = 0.015T_\star^3$ from quenched lattice QCD [10] $A \approx 3 \times 10^{-5}$. In the bag model $A \approx 8 \times 10^{-2}(\sigma/T_\star^3)^3$.

The amount of supercooling that is necessary to complete the transition, $\Delta_{\rm sc}$, can be estimated from the schematic case of one single bubble nucleated per Hubble volume per Hubble time, which is

$$\mathcal{O}(\Delta_{\rm sc}) = \left[\frac{A}{4\ln(T_\star/H_\star)}\right]^{1/2} \approx 4 \times 10^{-4} \tag{3.5}$$

for the values of l and σ from quenched lattice QCD [10]. For the bag model I assume $\sigma < 0.1T_\star^3$, which implies that $\Delta_{\rm sc} < 10^{-3}$. It has been shown in [12] that for such a tiny supercooling the formation of detonation bubbles is forbidden. This justifies the approximation of small supercooling made above.

The time lapse during the supercooling period follows from the conservation of entropy and reads

$$\Delta t_{\rm sc}/t_{\rm H} = \Delta_{\rm sc}/(3c_s^2) = \mathcal{O}(10^{-3}) \ . \tag{3.6}$$

Here we used the relation $c_s^2 = {\rm d}\ln s/{\rm d}\ln T$ for the sound speed in the supercooled phase. For realistic models $0 < c_s(\Delta) < 1/\sqrt{3}$. In the bag model $c_s(\Delta) = 1/\sqrt{3}$.

The critical size of the bubbles created at the supercooling temperature is

$$R_{\rm crit}(\Delta_{\rm sc}) \approx \frac{2\sigma}{l\Delta_{\rm sc}} \approx 30 \ {\rm fm} \ . \tag{3.7}$$

The critical radius is large compared to the QCD scale, and this justifies the thin wall approximation, which was made implicitly above.

After the first bubbles have been nucleated, they grow most probably by weak deflagration [4, 8, 9, 12]. The deflagration front (the bubble wall) moves with the velocity $v_{\rm defl} \ll 1/\sqrt{3}$ [97]. The energy that is released from the bubbles is distributed into the surrounding QGP by a supersonic shock wave and by neutrino radiation. This reheats the QGP to $T_\star$ and prohibits further bubble formation. Since the amplitude of the shock is very small [8], on scales smaller than the neutrino mean free path heat transport by neutrinos is most efficient. Neutrinos have a mean free path of $10^{-7}R_{\rm H}$ at $T_\star$. When they do most of the heat transport, heat goes with $v_{\rm heat} = \mathcal{O}(c)$. For larger scales heat transport is much slower. Figure 3.1 shows a sketch of the homogeneous bubble nucleation scenario.

Let us now calculate the mean bubble separation, $d_{\rm nuc}$, and the final supercooling, $\Delta_{\rm sc}$, for a scenario with weak deflagration. Bubbles present at a given time have been nucleated typically during the preceding time interval

$$\Delta t_{\rm nuc} \equiv I/({\rm d}I/{\rm d}t) \ . \tag{3.8}$$

Using the relation between time and supercooling, ${\rm d}\Delta/{\rm d}t = 3c_s^2/t_{\rm H}$, we find

$$\Delta t_{\rm nuc}/t_{\rm H} = \Delta^3/(6Ac_s^2) = \mathcal{O}(10^{-5}) \tag{3.9}$$

and

$$\Delta_{\rm nuc} = \frac{\Delta t_{\rm nuc}}{\Delta t_{\rm sc}}\Delta_{\rm sc} = \mathcal{O}(10^{-2})\Delta_{\rm sc} \ . \tag{3.10}$$

During the time interval $\Delta t_{\rm nbucl}$ each bubble has distributed released latent heat over a distance $\approx \Delta 2 v_{\rm heat} t_{\rm nuc}$. This distance has a weak dependence on the precise value of $\Delta_{\rm sc}$, but the bubble nucleation rate increases exceedingly strongly with Δ until one bubble per volume $\sim (\Delta t_{\rm nuc} v_{\rm heat})^3$ is nucleated. Therefore the mean bubble separation is

$$d_{\rm nuc} \approx 2 v_{\rm heat}\Delta t_{\rm nuc} \approx \frac{v_{\rm heat}}{3c_s^2}\frac{\Delta_{\rm sc}^3}{A}R_{\rm H} = \mathcal{O}(10^{-6}R_{\rm H}) = \mathcal{O}(1{\rm cm}), \tag{3.11}$$

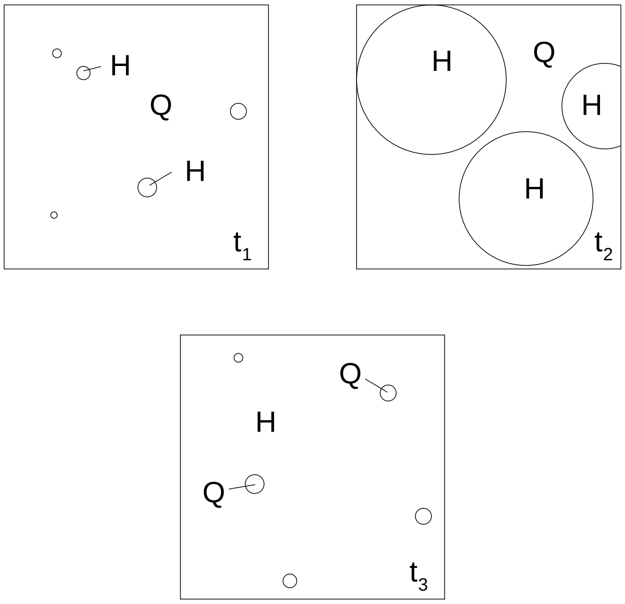

Figure 3.1: Sketch of a first-order QCD transition via homogeneous bubble nucleation: Above the critical temperature the Universe is filled with a quark-gluon plasma (Q). After a small amount of supercooling the first hadronic bubbles (H) nucleate with mean separation $d_{\rm nuc}$ at t_1. At $t_2 > t_1$ these bubbles have grown and have released enough latent heat to quench the formation of new bubbles. The supercooling, bubble nucleation, and quenching takes just 1% of the full transition time. In the remaining 99% of the transition time the bubbles grow due to the adiabatic expansion of the Universe. At t_3 the transition is almost finished. The shrinking QGP drops are separated by the typical distance $d_{\rm nuc}$.

where I used $v_{\rm heat} = \mathcal{O}(0.1), 3c_s^2 = \mathcal{O}(0.1)$, which gives a typical value for the nucleation distance. The suppression of bubble nucleation due to already existing bubbles is neglected.

The estimate (3.11) of the mean bubble separation applies if the released latent heat by means of sound waves and by neutrino free streaming is sufficient to reheat the QGP to $T_\star$, i.e. to quench the nucleation of new bubbles. On the other hand the typical bubble separation could be given by the rate of release of latent heat, i.e. by the bubble wall velocity $v_{\rm defl}$. Since the period of supercooling lasts about 1% of the time needed for completing the entire first-order phase transition, 1% of the QGP must be converted to HG in the process of sudden reheating to $T_\star$, hence the bubble radius at quenching must reach 0.2 of the bubble separation, $R_{\rm bubble} \approx 0.2 d_{\rm nuc}$. With $R_{\rm bubble} \approx v_{\rm defl}\Delta t_{\rm nuc}$ and using the above relation $d_{\rm nuc} \approx 2 v_{\rm heat} \Delta t_{\rm nuc}$, we require $v_{\rm defl} \geq 0.4 v_{\rm heat}$ for consistency. If $v_{\rm defl}$ is smaller than this, the limiting factor for quenching is the rate of release of latent heat by bubble growth, and the bubble separation is

$$d_{\rm nuc} \approx 2 v_{\rm defl} \Delta t_{\rm nuc} \approx \frac{v_{\rm defl}}{3c_s^2} \frac{\Delta_{\rm sc}^3}{A} R_{\rm H} \ , \tag{3.12}$$

i.e. the bubble separation will be smaller than the estimate Eq. (3.11).

We are now in a position to improve the estimate of $\Delta_{\rm sc}$: One bubble nucleates in the volume $(v_{\rm heat}\Delta t_{\rm nuc})^3$ during $\Delta t_{\rm nuc}$. This can be written as

$$1 \approx (v_{\rm heat}\Delta t_{\rm nuc})^3 \Delta t_{\rm nuc} I(t_{\rm sc}) \ , \tag{3.13}$$

which in terms of the supercooling parameter $\Delta_{\rm sc}$ is given by:

$$\begin{aligned} 1 &\approx \frac{v_{\rm heat}^3}{(3c_s^2 A)^4} \left(\frac{T_\star}{H_\star}\right)^4 \Delta_{\rm sc}^{12} \exp\left(\frac{-A}{\Delta_{\rm sc}^2}\right) \\ &\approx 10^{94} \Delta_{\rm sc}^{12} \exp\left(\frac{-2.89 \times 10^{-5}}{\Delta_{\rm sc}^2}\right) \ . \end{aligned} \tag{3.14}$$

Also the pre-exponential factor is smaller by a factor of 10^{20} compared to the naive estimate (3.5), the amount of supercooling is just 20% larger than in (3.5), i.e. $\Delta_{\rm sc} = 5 \times 10^{-4}$. This also demonstrates that numerical prefactors in (3.13) are irrelevant for the calculation of $\Delta_{\rm sc}$.

To summarize, the scales on which non-equilibrium phenomena occur are given by the mean bubble separation, which is about $10^{-6} R_{\rm H}$. The entropy production is tiny, i.e. $\Delta S/S \sim 10^{-6}$, since the supercooling is small $\sim 10^{-3}$. After supercooling, which lasts $10^{-3} t_{\rm H}$, the Universe reheats in $\Delta t_{\rm nuc} \approx 10^{-6} t_{\rm H}$. After reheating the thermodynamic variables follow their equilibrium values and bubbles grow due to the expansion of the Universe only.

3.2 Heterogeneous bubble nucleation

In first-order phase transitions that we know from our everyday experience, an example is the condensation of water drops in clouds, bubbles resp. drops are nucleated at impurities ('dirt'). This could happen in the early Universe as well. Candidates for cosmic 'dirt' are primordial black holes, monopoles, strings, and other kinds of defects. Of course, the existence of any of these objects has not been verified so far. Nevertheless, let me discuss in what manner cosmic 'dirt' would change the nucleation of bubbles. The following considerations are based on the work of Christiansen and Madsen [13].

Let n be the number density of the impurities. Further assume that at time $t_{\rm i}$ with $t_\star \leq t_{\rm i} < t_{\rm sc}$ bubbles nucleate at the locations of the impurities.

(It is easy to see that $t_{\rm i}$ is restricted to the mentioned interval: Before $t_\star$ a bubble cannot grow because $T > T_\star$, after $t_{\rm sc}$ homogeneous nucleation already happened.)

There are two limiting cases: If $n \gg d_{\rm nuc,\ hom}^{-3}$, the mean nucleation distance is $d_{\rm nuc} = n^{-1/3} \ll d_{\rm nuc,\ hom}$. If $n \ll d_{\rm nuc,\ hom}^{-3}$, the impurities are so rare that $d_{\rm nuc} = d_{\rm nuc,\ hom}$.

The most interesting situation occurs when the typical distance between the impurities is something bigger than the mean homogeneous nucleation distance. But it should be small enough such that the bubbles nucleated at the impurities can reheat the Universe just before homogeneous nucleation starts. For a quantitative estimate let me determine the amount of supercooling for heterogeneous nucleation. As in homogeneous nucleation [see Eq. (3.13)] I use the condition that one bubble is nucleated per reheated volume, i.e. the sum of the probabilities to form a bubble from an impurity and to form the bubble from a thermal fluctuation:

$$1 \approx n(v_{\rm heat}\Delta t)^3 + (v_{\rm heat}\Delta t_{\rm nuc})^3 \Delta t_{\rm nuc} I(t_{\rm sc}) \ . \tag{3.15}$$

$\Delta_{\rm i} = t_{\rm sc} - t_{\rm i}$ is the growth time of bubbles from impurities and $\Delta t_{\rm nuc}$ the growth time of bubbles from thermal fluctuations, as defined in (3.8). Note that here $t_{\rm sc}$ may be smaller than in homogeneous nucleation. If $\Delta t/\Delta t_{\rm nuc}$ is of order unity both mechanisms work independently and

$$d_{\rm nuc} \approx \frac{1}{(n + \Delta t_{\rm nuc} I(t_{\rm sc}))^{1/3}} \leq d_{\rm nuc,\ hom} \ . \tag{3.16}$$

The most interesting situation arises when $\Delta t/\Delta t_{\rm nuc} \gg 1$. This means that the probability for a bubble from a thermal fluctuation is reduced because the available volume for thermal fluctuations in the QGP has been reduced by a factor of $(1 - n(v_{\rm heat}\Delta t)^3)$. This factor should be taken into account in (3.15) which now reads

$$1 \approx n(v_{\rm heat}\Delta t)^3 + (v_{\rm heat}\Delta t_{\rm nuc})^3 \Delta t_{\rm nuc} I(t_{\rm sc})[1 - n(v_{\rm heat}\Delta t)^3] \ . \tag{3.17}$$

The unique solution to this equation is $n(v_{\rm heat}\Delta t)^3 \approx 1$ and thus

$$d_{\rm nuc} \approx \frac{1}{\{n + \Delta t_{\rm nuc} I(t_{\rm sc})[1 - n(v_{\rm heat}\Delta t)^3]\}^{1/3}} \approx n^{-1/3} \ . \tag{3.18}$$

The maximal mean nucleation distance from heterogeneous nucleation is found from $\Delta t \leq \Delta t_{\rm sc,\ het}$ to be

$$\max(d_{\rm nuc}) \approx v_{\rm heat} \max(\Delta t_{\rm sc,\ het}) \approx v_{\rm heat}\Delta t_{\rm sc,\ hom} \approx 10^{-3} R_{\rm H} = \mathcal{O}(10\ {\rm m}) \ . \tag{3.19}$$

For a narrow range in parameter space, namely $n(v_{\rm heat}\Delta t)^3 \approx 1$, nucleation distances may be by a factor of 100 larger than in homogeneous nucleation. That means that n should be $n \sim 10^9/R_{\rm H}^3$.

As an example for 'dirt' I consider primordial black holes (PBH): PBHs with the appropriate density, $n_{\rm PBH}(T_\star) \sim 10^9/R_{\rm H}^3$, are produced at the temperature $T_{\rm PBH} \sim 10^7$ GeV [see Eq. (2.21)] with a mass of $m_{\rm PBH} \sim 10^{-16} M_\odot$. PBHs of this mass are excluded observationally because they start to evaporate now and should be observed as γ-sources [70]. Thus PBHs cannot be considered as seeds which yield the maximum nucleation distance. Nevertheless, larger PBH masses still may seed bubbles, but their mean separation is so large that thermal bubble nucleations cannot be suppressed.

3.3 Bubble nucleation in the inhomogeneous Universe

The ideas presented in this section are based on recent work of Ignatius and Schwarz [14].

The local temperature $T(t, \mathbf{x})$ of the radiation fluid fluctuates, because cosmological perturbations have been generated during inflation [57]. Let me denote the temperature fluctuation by $\Delta_T \equiv \delta T/T$. Inflation predicts a Gaussian distribution of perturbations,

$$P(\Delta_T)\mathrm{d}\Delta_T = \frac{1}{\sqrt{2\pi}\Delta_T^{\rm rms}} \exp\left(-\frac{1}{2}\frac{\Delta_T^2}{(\Delta_T^{\rm rms})^2}\right) \mathrm{d}\Delta_T \ . \tag{3.20}$$

If one allows for a tilt in the power spectrum of density fluctuations, the COBE [60] normalized rms temperature fluctuation reads

$$\Delta_T^{\rm rms} \approx 10^{-5}\left(\frac{k}{k_0}\right)^{(n-1)/2} , \tag{3.21}$$

where k_0 is the wavenumber of the mode that crosses the Hubble radius today. The case $n = 1$ gives the Harrison-Zel'dovich spectrum [61]. For $k = (aH)_{\rm QCD}$ even a moderate tilt of $n - 1 = 0.2$ gives $\Delta_T^{\rm rms}(k_{\rm QCD}) \approx 10^{-4}$.

From the above we conclude that $\Delta_T^{\rm rms}$ and $\Delta_{\rm nuc}$ [see Eq. (3.10)] may be of the same magnitude or $\Delta_T^{\rm rms}$ may even be larger. The picture of homogeneous bubble nucleation, bubbles form due to statistical fluctuations, is false for the most probable cosmological scenarios.

We thus developed a new scenario for the cosmological QCD transition [14]. To do that we have to learn more about the primordial temperature fluctuations first. A small scale cut-off in the spectrum of primordial temperature fluctuations comes from collisional damping by neutrinos [62, 24] (see

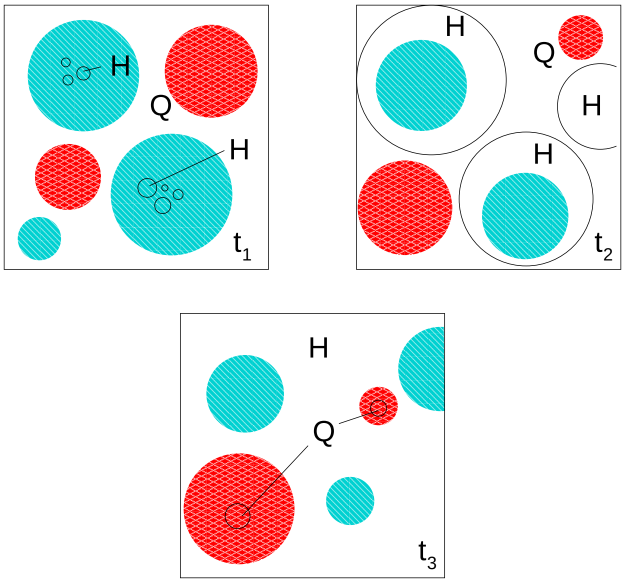

Figure 3.2: Sketch of a first-order QCD transition in the inhomogeneous Universe: At t_1 the coldest spots (dark grey) are cold enough to render the nucleation of hadronic bubbles (H) possible, while most of the Universe remains in the quark-gluon phase (Q). At $t_2 > t_1$ the bubbles from the cold spots have merged and have grown to bubbles as large as the fluctuation scale. Only the hot spots (light grey) are still in the QGP phase. At t_3 the transition is almost finished. The last QGP drops are found in the hottest spots of the Universe. The mean separation of these hot spots can be much bigger than the homogeneous bubble nucleation separation.

also section 5.3). Because the neutrinos interact only weakly, their mean free path is large compared to the strong and electro-magnetic interacting particles. The interaction rate of neutrinos is $\Gamma \sim G_{\rm F}^2 T^5$. This has to be compared with the frequency $c_s k_{\rm phys}$. We find that at the QCD transition neutrinos travel freely on scales $\lambda_{\rm phys}^{\nu-{\rm dec}} \approx 10^{-6} R_{\rm H}$. Fluctuations on the diffusion scale of neutrinos are washed out by the time of the QCD transition,

$$\lambda_{\rm phys}^{\nu-{\rm diff}} = \frac{1}{3}\sqrt{\lambda_{\rm phys}^{\nu-{\rm dec}} c t_{\rm H}} \approx 10^{-4} R_{\rm H} \ . \tag{3.22}$$

Thus the old picture of homogeneous bubble nucleation still applies within the small homogeneous patches of $\lambda_{\rm smooth} = 10^{-4} R_{\rm H}$.

The compression time scale for a homogeneous patch is $\delta t = \lambda_{\rm smooth}/c_s \sim 10^{-3} t_{\rm H}$. If the compression time scale is larger than $\Delta t_{\rm nuc}$ the temperature fluctuations are frozen with respect to the time scale of nucleations.

A sketch of inhomogeneous bubble nucleation is shown in Fig. 3.2. The basic idea is that temperature inhomogeneities determine the location of bubble nucleation. In cold regions bubbles nucleate first. There are three cases which we have to investigate separately:

(i) $\Delta_{\rm nuc} \gg \Delta_T^{\rm rms}$: The temperature inhomogeneities are negligible and the phase transition proceeds via homogeneous nucleation (see section 3.1).

(ii) $\Delta_{\rm sc} > 2\Delta_T^{\rm rms} > \Delta_{\rm nuc}$: The quenched lattice QCD data for latent heat and surface tension and the assumption of a Harrison-Zel'dovich spectrum provide the values: $\Delta_{\rm sc} \sim 10^{-4}, \Delta_T^{\rm rms} \sim 10^{-5}, \Delta_{\rm nuc} \sim 10^{-6}$. Thus it is very likely that the cosmological QCD transition belongs to this case.

(iii) $\Delta_T^{\rm rms} \gg \Delta_{\rm sc}$: This situation could be realized if it turns out that the primeval spectrum has a positive tilt and/or if quenched lattice QCD overestimates the quantity A in Eq. (3.4).

Let me start with the analysis of case (iii): As soon as any cold spot has a local temperature $T_{\rm f}$ hadronic bubbles will nucleate. However the temperature fluctuations are so large that the next compression phase will heat up the hadronic bubbles well above $T_{\rm c}$ and the bubbles disappear again. As the Universe is cooling, the smallest density fluctuations (I call them 1σ events) are the first ones for which the compression phase does not reheat the hadronic bubbles above T_c. Therefore these 1σ fluctuations set the scale of the nucleation distance. Within each volume $V_{\rm smooth} \sim (4\pi/3)\lambda_{\rm smooth}^3$ bubbles nucleate according to the homogeneous nucleation mechanism. In the limit of tiny supercooling many bubbles nucleate in each 1σ cold spot. These bubbles quickly merge to make up one bubble of typical radius $\lambda_{\rm smooth}$. The average distance between 1σ events is $\approx 2.4\lambda_{\rm smooth}$. Thus the effective nucleation distance is

$$d_{\rm nuc} \approx 2.4\lambda_{\rm smooth} \sim 10^{-3} R_{\rm H} = \mathcal{O}(10 \text{ m}) \ . \tag{3.23}$$

The space in between the 1σ cold spots remains in the QGP phase.

Let me estimate the duration of the inhomogeneous nucleation: The number of bubble nucleations in any 1σ cold spot is $N = V_{\rm smooth}/(2v_{\rm heat}\Delta t_{\rm nuc})^3$. Thus the volume filled by the new phase after the growth time $\Delta t_{\rm gr}$ from a single cold spot is

$$V_{\text{new phase}} = N(2v_{\rm def}\Delta t_{\rm gr})^3 = \left(\frac{v_{\rm def}\Delta t_{\rm gr}}{v_{\rm heat}\Delta t_{\rm nuc}}\right)^3 V_{\rm smooth} \ . \tag{3.24}$$

The cold spot is filled up by the new phase when $\Delta t_{\rm gr} = (v_{\rm heat}/v_{\rm def})\Delta t_{\rm nuc}$. Because $\Delta t_{\rm nuc} \ll \delta t$, the whole cold-spot volume is in the new phase long before the compression wave decelerates bubble growth.

Comparing the released latent heat per 1σ cold spot to the energy difference from the temperature fluctuation $\Delta_T^{\rm rms}$ we find $l/(T^3\Delta_T^{\rm rms}) \gg 1$, for $l \sim T_{\rm c}^4$. Thus the released latent heat may reheat the remaining QGP such that new bubble nucleations are quenched. Within one compression period the latent heat is distributed in the volume fraction

$$\frac{V_{\rm heat}(\Delta t_T)}{V_{\rm H}} \sim 0.3 \left(\frac{\Delta t_T}{\Delta t_{\rm nuc}}\right)^3 \frac{V_{\rm smooth}}{V_{\rm H}} \ . \tag{3.25}$$

The factor 0.3 is the volume fraction with $\Delta_T \in (-\Delta_T^{\rm rms}, 0)$, i.e. the 1σ cold spots where nucleation takes place. When the fraction (3.25) is of order unity, all regions with $T < T_{\rm c}$ are converted into the HG phase by the growth of the bubbles from the cold spots. In this situation the mean separation of relics from bubble nucleation will be close to the maximum value $2.4\lambda_{\rm smooth}$. This is indeed the case if one inserts the values from quenched lattice QCD for the latent heat and the surface tension. This completes the proof of Eq. (3.23).

In the limit of vanishing supercooling the nucleation distance for case (iii) is much larger than the distance scale from homogeneous nucleation. In contrast to homogeneous nucleation in inhomogeneous nucleation the mean separation between the first nucleations is not necessarily the mean separation for the inhomogeneity scale for the last QGP drops. However the mean nucleation distance sets a strict upper limit for the baryon number fluctuation distance.

Let me now turn to case (ii): Now the 1σ temperature fluctuations do no longer destroy the new phase once it has been nucleated because $2\Delta_T^{\rm rms} < \Delta_{\rm sc}$. However $N\sigma$ fluctuations may be large enough so that $2N\Delta_T^{\rm rms} > \Delta_{\rm sc}$. This gives $N_{\rm max} = \Delta_{\rm sc}/2\Delta_T^{\rm rms}$.

Assume that bubbles nucleate in a $N\sigma$ cold spot ($N \leq N_{\rm max}$) at $T = T_f$. Let $\Delta t_{\rm heat}$ be the time heat fronts from neighboring bubbles need to meet. We now have to ask: does the average temperature $\bar{T}$ drop in $\Delta t_{\rm heat}$ by more than $\Delta_T^{\rm rms}$. If yes, bubbles would nucleate from $(N-1)\sigma$ cold spots before the transition could be completed by the bubbles from the $N\sigma$ cold spots. In that case consider $(N-1)\sigma$ events. If no, N is known (having started at $N = N_{\rm max}$). The mean separation between two $N\sigma$ cold spots is given by

$$d_N \approx 1.6\lambda_{\rm smooth} f(N)^{-\frac{1}{3}} \ , \tag{3.26}$$

where the probability that a cold spot has a temperature below $\bar{T}(1-N\Delta_T^{\rm rms})$ reads

$$f(N) = \int_{-\infty}^{-N\Delta_T^{\rm rms}} P(\Delta_T) {\rm d}\Delta_T \ . \tag{3.27}$$

The heating time is given by $\Delta t_{\rm heat}(N) \sim d_N/(2v_{\rm heat})$. During that time the drop of the mean temperature is $|\Delta T/\bar{T}| = 3c_s^2\Delta t_{\rm heat}(N)/t_{\rm H}$, which should be smaller than $\Delta_T^{\rm rms}$. Thus N follows from

$$\frac{3c_s^2}{2v_{\rm heat}}\frac{1.6\lambda_{\rm smooth}}{R_{\rm H}}f(N)^{-\frac{1}{3}} \le \Delta_T \ , \tag{3.28}$$

which gives for the correct N, denoted by N_*

$$f(N_*) = \left(\frac{3c_s^2}{2v_{\rm heat}}\frac{1.6\lambda_{\rm smooth}}{R_{\rm H}}\frac{1}{\Delta_T^{\rm rms}}\right)^3 \approx \left(\frac{3c_s^2}{v_{\rm heat}}\frac{10^{-4}}{\Delta_T^{\rm rms}}\right)^3 \ . \tag{3.29}$$

The maximum of f is given for $N_* = 0$, $f(0) = 0.5$. This gives the consistency condition $\Delta_T^{\rm rms} \ge (3c_s^2/v_{\rm heat})10^{-4}$. If I assume that $3c_s^2/v_{\rm heat} = \mathcal{O}(1)$, $\Delta_T^{\rm rms} \ge 10^{-4}$. For large rms fluctuations the rare events dominate: E.g. for $\Delta_T^{\rm rms} \approx 10^{-3}$ the 3σ events set the nucleation scale, provided $N_* < N_{\rm max}$. Putting everything together one finds that

$$d_{\rm nuc} \sim 1.6\lambda_{\rm smooth} f(N_*)^{-\frac{1}{3}} \sim \frac{v_{\rm heat}}{3c_s^2}2\Delta_T^{\rm rms}R_{\rm H} \ . \tag{3.30}$$

For the latent heat and surface tension from quenched lattice QCD and for the COBE normalized spectrum with the measured tilt from COBE the nucleation distance is $d_{\rm nuc} \approx 2\times 10^{-4}R_{\rm H} = \mathcal{O}(2\ {\rm m})$, which is a factor of 10 bigger than the nucleation distance in the homogeneous nucleation scenario.

Chapter 4

Isothermal baryon fluctuations

The nucleation of bubbles in a first-order QCD transition may affect the distribution of baryons in the Universe strongly [5, 6]. Isothermal baryon number fluctuations are created at the end of the QCD phase transition (see Sec. 4.1). These fluctuations are smoothened by baryon diffusion after the QCD transition (Sec. 4.2). As the temperature of the Universe drops below 1 MeV neutrons and protons decouple chemically (freeze-out). The mean free path of the neutrons exceeds the proton mean free path and thus protons and neutrons segregate. I.e., regions of high baryon density become proton-enriched and regions of low baryon density become neutron-enriched. This affects the local nucleosynthesis yields, giving rise to inhomogeneous big bang nucleosynthesis (IBBN) [15] (in contrast to homogeneous BBN [18]), which is sketched in section 4.3.

4.1 Baryon inhomogeneities

Isothermal fluctuations of baryon number are an inevitable consequence of any first-order QCD transition in the early Universe. After the tiny period of supercooling, bubble nucleation, and reheating, the HG bubbles grow adiabatically and merge (perlocate). For tiny supercooling the perlocation happens very close to equilibrium, because this process is extremely slow compared to the QCD time scale. Just before the transition is completed the Universe is filled with a phase of HG in which shrinking drops of QGP are embedded. Usually these drops are assumed to be spheres, which is the case if the surface tension is reasonably large. The typical distance between QGP drops is given by the typical bubble nucleation distance d_{nuc}. The bulk properties of growing HG bubbles and shrinking QGP drops (except for the very last moments before the drops evaporate) are governed by the hydrodynamic equations for the radiation fluid only, i.e. the baryons do not influence the bulk properties. The hydrodynamics of growing HG bubbles and decaying QGP drops has been studied in detail in Refs. [8, 9, 98]. Without baryons no relics remain from the bubble scale today, thus let me concentrate on the role of baryons during a first-order QCD transition.

Let me assume for a while that chemical and thermal equilibrium is maintained from the formation of the QGP drops until the completion of the phase transition (evaporation of the last QGP drops). In chemical equilibrium baryon number prefers to reside in the QGP because the deconfined quarks are almost massless. The ratio κ of the baryon number density in both phases is a constant for chemical equilibrium, given by

$$\begin{aligned} \kappa &\equiv \frac{n_{\mathrm{B}}^{\mathrm{QGP}}}{n_{\mathrm{B}}^{\mathrm{HG}}} \qquad (4.1)\\ &\approx \frac{N_f}{9}\left(\frac{\pi}{2}\right)^{\frac{3}{2}}\left(\frac{m_{\mathrm{p}}}{T_\star}\right)^{-\frac{3}{2}}\exp\left(\frac{m_{\mathrm{p}}}{T_\star}\right) \qquad (4.2)\\ &\approx 15 \qquad \text{for } T_\star = 150 \text{ MeV}\ , \end{aligned}$$

evaluated for the bag model with $N_f = 2$. The mean baryon number density is given by

$$n_{\mathrm{B}} = (1-f)n_{\mathrm{B}}^{\mathrm{QGP}} + f n_{\mathrm{B}}^{\mathrm{HG}}\ , \qquad (4.3)$$

where f is the volume fraction filled by the HG. f rises from 0 to 1 during the transition. After reheating $f \sim 10^{-3}$. At perlocation $f \sim 0.7$ (for spherical bubbles with a single radius) [99]. The baryon number $N_{\mathrm{B}} = n_{\mathrm{B}}V$ is conserved in the comoving volume V. From the equations (4.1) and (4.3) one finds that both $n_{\mathrm{B}}^{\mathrm{QGP}}/n_{\mathrm{B}}$ and $n_{\mathrm{B}}^{\mathrm{HG}}/n_{\mathrm{B}}$ grow during the transition:

$$\begin{aligned} n_{\mathrm{B}}^{\mathrm{QGP}} &= \frac{n_{\mathrm{B}}}{f/\kappa + (1-f)} \qquad (4.4)\\ n_{\mathrm{B}}^{\mathrm{HG}} &= \frac{n_{\mathrm{B}}}{f + (1-f)\kappa}\ . \qquad (4.5) \end{aligned}$$

The maximum values are reached for $f \approx 1$, where $n_{\mathrm{B}}^{\mathrm{QGP}}/n_{\mathrm{B}} \approx \kappa = \mathcal{O}(10)$ and $n_{\mathrm{B}}^{\mathrm{HG}}/n_{\mathrm{B}} \approx 1$. Of course, if equilibrium was maintained throughout the transition, no baryon inhomogeneity would arise from the preference of baryons to reside in the QGP. If baryons drop out of equilibrium before the transition is completed, baryon inhomogeneities are produced necessarily.

There are three mechanisms that drive the baryons out of chemical equilibrium:

- The baryon flux through the surface of the QGP drop might be suppressed. This was elaborated in Refs. [6, 11, 50]. Any suppression of the baryon flux results in a deviation from chemical equilibrium. Since the net flow of baryons is directed from inside the QGP drops to the HG, flux suppression increases the value of κ and baryon number fluctuations are generated.

However, we do not know the physics of the phase interface so far. Thus it is unclear how large this flux suppression might be. The simplest model is based on phase-space arguments [11]. A more sophisticated model attaches chromoelectric flux tubes to the surface at the points where a quark penetrates the interface. These flux tubes then break up and produce mainly pions, and rarely nucleons or heavier baryons [50]. Both models give a large suppression of baryon number flux. However, in both models it is assumed that no bound states or cluster states exist in the QGP near the critical temperature. If, e.g., a significant fraction of quarks in the QGP would form diquarks near the critical temperature, the arguments for flux suppression would break down [53].

Our ignorance about the physics of the phase interface has been encoded in the so-called filter factor F [11], which is any number between 0 and 1 and gives the probability that a baryon penetrates the interface. The flux suppression is strongest and most simple to analyze when $F = 0$, which means that all baryon number is trapped into the QGP phase. In such a situation the only relevant quantity is the typical nucleation distance. Any QGP drop contains a baryon number of about $N_{\mathrm{B}} = n_{\mathrm{B}} d_{\mathrm{nuc}}^3$, which gives $\sim 10^{30}(10^{36})$ baryons per QGP drop for $d_{\mathrm{nuc}} \sim 10^{-6}(10^{-4}) R_{\mathrm{H}}$ after the annihilation of all anti-baryons in the QGP drop. The baryon density in the QGP drops reaches nuclear matter density ($\sim$ 200 MeV/fm^3) at a drop radius of 10 μm(1 mm). This demonstrates that the produced inhomogeneities may be enormous. On the other hand it is clear that the filter factor cannot vanish exactly, because all baryons would be trapped in the QGP drops (quark nuggets) by the end of the QCD transition and no nucleosynthesis could have taken place.

- Even if the baryon flux through the phase interface is large enough to maintain chemical equilibrium locally, we have to ask for the diffusion length of baryons during the evaporation of the QGP. Only if baryons diffuse over scales d_{nuc} chemical equilibrium could be maintained globally. According to Eq. (4.5) $n_{\mathrm{B}}^{\mathrm{HG}} \approx n_{\mathrm{B}}/\kappa \ll n_{\mathrm{B}}$ at the early stages of the transition and thus the regions where HG bubbles nucleate are underdense in baryon number.

  The typical collision time for baryons is $\tau_{\mathrm{b}} \sim 1/T_\star$ (collisions with πs dominate at $T_\star$). The duration of the transition is $\sim 0.1 t_{\mathrm{H}}$. Thus, baryons make $N \sim 10^{19}$ collisions during the phase transition. Their typical velocity is $v_{\mathrm{b}} \sim (T_\star/m_{\mathrm{p}})^{1/2}$ and thus they diffuse a distance of

$\lambda_{\mathrm{b-diff}} \sim \sqrt{N} v_{\mathrm{b}} \tau_{\mathrm{b}} \sim 10^{-11} R_{\mathrm{H}}$, which is much smaller than d_{nuc}. Thus baryon diffusion alone is not able to keep the mixed phase at chemical equilibrium globally.

The consequences of baryon diffusion have been studied by Kurki-Suonio [100] and have been incorporated into numerical simulations [101]. Since $R_{\mathrm{drop}} \gg \lambda_{\mathrm{b-diff}}$ initially, chemical equilibrium cannot be established globally (not even within a single phase). At the QGP side of the interface baryon number is piled up in a thin surface layer of dimension $r_{\mathrm{s}} \sim \lambda_{\mathrm{b-diff}}^2 / R_{\mathrm{drop}}$ [100]. Since locally $n_{\mathrm{B}}^{\mathrm{QGP}} = \kappa n_{\mathrm{B}}^{\mathrm{HG}}$, more baryons leak into the HG than without diffusion. The baryon density grows when the QGP drops shrink, and thus the baryon density in the HG close to the QGP drop grows as well. Due to the small diffusion length the baryons that penetrate the interface cannot be redistributed in the whole volume. In this way core-concentrated clouds of baryons are formed.

- The third mechanism is the extraction of entropy once the mean free path of any relativistic species exceeds the size of the QGP drops. First this happens for the neutrinos, $\lambda_\nu \sim 10^{-6} R_{\mathrm{H}}$, later for the charged leptons. A radiative flux is established which carries away entropy but not baryon number. In contrast the hydrodynamic flux carries away entropy as well as baryon number. Thus baryons are compressed in the QGP drop (it is the ratio n_{B}/s that is important). This mechanism has been found by Applegate and Hogan [6] and was further studied in [100, 11, 101]. It turns out that entropy extraction is most efficient for large initial drop size ($R_{\mathrm{drop}} \gg \lambda_\nu$).

All three mechanisms lead to the formation of baryon number fluctuations by the end of a first-order QCD transition. Because the baryons are tightly coupled to the radiation fluid on scales of $\mathcal{O}(d_{\mathrm{nuc}})$ the baryon fluid has the same local temperature as the radiation fluid an thus isothermal fluctuations are generated (in contrast to isentropic fluctuations).

Let me estimate the fluctuation amplitude and the fraction of baryons affected: The most extreme case happens for the observationally excluded situation $F = 0$. For small values of F we still find extremely high baryon densities and a large fraction of affected baryons. Given the large uncertainties on the value of F it is most interesting to ask, what happens if $F = 1$. Since the physics of baryon diffusion and entropy extraction are well understood, this case gives a lower limit on the fraction of baryons that is concentrated in clouds. I will focus on large nucleation distances, I take $d_{\mathrm{nuc}} \sim 10^{-4} R_{\mathrm{H}}$, because, as will be shown below, $d_{\mathrm{nuc}} \geq 1$ m is necessary in order to affect BBN.

The first substantial departure from chemical equilibrium happens when $R_{\text{drop}} \sim \lambda_\nu \sim 10^{-6} R_{\text{H}}$. For inhomogeneous bubble nucleation $d_{\text{nuc}} \sim 10^{-4} R_{\text{H}}$. The volume fraction in QGP drops at $R_{\text{drop}} \sim \lambda_\nu$ is $f_{\text{QGP}} \sim 10^{-6}$. Since at that time $\lambda_{\text{b-diff}} \ll R_{\text{drop}}$ the fraction of baryons that is piled up in an surface layer on the QGP side of the interface is negligible. This means that the fraction of baryons that is inside the QGP drops at neutrino decoupling is $\sim \kappa f_{\text{QGP}}$, according to Eq. (4.4). This shows that at most $\sim 10^{-5} N_{\text{B}}$ baryons are in core-concentrated clouds by the end of the QCD transition.

It was shown in Refs. [6, 100] that for $R_{\text{drop}} \gg \lambda_{\text{b-diff}}$ the baryon number distribution of such a cloud is given by

$$n_{\text{B}}(r) \approx \bar{n}_{\text{B}} \left[\left(\frac{R_{\text{cloud}}}{r} \right)^{\alpha} - 1 \right] , \tag{4.6}$$

where $R_{\text{cloud}} \sim \lambda_\nu$ and α is the ratio of the neutrino radiation flux and the hydrodynamic flux, i.e.

$$\alpha \equiv \frac{F_\nu}{F_{\text{hydro}}} \propto \sqrt{\frac{\Delta T}{T_\star}} \ll 1 . \tag{4.7}$$

This ratio depends on the temperature difference between the QGP drop and the surrounding HG. The temperature gradient is necessary to establish a hydrodynamic flux. The hydrodynamic flux originates from a surface layer, whereas the neutrino flux origins from the volume of the drop. When the QGP drop shrinks, the ratio α grows because ΔT has to grow to keep both phases close to $T_\star$. Within the bag model $\alpha \sim 10^{-4}$ at most. The parameters from quenched lattice QCD give $\alpha \sim 10^{-6}$. The resulting baryon distribution (4.6) is very broad and high baryon densities are reached at the center of the clouds only. The fraction of baryons in the clouds has been estimated to be $\alpha/3$ [100], which is in consistent with the estimate $\sim \kappa f_{\text{QGP}}$ from above. In general, increasing the nucleation distance reduces the fraction of baryons in high density regions.

It was shown numerically in Ref. [101] that enormous baryon densities are reached in the inner 10^4 fm of the drop. However, it is hard to have a cosmologically significant fraction of baryons residing in these inner regions if there is no baryon flux suppression. I conclude that large separations of baryon clouds and high baryon fraction within these clouds are mutually exclusive, except for significant baryon flux suppression.

4.2 Baryon diffusion

The isothermal baryon number fluctuations formed at the end of a first-order QCD transition are smoothened by two mechanisms, baryon diffusion

[102, 103, 16] and neutrino inflation [6, 104, 105]. The latter is important for baryon clouds with high $\eta \equiv n_{\rm B}/n_\gamma > 10^{-4}$. These baryon clouds are in pressure equilibrium with the regions of lower baryon density. Thus the temperature of a baryon could is below the mean temperature, because the baryons give an additional contribution to the pressure besides the radiation quanta. If the size of the cloud is smaller than the mean free path of neutrinos, heat is transported into the baryon clouds. This leads to an increase in pressure inside the cloud and thus to an expansion (inflation) of the cloud. Neutrino inflation provides an upper limit $\eta \leq 10^{-4}$ for clouds with $R_{\rm cloud} \leq 1$ m at the time of the QCD transition. In contrast to neutrino inflation, baryon diffusion is an efficient smoothing mechanism for any value of η.

After the annihilation/decay of pions the baryon mean free path increases (below $T \sim 40$ MeV). At temperatures above the decoupling of the weak interaction (~ 1 MeV) protons and neutrons are in chemical equilibrium and thus nucleons change isospin currently. A nucleon spends a fraction $X_{\rm n}(T) \equiv n_{\rm n}/n_{\rm B} = 1/[1+\exp(Q/T)]$ of its time as a neutron, where $Q = 1.29$ MeV is the neutron-proton mass difference. The mean free path of neutrons is much larger than the mean free path of protons. Thus at $T > 1$ MeV the diffusion length of nucleons is given by $\lambda_{\rm N-diff}(t) \sim \sqrt{\lambda_{\rm n-mfp} v_{\rm n} X_{\rm n} t}$, where $\lambda_{\rm n-mfp}$ is the neutron mean free path and $v_{\rm n} \sim (T/m_{\rm N})^{1/2}$ the thermal velocity of neutrons. The neutron mean free path is determined from neutron-electron scattering (the neutron has an electric dipole moment) and from neutron-proton scattering. At 1 MeV the nucleon diffusion length is ~ 100 m [102]. This corresponds to a comoving distance at the QCD transition of ~ 1 m or $\sim 10^{-4} R_{\rm H}$.

After weak decoupling (at ~ 1 MeV) neutrons diffuse much larger distances than protons. The proton diffusion is determined by electron-proton scattering, which gives a diffusion distance much smaller than that of the neutron. The proton diffusion at the time nucleosynthesis starts (at ~ 0.1 MeV) is completely negligible compared to the nucleon diffusion before weak decoupling. Thus $\lambda_{\rm p-diff} \sim 1$ km at the start of BBN and

$$\lambda_{\rm p-diff} \sim 10^{-4} R_{\rm H} \text{ comoving at } T_\star. \tag{4.8}$$

The neutron diffusion length is $\lambda_{\rm n-diff} \sim 100$ km at the start of BBN or

$$\lambda_{\rm n-diff} \sim 10^{-2} R_{\rm H} \text{ comoving at } T_\star. \tag{4.9}$$

The typical scale for baryon inhomogeneities are given by the typical bubble nucleation distance, $d_{\rm nuc}$. Thus all baryon inhomogeneities on scales $d_{\rm nuc} < \lambda_{\rm p-diff}$ are washed out due to baryon diffusion by the time of BBN. Most interesting are baryon inhomogeneities on scales $\lambda_{\rm p-diff} < d_{\rm nuc} < \lambda_{\rm n-diff}$.

The situation $d_{\rm nuc} > \lambda_{\rm n-diff}$ seems to be highly disfavored, according to the discussion in chapter 3.

The different diffusion lengths lead to the segregation of protons and neutrons. Neutrons escape from the high baryon density clouds, while the protons remain in the cloud. Thus the surrounding a cloud becomes neutron-rich, whereas the baryon cloud itself becomes proton-rich. This provides inhomogeneous initial conditions for nucleosynthesis.

4.3 Inhomogeneous nucleosynthesis

The baryon segregation, which leads to an inhomogeneous neutron-to-proton ratio, and inhomogeneities in the entropy per baryon both lead to inhomogeneous nucleosynthesis [15, 108]. Let me first discuss what happens to the element abundances in an homogeneous patch when we change η and $X_{\rm n}$.

η In homogeneous BBN η is the single free parameter of the theory. Its value is obtained from a fit to the data, which gives $\eta = (5.1 \pm 0.5) \times 10^{-10}$ or $\Omega_{\rm B} h^2 = 0.019 \pm 0.002$ [106]. The key role of η is to determine the time when nucleosynthesis starts. The first step in nucleosynthesis is the generation of deuterium ($\mathrm{p} + \mathrm{n} \rightarrow \mathrm{d} + \gamma$). Since deuterium has a small binding energy ($\approx$ 2.2 MeV) it is very easy to photo-dissociate it. The condition that deuterium does not see photons with energy above 2.2 MeV is $\eta^{-1} \exp(2.2\ \mathrm{MeV}/T) < 1$, which gives the temperature at the beginning of nucleosynthesis. The higher η, the earlier BBN starts, which means that baryons can be burned more efficiently. For higher η more ^{4}He and less D are produced. Typical mass fractions in homogeneous BBN are $0.24, 5\times10^{-5}, 2\times10^{-5}, 2\times10^{-10}$ for ^{4}He, D, ^{3}He, and ^{7}Li, respectively. For very high baryon densities, i.e. $\eta \sim 10^{-4}$ heavy elements like ^{12}C, ^{13}C, and ^{14}N could be generated with mass abundances of $\mathcal{O}(10^{-9})$ [19].

$X_{\rm n}$ The neutron-proton fraction basically determines the mass abundance of ^{4}He, given by $Y_{\rm p} \equiv 4 n_{^4{\rm He}}/n_{\rm B} \approx 2 X_{\rm n}$. Here I used the approximation that all neutrons end up in ^{4}He eventually. For homogeneous BBN $X_{\rm n} \approx 1/8$ and thus $Y_{\rm p} \approx 0.25$ from this simple argument. An inhomogeneous distribution of $X_{\rm n}$ could change the local ^{4}He abundance. Of course, the other abundances change as well.

In order to produce a global change in the elements abundances, nonlinear fluctuations in η and/or $X_{\rm n}$ are needed. Linear fluctuations would yield the same average abundances as homogeneous BBN. In addition the IBBN yields depend on the geometry of the baryon fluctuations.

Originally, interest in IBBN arose because it was thought that $\Omega_{\rm B} = 1$ could be possible [102]. It was shown that even with IBBN a baryon dominated, flat Universe is impossible, due to a severe overproduction of ^{7}Li [107, 11, 108]. Nevertheless there are interesting, probably in the future observable, consequences from IBBN: The precision measurements of the primordial abundances will need to take effects from IBBN into account [17] and, more speculative, higher mass elements (C, N, O) might have been generated during IBBN at an amount which could be observable [19].

The following conditions are necessary in order to have significant effects from IBBN: 1. $d_{\rm nuc} > \lambda_{\rm p-diff}$, 2. $\eta_{\rm high}/\eta_{\rm low}$ should be large, and 3. the fraction of baryons in the high density region has to be well above the ^{7}Li abundance. Heavy elements could be produced, leaving the ^{4}He abundance unchanged, if this fraction is small, and $\eta_{\rm high}$ is at its upper limit $\sim 10^{-4}$. On the other hand, significant corrections to the light element yields are obtained if the fraction of baryons in high density regions is high. In a recent work Suh and Mathews found that two fluctuation scales are consistent with the observed abundances: < 1 m (homogeneous BBN) and $10 - 40$ m, measured at $T_\star$. It seems that the nucleation distances obtained from nucleation in the inhomogeneous Universe are consistent with these constraints.

Chapter 5

Amplification of primordial inhomogeneities

Due to the vanishing of the sound speed during a first-order QCD transition (see section 2.1.3) the restoring forces for compressional perturbations vanish and thus density inhomogeneities on scales below the Hubble scale are amplified [23, 24, 74]. Below the evolution of cosmological perturbations is analyzed for perfect fluids. The Einstein equations are linearized, e.g. $\rho(\mathbf{x}, t) =: \rho_0(t) + \delta\rho(\mathbf{x}, t)$. The perturbed metric and energy momentum tensor are decomposed in a scalar, a vector, and a tensor part with respect to spatial coordinate transformations. See appendix B for an introduction to the theory of linear cosmological perturbations. Here we are interested in the density perturbations, which means the scalar sector. Below I work in the uniform expansion gauge (UEG), which is characterized by the vanishing of the perturbation of the volume expansion. The analysis is conveniently done in the dimensionless variables (see appendix B) $\delta \equiv \delta\rho/\rho_0$, the density contrast, $\hat{\psi}$, which is the peculiar velocity up to a factor of $\rho/(\rho + p)$, and α, the relativistic generalization of Newton's gravity potential (the perturbation of the lapse function). These quantities are determined by the relativistic continuity and Euler equations for each fluid separately, and by a relativistic Poisson equation:

$$
\begin{aligned}
\frac{1}{\mathcal{H}}\delta' + 3(c_s^2 - w)\delta &= \frac{k}{\mathcal{H}}\hat{\psi} - 3(1+w)\alpha && (5.1) \\
\frac{1}{\mathcal{H}}\hat{\psi}' + (1-3w)\hat{\psi} &= -c_s^2\frac{k}{\mathcal{H}}\delta - (1+w)\frac{k}{\mathcal{H}}\alpha && (5.2) \\
\left[\left(\frac{k}{\mathcal{H}}\right)^2 + \frac{9}{2}(1+w)\right]\alpha &= -\frac{3}{2}(1+3c_s^2)\delta\ , && (5.3)
\end{aligned}
$$

where derivatives $()' \equiv \partial_\eta \equiv a\partial_t$ are taken with respect to conformal time η. A derivation of these equations can be found in appendix B.

In this chapter I first discuss the perturbations in the dominant radiation fluid (section 5.1). I then comment on the possibility to form black holes during the QCD transition (section 5.2). The fate of the large peaks in the radiation spectrum is treated in section 5.3. In the following section (5.4) inhomogeneities of the subdominant component of the Universe at the QCD scale, kinetically decoupled CDM, is analyzed. The chapter is closed by a section on the clumps in CDM that form due to the amplification of inhomogeneities by the QCD transition (section 5.5).

5.1 Perturbations of the radiation fluid

The transfer functions, i.e. the change in the primordial spectrum, for the radiation fluid and the cold dark matter (CDM) are calculated by integrating the exact general relativistic set of equations (5.1)–(5.3) throughout the QCD transition. The initial conditions are fixed at $T = 100$ GeV, where all scales under considerations were far above the horizon. We fix the initial amplitude of the radiation fluid, $A_{\rm in}$, by the growing mode of an exactly radiation dominated solution, Eqs. (B.20) and (B.21). The normalization constant is given by the COBE normalized [60] Harrison-Zel'dovich spectrum [61], but it drops out in the transfer functions. The initial conditions for CDM are obtained assuming adiabatic perturbations, i.e. the entropy per cold particle is unperturbed $\delta\left(s^{\rm RAD}/n^{\rm CDM}\right) = 0$. Since $\rho^{\rm CDM} = mn^{\rm CDM} \propto 1/V_{\rm comoving}$ and $\rho_{\rm RAD} \propto (1/V_{\rm comoving})^{4/3}$, the adiabatic initial conditions for $\delta^{\rm CDM}$ can be written

$$\delta^{\rm CDM} = \frac{3}{4}\delta^{\rm RAD}. \tag{5.4}$$

The initial fluid velocities are equal. Since we are in the linear regime, each spatial Fourier mode evolves independently.

For a first-order phase transition it is convenient to use the volume of a comoving box $\propto a^3$ instead of time as the evolution variable. Thus, the derivatives in Eqs. (5.1) and (5.2) have to be replaced, $\mathcal{H}^{-1}(d/d\eta) = a(d/da)$. In sections 2.1.2 and 2.1.3 we have given w and c_s^2 in terms of the scale factor. In the case of a crossover we use the temperature T as the independent evolution variable, since temperature is decreasing strictly monotonically in time. The derivatives in Eqs. (5.1) and (5.2) are replaced by $\mathcal{H}^{-1}(d/d\eta) = -3c_s^2 T(d/dT)$. We obtain $p(T)$ by integrating the entropy density $s(T)$, Eq. (2.1).

The transfer functions are evaluated by evolving each mode from the initial temperature $T_{\rm in} = 100$ GeV to the final temperature $T_{\rm f} = T_\star/10 = 15$ MeV, i.e. until the peculiar velocity of CDM has redshifted away. At $T_{\rm f}$ the universe is exactly radiation dominated. The amplitude of the acoustic oscillations is $A^{\rm RAD} \equiv (\delta^2_{\rm RAD} + 3\hat\psi^2_{\rm RAD})^{1/2}$. The final amplitude of CDM is $A^{\rm CDM} = |\delta^{\rm CDM}|$. The transfer functions for the radiation and the CDM fluid are defined by

$$\mathcal{T}^{\rm RAD}(k, {\rm in} \to {\rm f}) \equiv \frac{A^{\rm RAD}(k)|_{T_{\rm f}}}{A_{\rm in}} \qquad (5.5)$$

$$\mathcal{T}^{\rm CDM}(k, {\rm in} \to {\rm f}) \equiv \frac{A^{\rm CDM}(k)|_{T_{\rm f}}}{A_{\rm in}} \ , \qquad (5.6)$$

where $A_{\rm in} = A^{\rm RAD}_{\rm in}$.

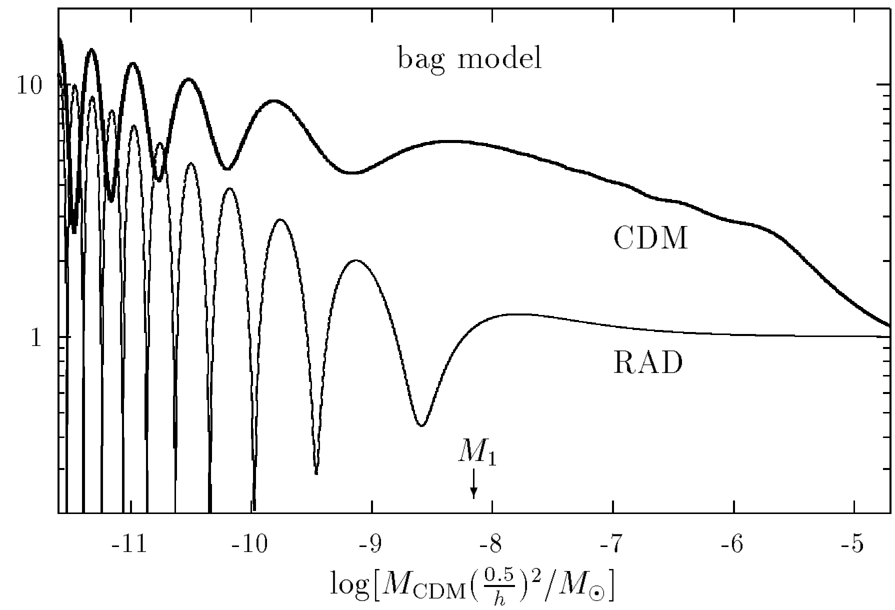

Figure 5.1: The modifications of the density contrast for kinetically decoupled CDM (like axions or primordial black holes) $A^{\rm CDM} \equiv |\delta^{\rm CDM}|(T_\star/10)$ and of the radiation fluid amplitude $A^{\rm RAD} \equiv (\delta^2_{\rm RAD} + 3\hat\psi^2_{\rm RAD})^{1/2}$ due to the QCD transition in the bag model. Both quantities are normalized to the pure Harrison-Zel'dovich radiation amplitude. On the horizontal axis the wave number k is represented by the CDM mass contained in a sphere of radius π/k.

For the bag model the transfer functions are shown in Fig. 5.1. Both transfer functions show huge peaks on small scales. The different scales $k = 2\pi/\lambda$ are represented by the invariant CDM mass contained in a sphere with radius $\lambda/2$,

$$M^{\rm CDM}(\lambda^{\rm phys}) \equiv \frac{4\pi}{3}\rho^{\rm CDM}\left(\frac{\lambda^{\rm phys}}{2}\right)^3 \ , \qquad (5.7)$$

assuming that $\Omega_{\rm CDM} \approx 1$ today. The largest scales in Fig. 5.1 correspond to the horizon at $T_{\rm f} = T_\star/10$. The CDM curve also shows the logarithmic growth of subhorizon scales of CDM in a radiation dominated universe. The CDM peaks lie on top of this logarithmic curve.

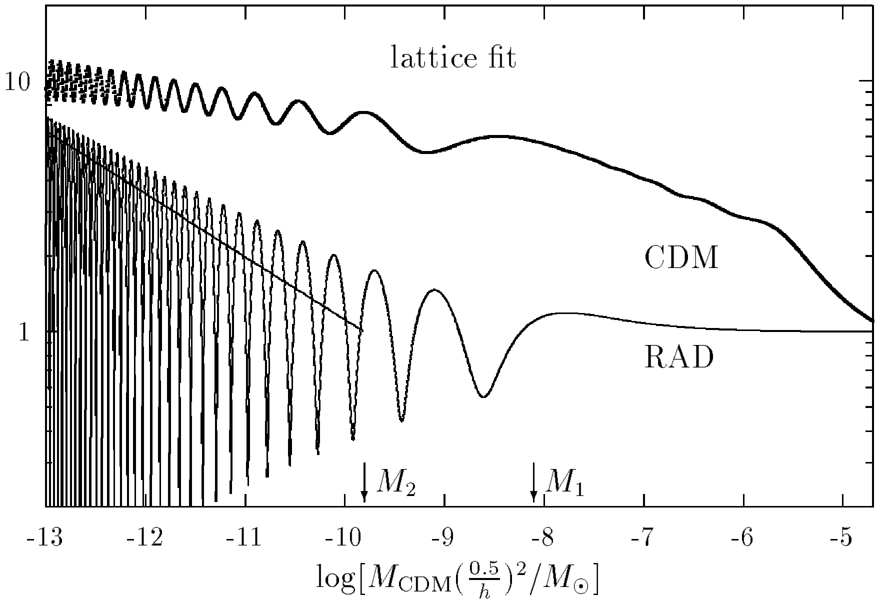

Figure 5.2: The same as Fig. 5.1, but for the lattice QCD fit, Eq. (2.5). The straight line denotes the asymptotic envelope for small scales $\propto k^{3/4}$.

The peak structure starts at a scale $\approx 10^{-8} M_\odot$ in CDM mass. This scale corresponds to the horizon scale at the QCD transition, $M_{\rm H} \equiv (4\pi/3)\rho^{\rm CDM}$ $(R_{\rm H}/2)^3$. The radiation energy inside the horizon at $T_\star$ is $\sim 1 M_\odot$, but it is redshifted as $M^{\rm RAD}(a) \sim (a_{\rm equality}/a) M^{\rm CDM}$. Scales which are above the horizon at the QCD transition are not affected in accordance with the general proof in appendix B, Eq. (B.14). For scales below $M_1^{\rm CDM} \approx 9 \times 10^{-9} M_\odot$ the radiation peaks grow linearly in wave number. This linear growth comes from the fact that the vanishing sound speed during the QCD transition implies a vanishing restoring force in the acoustic oscillations on subhorizon scales. Therefore, the radiation fluid falls freely during the transition, with a constant velocity given at the beginning of the transition. The density contrast $\delta^{\rm RAD}$ grows linearly in time with a slope k. CDM is moving in an external potential provided by the dominant radiation fluid, and is pushed by the strong increase in the gravitational force during the transition. The highest peaks have $k/k_1 \sim 10^4$, because on smaller scales the acoustic oscillations are damped away by neutrino diffusion already before the QCD transition (see section 5.3).

For the fit (2.5) to lattice QCD the transfer functions $\mathcal{T}^{\rm RAD}, \mathcal{T}^{\rm CDM}$ are shown in Fig. 5.2. The peak structure starts at the horizon scale M_1, but the asymptotic growth on small scales is different. It grows $\propto k^{3/4}$ starting at a scale k_2 which corresponds to an invariant CDM mass of $M_2 = 2 \times 10^{-10} M_\odot$. The asymptotic envelope for small scales is indicated by the straight line in Fig. 5.2. The highest peaks show an amplification of a factor of 400 and correspond to wave numbers $k/k_2 \sim 3 \times 10^3$. The smaller amplification compared to the bag model is due to the decrease of the radiation fluid velocity before the transition. This happens because the sound speed drops below $1/\sqrt{3}$ already before the transition. The values for M_2 and the exponent of asymptotic growth depend on the specific choice of the latent heat ($R_L = 0.2$) and the thermodynamic behavior at $T > T_\star$, parametrized by γ ($\gamma = 1/3$). In the next chapter we will show, that the exponent of the asymptotic envelope for $\gamma \in (0,1)$ varies between 1/2 and 1.

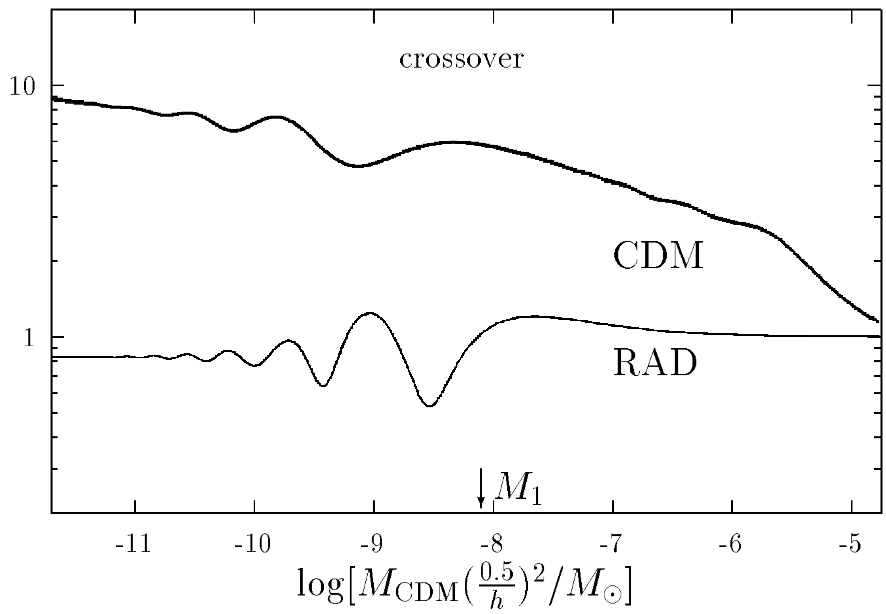

Figure 5.3: The same as Fig. 5.1, but for a QCD crossover.

The processed spectrum for the crossover with equation of state (2.6), Fig. 5.3, shows a similar behavior as for the bag model and the lattice fit on superhorizon and horizon scales. The peak structure starts at M_1, but on subhorizon scales there are no peaks. The level of the subhorizon transfer function for the radiation fluid is reduced to 0.83. This comes from the damping of the acoustic oscillations during the time with $c_s^2 \neq 1/3$.

The time evolution for subhorizon modes, $\lambda^{\rm phys} \ll R_{\rm H} = H^{-1}$, at the transition can be solved analytically. For the dynamics of the radiation fluid (QCD, photons, leptons) one can neglect cold dark matter (CDM), since $\rho^{\rm CDM}/\rho^{\rm RAD} = a/a_{\rm equality} \approx 10^{-8}$. The transition time is short compared to the Hubble time at the transition, $(t_+ - t_-) < t_{\rm H} = H^{-1}$. For subhorizon modes we can neglect gravity during the whole transition as we will show below. The damping terms in the continuity equation (B.15) and Euler equation (B.16) are absent in the purely radiation dominated regime. During the transition the damping terms can be neglected in view of the huge amplification for a first-order phase transition. Eqs. (B.15) and (B.16) now read:

$$\begin{aligned} \delta' - k\hat{\psi} &= 0 \\ \hat{\psi}' + c_s^2 k\delta &= 0 \ . \end{aligned} \tag{5.8}$$

Written as a second order differential equation for δ, this is just an oscillator equation

$$\delta'' + \omega^2\delta = 0 \ , \tag{5.9}$$

with the time-dependent frequency $\omega(\eta) \equiv kc_s(\eta)$.

Bag model

We first discuss the origin of large amplifications for small scales in the bag model. Before and after the QCD transition the radiation fluid makes standing acoustic oscillations in each mode k with sound speed $c_s^2 = 1/3$ and with amplitude $A_{\rm in}$ and $A_{\rm out}$ for the incoming and outgoing solution respectively, see Fig. 5.4. The incoming solution for the density contrast δ and the peculiar velocity $\sqrt{3}\hat{\psi}$ reads

$$\begin{aligned} \delta &= -A_{\rm in}\cos\left(\omega(\eta - \eta_-) + \varphi_-\right) \\ \sqrt{3}\hat{\psi} &= A_{\rm in}\sin\left(\omega(\eta - \eta_-) + \varphi_-\right) \ . \end{aligned} \tag{5.10}$$

This solution is valid until the beginning of the transition at $\eta = \eta_-$, and φ_- denotes the phase of the oscillation at η_-. During the transition the sound speed is zero. There are no restoring forces from pressure gradients and the radiation fluid falls freely. Since the duration of the transition is short compared to the Hubble time $\Delta t \equiv (t_+ - t_-) < H^{-1}$, gravity is negligible during this free fall. If we estimate the contribution of the gravity term in the Euler equation (B.16) during the transition we get $(t_+ - t_-)\partial_t\hat{\psi}_- = \mathcal{O}(\Delta t k_{\rm phys})\alpha_- = \mathcal{O}[(H\Delta t)(H/k_{\rm phys})]\delta_- = \mathcal{O}[(H\Delta t)(H/k_{\rm phys})]\hat{\psi}_- \ll \hat{\psi}_-$ except for an initial phase $\varphi_- = 0 \bmod \pi$ (which leads to a dip in the spectrum). Thus, the fluid is moving inertially in the sense of Newton, the velocity stays

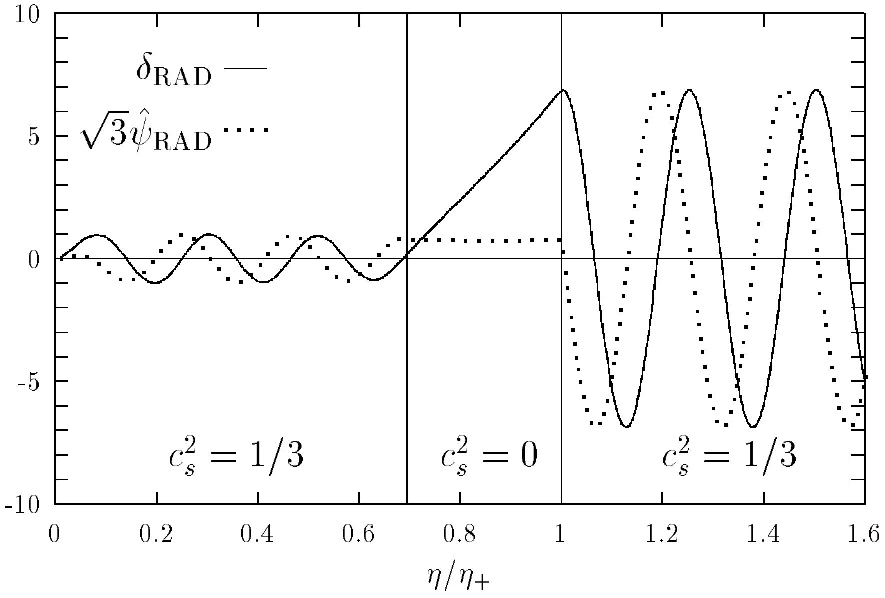

Figure 5.4: The time evolution of the density contrast, $\delta^{\rm RAD}$, and the peculiar velocity, $\frac{3}{4}\hat{\psi}^{\rm RAD}$, of the radiation fluid for the mode $k/k_1 = 7$ in uniform expansion gauge. During the QCD transition in the bag model — marked by the 2 vertical lines — the velocity stays approximately constant and the density contrast grows linearly. The amplitude is normalized to 1 long before the transition.

constant, and the density contrast grows linearly in time

$$\begin{aligned} \delta &= \delta_- + k(\eta - \eta_-)\hat{\psi}_- , \\ \sqrt{3}\hat{\psi} &= \sqrt{3}\hat{\psi}_- , \end{aligned} \tag{5.11}$$

where $\sqrt{3}\hat{\psi}_- = A_{\rm in}\sin(\varphi_-)$ is the peculiar velocity at η_-.

Since we have no jumps in pressure p_0, the density contrast δ and the fluid velocity $\hat{\psi}$ stay continuous throughout the whole transition, in particular at the matching points of the different regimes. Gravity remains negligible during the entire transition since the growth of $\hat{\psi}$ due to gravity at the end of the transition can be estimated by $\hat{\psi}_+ - \hat{\psi}_- = \mathcal{O}(\Delta t k_{\rm phys}\alpha_+) = \mathcal{O}[H\Delta t(H/k_{\rm phys})\delta_+] = \mathcal{O}[(H\Delta t)^2\hat{\psi}_-] \ll \hat{\psi}_-$, in the limit under consideration. At the end of the transition this solution has to be joined to the pure radiation dominated regime for $T \leq T_\star$. Since the amplitude of the density contrast grows linearly during the transition, the final amplitude $A_{\rm out} = A_+$ is enhanced linearly in k, modulated by the incoming phase

$$\left(\frac{A_{\rm out}}{A_{\rm in}}\right)^2 = \left(\frac{k}{k_1}\right)^2 \sin^2(\varphi_-) \ , \tag{5.12}$$

with $k_1 \equiv \sqrt{3}/\Delta\eta$, $\Delta\eta \equiv \eta_+ - \eta_-$. The envelope of the linearly growing peak structure for subhorizon scales starts at the scale k_1 which corresponds to a CDM mass of $M_1 = 9 \times 10^{-9} M_\odot$.

Lattice QCD

For the fit to lattice QCD, Eq. (2.5), the time evolution separates into four regimes. First we have a WKB regime, where the sound speed is slowly changing compared to the frequency of the oscillation, i.e. the WKB condition $|dc_s/d\eta|/c_s \ll \omega = kc_s$ is satisfied. The WKB solution is

$$\begin{aligned} \delta &= -\frac{A_{\rm in}}{(3c_s^2)^{1/4}} \cos \int_0^\eta \omega(\eta')d\eta' \\ \sqrt{3}\hat{\psi} &= A_{\rm in}(3c_s^2)^{1/4} \sin \int_0^\eta \omega(\eta')d\eta' \ , \end{aligned} \tag{5.13}$$

where $A_{\rm in}$, as before, denotes the incoming subhorizon amplitude in a radiation dominated universe. The decreasing sound speed in the WKB regime leads to an increase in the density contrast and a decrease in peculiar velocity compared to the purely radiation dominated case. Close to η_- the WKB condition can no longer be satisfied: Since c_s decreases by some power in $(\eta_- - \eta)$, Eq. (2.15), the left hand side of the WKB condition diverges like $1/(\eta_- - \eta)$, whereas the right hand side for any fixed k goes to zero. Therefore, the WKB solution for a given mode is valid up to a certain time $\tilde{\eta}(k) < \eta_-$. $\tilde{\eta}(k)$ approaches η_- for increasing k.

Close to η_- there is a second regime (overlapping with the WKB regime for large enough k), where c_s can be approximated by the power law of Eq. (2.15),

$$\begin{aligned} c_s &= C\left(\frac{\eta_- - \eta}{\eta_-}\right)^{\frac{1}{2\beta}-1} \\ \beta &\equiv \frac{\gamma}{\gamma+1} \ , \end{aligned} \tag{5.14}$$

where β is defined for convenience below. Inserting this power law into the oscillator equation (5.9) gives a Bessel differential equation. The new variable z is the argument of the cosine in the WKB expansion,

$$z \equiv k\int_\eta^{\eta_-} c_s(\eta')d\eta' = 2C\beta(k\eta_-)\left(\frac{\eta_- - \eta}{\eta_-}\right)^{\frac{1}{2\beta}} \ . \tag{5.15}$$

The index $\bar{\beta}$ of the Bessel functions is obvious from the ratio of the two fundamental solutions $J_{\bar{\beta}}(z)/N_{\bar{\beta}}(z) \propto z^{2\bar{\beta}} \propto (\eta_- - \eta)^{\bar{\beta}/\beta}$. Since the two fundamental solutions for $c_s \to 0$ are $\delta \to$ const and $\delta \propto (\eta_- - \eta)$, it follows that $\bar{\beta} = \beta$. The prefactor must be z^β to make the second fundamental solution constant,

$$\delta = z^\beta \left[-B_1 J_\beta(z) + B_2 N_\beta(z)\right] \ . \tag{5.16}$$

The peculiar velocity follows via $\hat{\psi} = \delta'/k$, see Eq. (5.8). Matching the WKB solution with the Bessel solution in the overlap region $z \gg 1$, where $J_\beta(z), N_\beta(z) \to \sqrt{2/(\pi z)}\cos[z-(\pi/2)(\beta+1/2, 3/2)]$, gives the normalization $B^2 \equiv B_1^2 + B_2^2$,

$$B = A_{\rm in}\frac{\sqrt{\pi\beta}}{3^{1/4}}(2C\beta)^{-\beta}(k\eta_-)^{1/2-\beta} \ . \tag{5.17}$$

At the beginning of the first-order transition, $\eta = \eta_-$, the Bessel solution (second regime) is matched to the third regime, i.e. the free fall regime with $c_s^2 = 0$. As in the bag model, peaks in the transfer function for large k are obtained for the mixing angles φ in the Bessel solution ($B_1 = B\cos\varphi, B_2 = B\sin\varphi$) which give the maximal $|\hat{\psi}|$ at the matching point. With $J_\beta(z) \to (z/2)^\beta/\Gamma(\beta+1)$ for $z \ll 1$ and $N_\beta(z) = [J_\beta(z)\cos(\beta\pi) - J_{-\beta}(z)]/\sin(\beta\pi)$ we find

$$\hat{\psi}_-^{\rm max} = A_{\rm in}\frac{\sqrt{\pi\beta}}{3^{1/4}}\frac{(C\beta)^\beta}{\Gamma(\beta+1)\sin\beta\pi}\,(k\eta_-)^{\beta-\frac{1}{2}} \ . \tag{5.18}$$

The evolution in the third regime, $c_s^2 = 0$, is as before. The restoring force in the oscillator equation, Eq. (5.9), vanishes, the fluid moves with constant peculiar velocity, $\hat{\psi}(\eta) = \hat{\psi}_-$, and the density contrast grows linearly in time.

After the transition ($\eta > \eta_+$, fourth regime) the universe is radiation dominated ($c_s^2 = 1/3$) and the solutions are oscillations with amplitude $A_{\rm out} = A_+$. The amplification of peaks in the outgoing amplitude $A_{\rm out}$ is given by $A_{\rm out}|_{\rm peaks} = \hat{\psi}_-^{\rm max} k\Delta\eta$,

$$\left.\frac{A_{\rm out}}{A_{\rm in}}\right|_{\rm peaks} = \frac{\sqrt{\pi\beta}}{3^{1/4}}\frac{(C\beta)^\beta}{\Gamma(\beta+1)\sin\beta\pi}\,(k\eta_-)^{\beta-\frac{1}{2}}\,k\Delta\eta. \tag{5.19}$$

The dependence on the latent heat is encoded in the duration $\Delta\eta$ of the transition. C and β are determined by the normalization and the power law for $c_s(\eta)$ shortly before the onset of the first-order phase transition, Eq. (5.14). Replacing β by γ (= the exponent in the QCD fit to the entropy density) the amplification factor is

$$\left.\frac{A_{\rm out}}{A_{\rm in}}\right|_{\rm peaks} = \left(\frac{k}{k_2}\right)^{\frac{3\gamma+1}{2(\gamma+1)}} \tag{5.20}$$

for large k. Since $0 < \gamma < 1$ the exponent of the power law varies between 1/2 and 1. The normalization of the peak amplification for large k is encoded in k_2. In the fit (2.5) to lattice QCD we take $\gamma = 1/3$, hence $\beta = 1/4$

$$\left.\frac{A_{\rm out}}{A_{\rm in}}\right|_{\rm peaks} = \left(\frac{k}{k_2}\right)^{\frac{3}{4}} . \tag{5.21}$$

For $R_L = 0.2$, k_2 corresponds to a CDM mass of $M_2 = 2 \times 10^{-10} M_\odot$. The spectrum for this case together with the asymptotic envelope is plotted in Fig. 5.2.

Crossover

In the case of a crossover, the amplification is occurring for scales around the Hubble radius at the transition only. Subhorizon scales always stay in the WKB-regime and therefore the spectrum is flat for these scales. However, the amplitude for subhorizon scales is damped during the phase transition. The same damping occurs in the case of a first-order phase transition. It has been neglected in the analytic discussion, since it is a small correction. The time evolution of the density contrast of subhorizon scales, including damping terms, reads

$$\delta'' + (1 + 3c_s^2 - 6w)\frac{a'}{a}\delta' + \omega^2(\eta)\delta = 0 \ . \tag{5.22}$$

The friction term in this equation can be eliminated if we write the density contrast as $\delta =: \frac{\sqrt{1+w}}{a'}u(\eta)$. Inserting this ansatz into Eq. (5.22), using the Friedmann equation and $w' = 3aH(1+w)(w - c_s^2)$, we obtain an undamped oscillator equation with frequency $\omega(\eta) = kc_s(\eta)$ for the quantity $u(\eta)$. For a crossover the sound velocity never vanishes, and subhorizon modes always satisfy the WKB-condition. Therefore, we obtain for the density contrast and the peculiar velocity

$$\begin{aligned} \delta &= -\frac{A_{\rm in}}{(3c_s^2)^{1/4}}\frac{a'_{\rm in}}{a'}\frac{\sqrt{3(1+w)}}{2}\cos\int \omega(\eta)d\eta \\ \hat{\psi} &= A_{\rm in}(3c_s^2)^{1/4}\frac{a'_{\rm in}}{a'}\frac{\sqrt{3(1+w)}}{2}\sin\int \omega(\eta)d\eta. \end{aligned} \tag{5.23}$$

The reduction of the amplitude of subhorizon scales is given by

$$\frac{A_{\rm out}}{A_{\rm in}} = \frac{(Ha^2)_{\rm in}}{(Ha^2)_{\rm out}} = \left(\frac{g_+}{g_-}\right)^{1/6} . \tag{5.24}$$

Therefore the subhorizon amplitudes are reduced to 83 % of their initial value. This damping is a general feature appearing whenever the number of degrees of freedom is reduced. Also in the case of a first-order transition, this damping factor should be taken into account. However, it changes the huge amplifications merely by the constant factor of 0.83.

5.2 Formation of black holes?

It was suggested in the literature [25, 27, 71] that the QCD transition could lead to formation of $1M_\odot$ black holes, which could account for dark matter today. Jedamzik [27] proposed to identify such black holes with the MACHOs observed by microlensing [72]. He pointed out that the formation of black holes should be particularly efficient during the QCD epoch due to the significant decrease in the effective sound speed.

In order to form a black hole in a radiation dominated universe, the density contrast inside the Hubble radius should be in the range $1/3 < \delta_{\rm H} < 1$ [92]. For an observable amount of $1M_\odot$ black holes today, i.e. $\Omega_{\rm BH}^{(0)} = \mathcal{O}(1)$, the fraction of energy density converted to black holes at the QCD transition must be $\mathcal{O}(a_{\rm QCD}/a_{\rm equality}) \approx 10^{-8}$. For a Gaussian distribution this requires $\delta_{\rm rms} \approx 0.06$ (without including any enhancement from the QCD transition) [94]. The QCD transition gives an enhancement factor (at the horizon scale) of 2 for the bag model and of 1.5 for lattice QCD in the linear perturbation treatment, Figs. 5.1 - 5.3. This indicates a corresponding reduction in the required preexisting perturbation spectrum at the solar mass scale. Cardall and Fuller used a qualitative argument of Carr and Hawking [91] and the bag model and also obtained a factor of 2 reduction in the required preexisting perturbation spectrum [73]. These QCD factors of 1.5 or 2 are so modest that a preexisting Harrison-Zel'dovich spectrum with COBE normalization is very far from giving a cosmologically relevant amount of black holes [74]. One would have to put in a fine-tuned tilt $(n-1) \approx 0.4$ to get the desired amount of black holes. However, this tilted spectrum would overproduce primordial black holes on scales which are only a factor of 50 below the Hubble radius at the QCD transition. Therefore a break in the preexisting spectrum below the QCD scale would be required, a second fine tuning.

We conclude that the QCD transition enhances the probability of black hole formation, but the preexisting spectrum needs to be fine tuned around the QCD scale and the major effect would not be due to the QCD transition.

5.3 Collisional damping from neutrinos

The acoustic oscillations in the radiation fluid get damped by neutrino diffusion at the time of neutrino decoupling. This damping is analogous to Silk damping at photon decoupling. The muon resp. tau neutrinos, which are coupled to the RAD fluid via neutral current interactions only, decouple at $T^{\rm dec}_{\nu_\mu\,\nu_\tau} \sim 2.2$ MeV from the Hubble scale $R_{\rm H}$, which follows from Ref. [104]. The electron neutrinos interact by charged and neutral currents and decouple slightly later, $T^{\rm dec}_{\nu_e} \sim 1.4$ MeV. By the time of neutrino decoupling at the

Hubble scale all inhomogeneities in the RAD fluid on scales below $\approx 10^{-6} M_\odot$ in CDM mass are wiped out by neutrino diffusion (cf. the QCD horizon scale is $10^{-8} M_\odot$ in CDM mass), as shown below, Eq. (5.29). Therefore the QCD peaks cannot affect big bang nucleosynthesis (BBN).

It is important to distinguish the total decoupling of neutrinos, i.e. neutrino decoupling at the Hubble scale, when the neutrino scattering rate Γ is less than the Hubble rate, $\Gamma_\nu/H < 1$, from the neutrino decoupling with respect to a certain mode given by $\Gamma_\nu/\omega_{\rm phys} < 1$, when the typical neutrino scatters less than once during an acoustic oscillation time of one particular mode. The mode-dependent decoupling temperature $T_\nu^{\rm dec}(k)$ is related to the total decoupling temperature by

$$\frac{T_{\nu_i}^{\rm dec}(k)}{T_{\nu_i}^{\rm dec}(H)} \approx \left(\frac{c_s k_{\rm phys}}{H}\right)^{1/4}_{T=T_{\nu_i}^{\rm dec}(H)} . \tag{5.25}$$

This follows because the neutrino interaction rates Γ_ν are proportional to T^5 and $k_{\rm phys} \propto 1/a \propto T$, hence $\Gamma_\nu/\omega_{\rm phys} \propto T^4$.

To compute the damping of acoustic oscillations in the radiation fluid by neutrino diffusion we follow Weinberg [62]. For a radiation fluid shear viscosity is dominant, bulk viscosity vanishes and heat conduction is negligible. The shear viscosity is given by

$$\eta_{\rm visc} = \frac{4}{15}\sum_i \rho_{\nu_i}\tau_{\nu_i} . \tag{5.26}$$

ρ_{ν_i} denotes the energy density of a neutrino species, τ_{ν_i} is the typical collision time. In the subhorizon limit the Navier-Stokes equation and the continuity equation give

$$\delta'' + \frac{k_{\rm phys}}{\rho_{\rm tot}}\eta_{\rm visc} k\delta' + \omega^2\delta = 0, \tag{5.27}$$

a damped oscillator. The damping factor for the mode k at a given conformal time η is

$$D(k,\eta) = \exp\,[-\frac{1}{2}\int_0^{\eta_{\rm max}} (k_{\rm phys}/\rho_{\rm tot})\eta_{\rm visc} k d\eta'], \tag{5.28}$$

Here the upper limit of the integral is the conformal time $\eta_{\rm max} = {\rm Min}[\eta, \eta_{\rm dec}(k)]$, because collisional damping of the γ-$\ell^\pm$-hadron fluid by neutrinos ceases at decoupling of the mode k considered. The damping per oscillation is largest for $\omega\tau_\nu \equiv \omega/\Gamma_\nu \approx 1$, i.e. immediately before neutrino decoupling for a given mode. But note that subhorizon modes get strongly damped long before the mode decouples from neutrinos, because a weak damping per oscillation is compensated by many oscillations per Hubble time.

For a first application we ask what modes are already damped by the time of the QCD transition. At the QCD transition, $T = T_\star$, the interaction rates for electron and muon neutrinos (resp. antineutrinos) with the leptons are the same, $\Gamma_{\nu_e} = \Gamma_{\bar{\nu}_e} = \Gamma_{\nu_\mu} = \Gamma_{\bar{\nu}_\mu} = 3.1 G_{\rm F}^2 T^5$ [104], since electrons and muons are still relativistic. The $\tau-$neutrinos interact only via neutral currents with the leptons and have a lower interaction rate, $\Gamma_{\nu_\tau} = \Gamma_{\bar{\nu}_\tau} = 0.6 G_{\rm F}^2 T^5$. Evaluating the damping integral, Eq. (5.28), at $T = T_\star$ we find that the damping factor $D(k, T_\star)$ is $< 1/e$ for $(k_{\rm phys}/H)_{T_\star} > 10^4$, which corresponds to $M_{\rm CDM} < 10^{-20} M_\odot$, i.e. acoustic oscillations on these small scales are wiped out before the QCD transition. Therefore no peaks in the RAD or in the CDM transfer function can develop below this scale. This small-scale cut-off is independent of the bubble separation scale.

Next we consider $T < T_{\nu_e}^{\rm dec}(H) \approx 1.4$ MeV and evaluate the final damping factor $D(k)$. At the time of neutrino decoupling we take a purely radiation dominated universe, consisting of γ, $e^\pm$ and $\nu' s$ only to evaluate the damping. Muons have disappeared since $m_\mu \gg T$ and since $\tau_\mu \ll t_{\rm H}$. The interaction rate for electrons is still given by charged and neutral currents, $\Gamma_{\nu_e} = \Gamma_{\bar{\nu}_e} = 1.3 G_{\rm F}^2 T^5$, whereas muon and tau neutrinos have the same lower (neutral current) rate, $\Gamma_{\nu_\mu} = \Gamma_{\bar{\nu}_\mu} = \Gamma_{\nu_\tau} = \Gamma_{\bar{\nu}_\tau} = 0.3 G_{\rm F}^2 T^5$ [104]. The final damping of a certain scale (expressed in invariant CDM mass) from Eq.(5.28) is

$$D = \exp\left[-\left(\frac{M_{\rm D}}{M}\right)^{1/4}\right], \tag{5.29}$$

with the neutrino damping scale $M_{\rm D} \approx 1.9 \times 10^{-6} M_\odot$ in CDM mass. This is $3 \times 10^{-5} M_{\rm H}^{\rm CDM}$ at $T = 1.4$ MeV and corresponds to length scales $\lambda = 1/30 R_{\rm H}$.

We conclude that the large peaks in the spectrum of the radiation fluid are damped away by the time of BBN. The large peaks in the RAD fluid generated by the QCD transition do not give a new mechanism for inhomogeneous BBN.

5.4 Perturbations of decoupled matter

Cold dark matter (CDM) is assumed to be the major matter content of the universe today. At the time of the QCD transition, however, the contribution of CDM to the total energy density was negligible, $\rho^{\rm CDM}/\rho^{\rm RAD} = a/a_{\rm equality} \approx 10^{-8}$. We consider a type of CDM which is non-relativistic ($p \ll \rho$) at the QCD transition and which is only coupled via gravity to the radiation fluid. CDM moves in the external gravitational potential provided by the dominant radiation fluid. During the QCD transition, the big amplifications of the density contrast in the radiation fluid $\delta^{\rm RAD}$ leads to a big amplification in the gravitational potential, i.e., the force term in the Euler equation for CDM. The CDM is accelerated to higher velocities at the end of the transition. Therefore, we also get peaks and dips in the cold dark matter fluid.

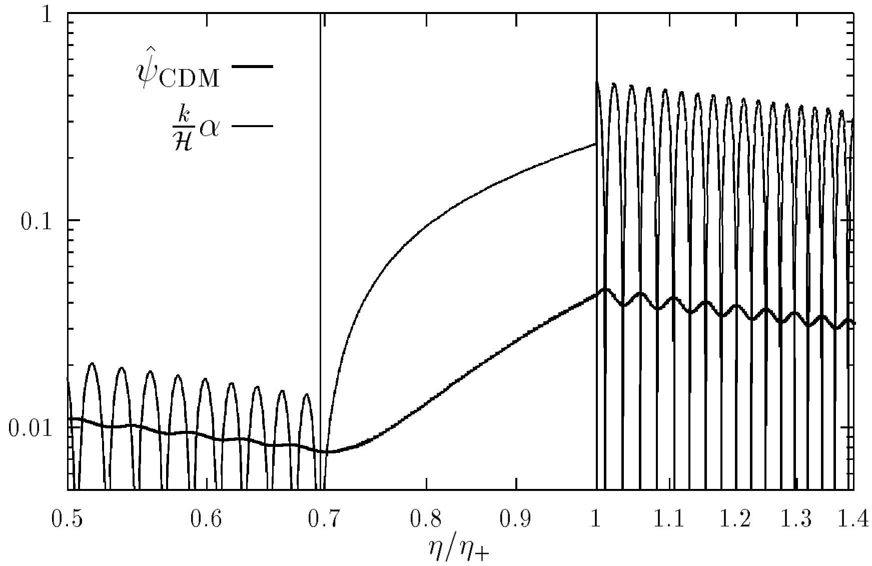

Figure 5.5: The time evolution of the peculiar velocity, $\hat{\psi}^{\rm CDM}$, of the kinetically decoupled cold dark matter fluid (axions or primordial black holes) and the external gravitational potential gradient $\frac{k_{\rm phys}}{H}\alpha$ for the mode $k/k_1 = 37$ in uniform expansion gauge. α is provided by the radiation fluid. During the QCD transition in the bag model — marked by the 2 vertical lines — the cold dark matter fluid is accelerated by the gravitational force.

The subhorizon evolution of CDM in a purely radiation dominated universe is just inertial motion. This can be seen from the Euler equation (B.16): The sound velocity of cold dark matter is zero, $c_s^2 \equiv 0$, and the gravitational potential α is given using the Poisson equation (B.17) for the dominant density contrast $\delta^{\rm RAD}$ Eq. (5.11). In the leading order in $x = k/\mathcal{H}$, the gravitational force can be neglected and the subhorizon evolution of the CDM velocity is obtained:

$$\hat{\psi}^{\rm CDM} = C\frac{1}{x}. \tag{5.30}$$

The velocity of CDM in a radiation dominated universe just redshifts to zero on subhorizon scales, see Fig. 5.5. C is an integration constant of order $A_{\rm in}$. The corresponding evolution of the density contrast $\delta^{\rm CDM}$ follows from the continuity equation (B.15),

$$\delta^{\rm CDM} = C \ln x + D. \tag{5.31}$$

This logarithmic growth of $\delta^{\rm CDM}$ [109] can be seen in Fig. 5.6 before and after the transition. The shape of $\delta^{\rm CDM}$ can also be seen in the transfer functions Figs. 5.1,5.2,5.3 on scales above the horizon scale M_1.

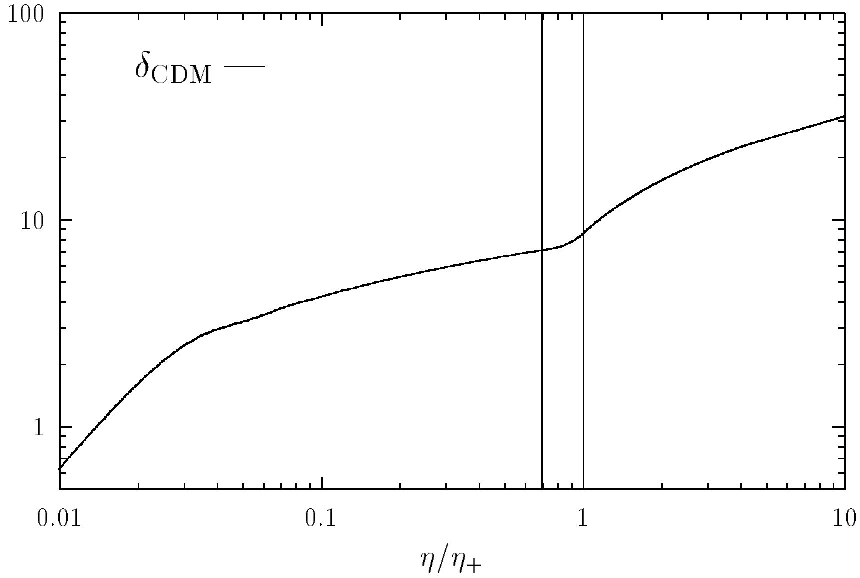

Figure 5.6: The time evolution of the CDM density contrast, $\delta^{\rm CDM}$, corresponding to the CDM velocity of Fig. 5.5. The major amplification of $\delta^{\rm CDM}$ is due to the higher peculiar velocity at the end of the transition.

During a first-order QCD transition the evolution of the gravitational potential is dominated by the linear growth in time of $\delta^{\rm RAD}$, Eq. (5.11). From the Poisson equation (B.17) follows that the gravitational potential grows linearly in time

$$\alpha = -\frac{3}{2}\mathcal{H}(\eta - \eta_-)\left(\frac{\mathcal{H}}{k}\right)\hat{\psi}_-^{\rm RAD}, \tag{5.32}$$

see Fig. 5.5. As before, we will take the transition time to be short compared to the Hubble time $\Delta t < H^{-1}$, hence $\Delta\eta < \mathcal{H}^{-1}$. The gravitational force in the Euler equation (B.16) and hence the fluid acceleration for CDM also grows linearly in time during the transition. The fluid velocity grows quadratically

$$\hat{\psi}_+^{\rm CDM} = \frac{3}{4}\left[\mathcal{H}\Delta\eta\right]^2 \hat{\psi}_-^{\rm RAD} + \hat{\psi}_-^{\rm CDM}. \tag{5.33}$$

The initial CDM velocity $\hat{\psi}_-^{\rm CDM}$ is given by Eq. (5.30). On scales well below the horizon the velocity is redshifted to small values and can be neglected. However, on subhorizon scales closer to the horizon the initial velocity dominates, because $[\mathcal{H}(\Delta\eta)]^2 \approx 0.1(0.01)$ for the bag model (lattice fit) is small. According to the continuity equation (B.15) the density contrast $\delta^{\rm CDM}$ grows cubically

$$\delta_+^{\rm CDM} = \delta_-^{\rm CDM} + \frac{1}{4}\left(\frac{k}{\mathcal{H}}\right)\left[\mathcal{H}\Delta\eta\right]^3 \hat{\psi}_-^{\rm RAD}. \tag{5.34}$$

Due to the cube the growth of $\delta^{\rm CDM}$ during the QCD transition is small.

The major amplification effect comes from the higher velocity at the end of the transition (see Fig. 5.5), which leads to

$$\delta^{\rm CDM}(\eta) = \hat{\psi}_+^{\rm CDM} k\eta_+ \ln(\frac{\eta}{\eta_+}) + \delta_+^{\rm CDM}. \tag{5.35}$$

The amplification of the density contrast during the transition is negligible compared to the enhancement of the velocity. This velocity enhancement during the transition leads to an additional logarithmic growth of $\delta^{\rm CDM}$ after the transition,

$$\delta^{\rm CDM}(\eta) = \left[\frac{3}{4}\left(\frac{\Delta\eta}{\eta_+}\right)^2 \hat{\psi}_-^{\rm RAD}\right] k\eta_+ \ln(\frac{\eta}{\eta_+}) + \delta_+^{\rm CDM}. \tag{5.36}$$

Here we have used (5.33) to obtain the leading subhorizon approximation. This additional logarithmic growth of $\delta^{\rm CDM}$ is most clearly seen in Fig. 5.6.

The number of CDM peaks in the numerical result, Figs. 5.1-5.3, is only half of the radiation peaks. This comes from the fact that the peaks in $\delta^{\rm CDM}$ lie on top of the logarithmic curve, which is still the main contribution at the scales plotted. The dips correspond to modes, with a maximal negative amplification.

The jump in the gravitational potential at the end of the QCD transition in Fig. 5.5 follows from the Poisson equation (B.17). Since δ is continuous, but c_s^2 jumps, the right hand side abruptly changes by a factor of 2. Therefore α jumps by the same factor.

Let us compare the 'QCD peaks' in the CDM spectrum with the CDM spectrum without phase transition. In the limit $\rho^{\rm CDM}/\rho^{\rm RAD} \ll 1$ the exact solution to Eqs. (5.1) – (5.3) in the radiation dominated universe without transition reads ($x = k/\mathcal{H}$):

$$\begin{aligned}\delta^{\rm CDM} &= \frac{3A_{\rm in}}{2}\left[\ln(\frac{x}{\sqrt{3}}) + \gamma_{\rm E} - \frac{1}{2} - {\rm Ci}(\frac{x}{\sqrt{3}}) + \right.\\ &\qquad \left. + \frac{3}{x^2+6}\left(\frac{x}{\sqrt{3}}\sin(\frac{x}{\sqrt{3}}) + \cos(\frac{x}{\sqrt{3}})\right)\right] \qquad (5.37)\\ \hat{\psi}^{\rm CDM} &= \frac{3A_{\rm in}}{2x}\left[1 - \frac{6}{x^2+6}\left(\frac{x}{\sqrt{3}}\sin(\frac{x}{\sqrt{3}}) + \cos(\frac{x}{\sqrt{3}})\right)\right]. \qquad (5.38)\end{aligned}$$

In the subhorizon limit this solution reduces to

$$\begin{aligned}\delta^{\rm CDM} &= \frac{3A_{\rm in}}{2}\left[\ln(\frac{x}{\sqrt{3}}) + \underbrace{\gamma_{\rm E} - \frac{1}{2}}_{\approx 0.077}\right] \qquad (5.39)\\ \hat{\psi}^{\rm CDM} &= \frac{3A_{\rm in}}{2}\frac{1}{x}, \qquad (5.40)\end{aligned}$$

which fixes the constants C and D in Eqs. (5.30) and (5.31).

We are now able to calculate the enhancement factor

$$\mathcal{E}(\eta) \equiv \left[\frac{\delta_{\rm transition}}{\delta_{\rm no\ transition}}\right]^{\rm CDM}(\eta)\ . \tag{5.41}$$

Let us evaluate $\mathcal{E}$ at equality, i.e., $\eta_{\rm eq}/\eta_+ \approx 2\times 10^8$:

$$\mathcal{E}(\eta_{\rm eq}) \approx 1 + \left[\frac{1}{2}\left(\frac{\Delta\eta}{\eta_+}\right)^2 \hat{\psi}_-^{\rm RAD}\right] k\eta_+ \ln(\frac{\eta_{\rm eq}}{\eta_+}) \Big/ \ln(\frac{k\eta_{\rm eq}}{\sqrt{3}})\ . \tag{5.42}$$

The enhancement at the smallest scales $M^{\rm CDM} \sim 10^{-20} M_\odot$ to which our calculation applies and at some intermediate scale $M^{\rm CDM} \sim 10^{-15} M_\odot$ reads

$$\mathcal{E}(\eta_{\rm eq}) \approx \left\{\begin{array}{ll} 600(20) & \text{bag model} \\ 10(2) & \text{lattice fit}\end{array}\right\} \quad \text{for } 10^{-20}(10^{-15})M_\odot\ , \tag{5.43}$$

where we have used Eq. (5.18) for the case of the lattice fit. This shows that both models lead to large enhancements of the CDM density contrast at equality for small enough scales. For the lattice fit the enhancement becomes important at scales below $M^{\rm CDM} \sim 10^{-15} M_\odot$.

5.5 CDM clumps

CDM in the form of axions or PBHs is not subject to damping as the radiation fluid, thus the peaks in CDM will survive until structure formation starts. The free streaming scale of CDM is way below our smallest scales, because the initial velocity of axions or PBHs is completely negligible. An overdensity of CDM in the form of axions or PBH (or any other matter that is kinetically decoupled at the QCD epoch) decouples from the cosmic expansion when its density contrast becomes nonlinear, $(\delta\rho/\rho)_R \sim 1$ (condition for turn around). It collapses and virializes by violent gravitational relaxations and forms a clump of CDM. For spherical collapse the final viral radius is half of the radius at turn around [126].

We take a COBE [60] normalized spectrum and allow for a tilt $|n-1| \leq 0.2$. During the radiation dominated regime, $(\delta\rho/\rho)_k$ for CDM continues to grow logarithmically. In $(\delta\rho/\rho)_R^2$ another logarithm comes from summing modes up to $k \sim 1/R$, where R is the radius of the window function. The enhancement factor $\mathcal{E}$ of CDM density fluctuations during the QCD transition has been obtained in Eq. (5.41). Putting these factors together we obtain the amplitude of CDM perturbations of size R at the time of equality:

$$\left(\frac{\delta\rho}{\rho}\right)_R^{\rm CDM}(t_{\rm eq}) \approx 2\times 10^{-4}\left(\frac{k}{k_0}\right)^{\frac{n-1}{2}}\left[\ln(\frac{k}{k_{\rm eq}})\right]^{\frac{3}{2}} \mathcal{E}_k(t_{\rm eq}) \tag{5.44}$$

k_0 denotes the comoving wave number of the mode crossing the horizon today. In the following we assume $\Omega_0 h^2 = 1/4$, and thus $z_{\rm eq} \approx 6000$. For a CDM mass of $10^{-15}(10^{-20})M_\odot$ a tilt of $n-1 = 0.2$ gives a factor $\approx 16(23)$. The logarithms contribute another factor $\approx 94(140)$. The enhancement factor has been calculated in section 5.4 to be $\mathcal{E}(t_{\rm eq}) \approx 2(8)$ for the lattice QCD fit. Looking at 3σ peaks we find without tilt $(n-1=0)$

$$\left(\frac{\delta\rho}{\rho}\right)_R^{3\sigma,n=1}(t_{\rm eq}) \approx 0.1(0.6) \quad \text{for } M_{\rm clump} = 10^{-15}(10^{-20})M_\odot \,. \tag{5.45}$$

This implies that these clumps go nonlinear at $z_{\rm nl} \approx 600(3600)$ and collapse to clumps of radius $R_{\rm clump} \approx 14(0.04)R_\odot$. With tilt $(n-1=0.2)$ we find

$$\left(\frac{\delta\rho}{\rho}\right)_R^{3\sigma,n=1.2}(t_{\rm eq}) \approx 2(16) \quad \text{for } M_{\rm clump} = 10^{-15}(10^{-20})M_\odot \,. \tag{5.46}$$

These over-densities start to collapse even before $t_{\rm eq}$ because locally CDM starts to dominate at $\sim 2(16)T_{\rm eq}$. This leads to clump radii of $R_{\rm clump} \approx 0.7(0.003)R_\odot$.

We conclude that the peaks in the CDM spectrum lead to clumps of masses $10^{-20} - 10^{-10}M_\odot$. Today, these clumps would have a density contrast of $10^{10} - 10^{17}$, where the lower value corresponds to a $10^{-15}M_\odot$ clump from an untilted CDM spectrum, the bigger value is for a $10^{-20}M_\odot$ clump from a tilted CDM spectrum. The evolution of these clumps in the late stages of structure formation remains to be investigated (disruption, mergers, etc.).

For larger enhancement, e.g., if it should turn out that the latent heat is bigger than the value from present lattice QCD calculations, more compact clumps are possible. These could be subject to femto-lensing [64]. With the values of the lattice fit (2.5), the CDM clumps are not compact enough to lie within the Einstein radius, which is $R_{\rm E} \sim 0.02R_\odot$ for a $10^{-15}M_\odot$ clump.

The clumping of CDM changes the expected reaction rates for some dark matter searches, because some of the rates depend on the space-time position of the detector, star, or planet. Especially experiments looking for axion decay in strong magnetic fields [63, 88] would not yield limits on the axion mass. Maybe these experiments just tell us that we are not sitting in an axion cloud currently. These consequences remain to be studied further.

Chapter 6

A smooth QCD crossover

It is possible that the cosmological QCD transition is a smooth crossover from a QGP to a HG. In this situation no bubbles are nucleated and the relevant scale is the Hubble scale. Below I use the equation of state (2.6) for a crossover. As can be seen from Figs. 2.3 and 2.4, $w \equiv p/\rho$ and the sound speed c_s^2 drop below 1/3 around the transition temperature $T_\star$. But note that neither w nor c_s^2 vanish. The reduction of w causes a change in the Hubble expansion. The reduction of the sound speed leads to an amplification of density perturbations at the Hubble scale and enhances the probability of black hole formation. The latter effect has no observable consequences unless the primordial spectrum of density fluctuations is fine-tuned, as discussed in section 5.2. The spectra of density perturbations [24] and gravitational waves [28] are modified. The modification is of order unity only, thus I expect that no effect survives in the small scale distribution of matter: In the radiation fluid a little peak at the Hubble scale is damped away by the time of BBN (see section 5.3 and in kinetically decoupled matter the effect might not be big enough to induce a preferred clumping scale.

Gravitational waves do not feel the various damping mechanisms and never undergo mode mixing due to nonlinearities. As I show below, a step is imprinted in the spectrum of primordial gravitational waves by the cosmological QCD transition. I discuss the evolution of gravitational waves through a crossover QCD transition and through a first-order transition below. It turns out that the effect is basically the same in both cases.

6.1 Evolution of gravitational waves

Primordial gravitational waves are predicted to be generated during inflation [75, 110] and could be detected with upcoming cosmic microwave background observations. Defects, like cosmic strings, produce stochastic gravitational waves as well [113]. Inflation and defects predict an almost scale-invariant energy density per logarithmic frequency interval for the most interesting frequencies ($\sim 10^{-8}$ Hz for pulsar timing, $\sim 10^{-3}$ Hz for LISA, and ~ 100 Hz for LIGO) of gravitational waves.

The line element of gravitational waves is given by

$$\mathrm{d}s^2 = -\mathrm{d}t^2 + a^2(\delta_{ij} + h_{ij})\mathrm{d}x^i \mathrm{d}x^j \ . \tag{6.1}$$

h_{ij} is a transverse, traceless tensor. The spatial average $\langle h_{ij}(x) h^{ij}(x+r)\rangle = \int j_0(kr) k^3 |h_k|^2 \mathrm{d}\ln k$ defines the power spectrum $|h_k|^2$. We define the rms amplitude h of a gravitational wave per logarithmic frequency interval: $h \equiv k^{3/2}|h_k|$. The linearized equation of motion for $h(t)$ reads

$$\ddot{h} + 3H\dot{h} + \frac{k^2}{a^2} h = 0 \ , \tag{6.2}$$

where the differentiation is taken with respect to cosmic time t. The amplitude of gravitational waves is constant on superhorizon scales and decays as $1/a$ after horizon crossing, $h \simeq C_k \sin(k\eta + \delta_k)/a$, where $\eta = \int \mathrm{d}t/a$ is conformal time. C_k and δ_k are determined by matching to the superhorizon solution.

For subhorizon modes, $k_{\mathrm{ph}} \gg H$, the energy density of gravitational waves can be defined. The space-time average of the energy-momentum tensor over several wavelengths gives $\rho_{\mathrm{g}} = -(M_{\mathrm{P}}^2/32\pi)\langle \dot{h}_{ij}\dot{h}^{ij}\rangle$. The energy density per logarithmic interval in k is related to the rms amplitude h:

$$k\frac{\mathrm{d}\rho_{\mathrm{g}}}{\mathrm{d}k} = \frac{M_{\mathrm{P}}^2}{32\pi} k_{\mathrm{ph}}^2 \frac{1}{2} h^2 \ . \tag{6.3}$$

The factor of $1/2$ comes from the time average over several oscillations. The energy fraction in gravitational waves, per logarithmic interval in k, is defined by

$$\Omega_{\mathrm{g}}(k) \equiv k \frac{\mathrm{d}\rho_{\mathrm{g}}}{\mathrm{d}k}\frac{1}{\rho_{\mathrm{c}}} \ , \tag{6.4}$$

where $\rho_c \equiv 3M_{\mathrm{P}}^2 H_0^2/(8\pi)$.

Figure 6.1 shows the transfer function $\Omega_{\mathrm{g}}(f)/\Omega_{\mathrm{g}}(f \ll f_\star)$ from a numerical integration of Eq. (6.2) through the cosmological QCD transition. The typical frequency scale is

$$f_\star \approx 1.36 \left(\frac{g}{17.25}\right)^{\frac{1}{2}} \frac{T_\star}{150\mathrm{MeV}} 10^{-7}\mathrm{Hz} \ , \tag{6.5}$$

which corresponds to the mode that crosses the Hubble horizon at the end of the bag model QCD transition. Scales that cross into the horizon after the

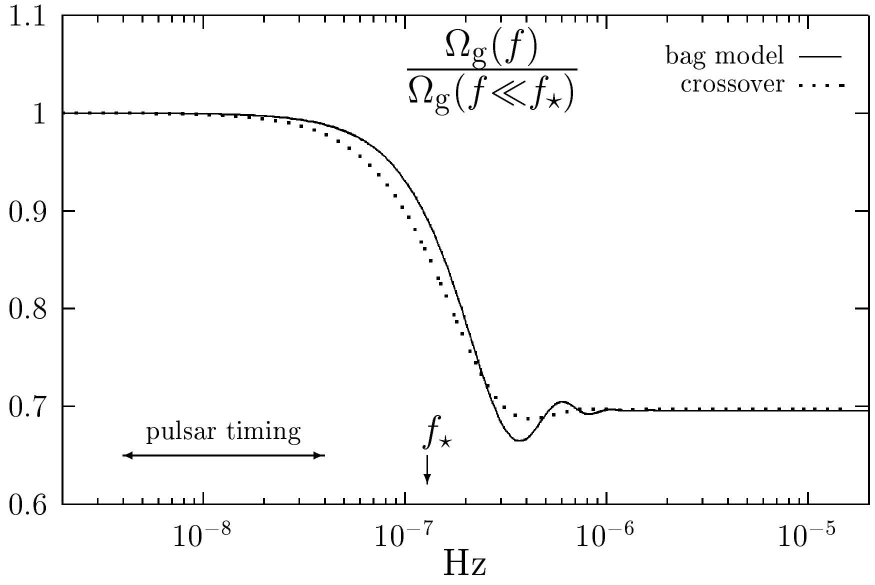

Figure 6.1: The modification of the energy density, per logarithmic frequency interval, for primordial gravitational waves from the QCD transition.

transition (l.h.s. of the figure) are unaffected, whereas modes that cross the horizon before the transition are damped by an additional factor ≈ 0.7. The modification of the differential spectrum has been calculated for a first-order QCD transition (bag model), Eqs. (1.11) and (1.12), and a crossover QCD transition, Eq. (2.6), with $\Delta T/T_\star = 0.3$. In both cases the step extends over one decade in frequency. The detailed form of the step is almost independent from the order of the transition. To solve Eq. (6.2) numerically, it proofs useful to use the scale factor as evolution parameter for the first-order transition and the temperature for the crossover transition. a and T are related by Eq. (2.7).

The size of the step can be calculated analytically: Long before and after the transition, in the radiation dominated era,

$$H \propto g^{-1/6} a^{-2} , \tag{6.6}$$

from the Friedmann equation and the conservation of entropy. On the other hand, $k_{\rm ph} \propto 1/a$, independently of the equation of state. Thus, the rate at which modes enter the Hubble horizon is changing during the transition. This change leads to the step in the transfer function.

For a fixed mode $k_{\rm a}$ that crosses the horizon after the phase transition the amplitude h is constant during the transition, the transfer function is one. Now, consider a mode $k_{\rm b}$ that crosses the horizon before the transition. Its amplitude decays proportionally to $a_{\rm hc}/a$. From Eqs. (6.3) and (6.4) we find

$$\Omega_{\rm g}(k_{\rm b}) \propto k_{\rm ph}^2 a_{\rm hc}^2 \propto g_{\rm b}^{-1/3} \ , \tag{6.7}$$

where we have used Eq. (6.6) and $k_{\rm ph} = H$ at horizon crossing. The constants of proportionality have been neglected in Eq. (6.7), because they drop out from the transfer function below. Comparing the differential energy spectrum for modes that cross into the horizon before the transition and for modes that cross into the horizon after the transition gives the ratio

$$\frac{\Omega_{\rm g}(f \gg f_\star)}{\Omega_{\rm g}(f \ll f_\star)} = \left(\frac{g_{\rm a}}{g_{\rm b}}\right)^{\frac{1}{3}} \approx 0.696 \ , \tag{6.8}$$

for the QCD transition, which coincides with the numerical integration in Fig. 6.1. The size and position of the step in the logarithmic spectrum is independent of the order of the transition!

The result (6.8) is in agreement with the entropy conservation of subhorizon gravitational waves [68, 111, 112]. However, for superhorizon modes the entropy is not defined.

Let us estimate the slope of the step in the transfer function. From the Friedmann equation and the 1st law of thermodynamics we obtain the Hubble rate as a function of the scale factor ($w \equiv p/\rho$)

$$\mathrm{d}\ln H(a) = -\frac{3}{2}[1 + w(a)]\mathrm{d}\ln a \ . \tag{6.9}$$

For $0 < w \leq 1/3$ during the phase transition the Hubble expansion changes during the transition, i.e., $H \propto a^{-\beta}$ with $\beta = \beta(a)$ in the range $(3/2, 2)$. This holds true if the change in w is small, i.e. $(\mathrm{d}w/\mathrm{d}a)\Delta a \ll 1 + w$. To estimate the exponent

$$n(f) \equiv \frac{\mathrm{d}\ln \Omega_{\rm g}(f)}{\mathrm{d}\ln f} \tag{6.10}$$

we use the relation $\mathrm{d}\ln f = \mathrm{d}\ln(Ha)_{\rm hc} = [-(1{+}3w)/2\ \mathrm{d}\ln a]_{\rm hc}$ and Eqs. (6.3) and (6.4). We find

$$n(f) \simeq -2\frac{1 - 3w(a_{\rm hc})}{1 + 3w(a_{\rm hc})} \ , \tag{6.11}$$

which takes values between -2 and 0 for w between 0 and $1/3$. From the numerical integration (see Fig. 6.1) we find that the minimum of the exponent is $n \approx -0.8$ for the bag model, which corresponds to an effective value $w_{\rm eff} \approx 0.15$. This is consistent with the values $w(a) \in (0.09, 1/3)$ that are taken during the first-order QCD transition. For the crossover transition the drop in w is smaller and thus the step is not as steep as in the first-order transition.

Similar steps in the differential spectrum have been studied for gravitational waves generated by cosmic strings [113]. These gravitational waves are generated on subhorizon scales when the cosmic strings decay. Their frequency is $> \alpha^{-1}H$, where α is the ratio between the typical size of a string loop and the Hubble radius at formation of the loop. α is smaller than 0.1 and might be as small as 10^{-5} [114]. In this situation steps in the differential spectrum follow from the conservation of entropy for decoupled species (gravitons) during cosmological phase transitions [115]. This interpretation applies to modes that have been inside the horizon long before the transition or that have been generated on subhorizon scales. However, for superhorizon modes entropy and energy of a gravitational wave are not defined. We therefore cannot rely on the conservation of entropy argument when dealing with gravitational waves from inflation.

In Fig. 6.1 we indicated the frequency range ($\sim 1\ \mathrm{yr}^{-1}$) in which limits on Ω_{g} have been reported from pulsar timing residuals [77]. The frequencies where the step of the QCD transition would be visible is of the order $0.3\ \mathrm{month}^{-1}$. For pulsar timing the power spectrum of gravitational waves is more relevant than the energy spectrum. The power spectrum is $\propto \Omega_{\mathrm{g}}(f) f^{-5}$. Our results show that the power spectrum might deviate from the f^{-5} behavior over a whole decade in frequency. Depending on the effective value of w during the transition it might be as steep as f^{-7} (for $w = 0$). However, a realistic estimate for the QCD transition gives $w_{\mathrm{min}} \geq 0.1$. Thus, the spectral index of the power spectrum, $n - 4$, lies, according to Eq. (6.11), between -6.1 and -5.

Chapter 7

Conclusions and open questions

The cosmological QCD transition might give rise to various interesting and important effects (clumps of CDM, inhomogeneous nucleosynthesis, quark nuggets, ...). However, none of these effects has been observed yet. What can be learned from that?

The observed primordial element abundances are consistent with the predictions of homogeneous BBN [18] and with the predictions of inhomogeneous BBN, if $d_{\rm nuc} = \mathcal{O}(10\ {\rm m})$ at $T_\star$ [16, 17]. Four possibilities are open: 1. the QCD transition is a crossover and there are no baryon inhomogeneities at all, 2. the QCD transition is of first order, but $d_{\rm nuc} < d_{\rm p-diff}$, thus BBN is homogeneous, 3. the QCD transition is of first order and $d_{\rm nuc} > d_{\rm p-diff}$, but the fraction of baryons that concentrate in clouds is negligible, thus BBN is homogeneous, 4. the QCD transition is of first order and $d_{\rm nuc} > d_{\rm p-diff}$ and a significant amount of baryons is concentrated in clouds, thus BBN is inhomogeneous.

How can we discriminate among those options? Eventually, lattice QCD will provide the order of the QCD phase transition and determine the most important parameters, like $T_\star, l$ and σ. If the QCD transition is found to be of first order, the amount of supercooling $\Delta_{\rm sc}$ might be determined from $T_\star, l$, and σ (see chapter 3).

Precision observations of the cosmic microwave background on small angular scales by MAP (launch in fall 2000) and PLANCK (launch in 2003) [117] will fix the spectral slope of density perturbations up to 1% or better. Thus $\Delta_T^{\rm rms}$ for subhorizon scales at the QCD epoch will be known in a few years. Together with $\Delta_{\rm sc}$ from lattice QCD we then know whether homogeneous or inhomogeneous bubble nucleation took place in the early Universe (see chapter 3).

Improved observations of element abundances [e.g. new deuterium observations in the ultraviolet by FUSE (launch in February 1999) [116]] and improved models of the chemical evolution of the Universe may rule out either homogeneous or inhomogeneous BBN (see chapter 4).

No quark nuggets have been observed yet. This does not tell us about the QCD transition in the first place. It probably means that strange matter is not the ground state of matter, or that the strange quark nuggets from the cosmological QCD transition are too small to survive evaporization. The nonexistence of quark nuggets might put strong limits on the spectral index of density perturbations, if quark nuggets are stable [118].

No CDM clouds have been observed so far. This is no surprise, since the sensitivity of the observations is not sufficient yet. First femto-lensing results became available only recently [119]. Compact objects with masses $10^{-16} M_{\odot}$ – $10^{-9} M_{\odot}$ are excluded to contribute more than $\Omega = 0.2$. The femto-lensing mass range overlaps with the predicted masses of CDM clumps from a first-order QCD transition (see chapter 5). Moreover, as long as it is unclear what the nature of the CDM is, we cannot draw any conclusions for the QCD transition.

Of course, no modification of the gravitational wave spectrum (see chapter 6) has been detected, since gravitational waves have not been seen yet [120]. This hopefully will change in the next years with large laser interferometers (LIGO, VIRGO, LISA) and with precision cosmic microwave background observations [121].

Upcoming observations and new lattice QCD data might be able to test our models of the cosmological QCD transition.

What to do, except waiting for new observations and new lattice QCD data? Some of the issues that deserve deep thoughts are:

- In order to determine $d_{\rm nuc}$ it is important to understand how latent heat is redistributed during bubble nucleation, i. e. what is $v_{\rm heat}(t)$?

- What happens at the phase interface? Is the baryon flux suppressed?

- Could the large inhomogeneities in the radiation fluid from the QCD transition induce turbulence? Would this wash out any baryon number inhomogeneity?

- How do preexisting axion mini-cluster [90] react on the large potential wells from the inhomogeneities in the radiation fluid?

- If axions come in clumps today, how does this affect the laboratory experiment in Livermore [122] quantitatively?

Let me mention that Brandenberger, Halperin, and Zhitnitsky [29] suggested a mechanism for baryogenesis at the QCD scale recently. In their mechanism baryon number is not violated globally (there are no baryon number violating processes in QCD), but their mechanism separates the baryons and the anti-baryons. Only the baryons would be visible today, the anti-baryons are trapped into so-called B-shells, which contribute to the dark matter today. If this scenario works, there would be at least one observable due to the QCD scale: the fact that we are made out of baryons.

Although the scale of the cosmological QCD transition is only two orders of magnitude above the scale of nucleosynthesis, there is plenty of fascinating physics and surprises should be expected in the future.

Appendix A

The Friedmann model

Let me briefly present the Friedmann model. Here I concentrate on those aspects that are important for the radiation dominated Universe. More details can be found in various textbooks [123, 112, 124, 125, 126].

The cosmological principle states that the Universe is spatially homogeneous and isotropic on large scales, i.e. $\lambda \gg 1$ Mpc, which is the typical distance between galaxies. This principle should be understood in a statistical sense, e.g. the expectation value of any physical observable should be independent of spatial position and direction. The isotropy with respect to one point (the Earth) has been confirmed observationally by the isotropy of the cosmic microwave background (CMB). Apart from a dipol due to our proper motion, anisotropies exist at the 10^{-5} level only [59, 60]. If we assume that we are not special observers (Kopernikanian principle) we have to conclude that space is isotropic with respect to all points in space. If we further assume that the metric of space-time is analytic, the homogeneity of space follows [127].

The most general spatially homogeneous and isotropic metric is given by the Robertson-Walker line element

$$\mathrm{d}s^2 = -\mathrm{d}t^2 + a^2(t)\left(\frac{\mathrm{d}r^2}{1-Kr^2} + r^2[\mathrm{d}\theta^2 + \sin^2\theta \mathrm{d}\phi^2]\right) , \tag{A.1}$$

with $K = 0, \pm 1$. $a(t)$ is the scale factor. All distances scale with a, a comoving volume V scales with a^3. The present value of the scale factor is denoted by a_0 and can be chosen arbitrarily. The values of K are related to the spatial geometry. The intrinsic 3-curvature reads:

$$\mathcal{R} = \frac{6K}{a^2} . \tag{A.2}$$

The expansion of 3-space is given by $\mathrm{d}V/V = 3H\mathrm{d}t$, where $H \equiv \dot{a}/a$ is the Hubble parameter. Recent measurements yield values of $H_0 = 100h$

km/s/Mpc with $0.5 < h < 0.8$. This sets the scale for the causal size and for the age of the Universe: the Hubble radius is $\approx 3000h^{-1}$ Mpc today and the Hubble age is $\approx 9.78h^{-1}$ Gyr. Due to the expansion of the Universe the momentum of a freely streaming particle is redshifted $\propto 1/a$. The redshift of photons is defined by $z \equiv \Delta\lambda/\lambda = a_0/a - 1$.

On large scales ($\gg 1$ Mpc) matter may be described as a fluid. From isotropy the vanishing of anisotropic stress and heat flow follows. Thus, the fluid is a perfect fluid. Let me denote the fluid 4-velocity by u^μ. Then, the energy momentum tensor reads

$$T^{\mu\nu} = (\rho + p)u^\mu u^\nu + p g^{\mu\nu} \tag{A.3}$$

where $\rho = \rho(t)$ denotes the energy density and $p = p(t)$ the pressure. The covariant conservation of the energy momentum tensor gives

$$\dot\rho = -(p + \rho)3H \ , \tag{A.4}$$

which is nothing but the first law of thermodynamics, $\mathrm{d}U = -p\mathrm{d}V$. As mentioned above, the heat flow vanishes due to the isotropy and thus the entropy is constant, $\mathrm{d}S = 0$, for reversible processes from the second law of thermodynamics. The relation between the pressure and the energy density is provided by the equation of state. For the most important cases in cosmology the equation of state reads:

$$p = \begin{cases} 0 & \text{matter(dust)} \\ \rho/3 & \text{radiation} \\ -\rho & \text{vacuum} \end{cases} . \tag{A.5}$$

From (A.4) we find:

$$\rho \propto \begin{cases} a^{-3} & \text{matter(dust)} \\ a^{-4} & \text{radiation} \\ 1 & \text{vacuum} \end{cases} . \tag{A.6}$$

Recent observations indicate that a cosmological constant $\Lambda \equiv 8\pi\rho_{\mathrm{VAC}}$ might exist. The Hubble diagram from high redshift Ia supernovae suggests that $\Lambda = 0.2h^2/\mathrm{Gpc}^2$ [128].

In the radiation dominated Universe spatial curvature and a cosmological constant can be neglected. This is easily seen from comparing (A.2) with (A.6). For $a \to 0$ the energy density of radiation grows much faster than $\mathcal{R}/G$. At very late times a cosmological constant would dominate the evolution. In the intermediate epochs matter and/or curvature might dominate.

The equation of motion for the scale factor follows from the time-time component of the Einstein equation. This equation is called the Friedmann equation:

$$H^2 + \frac{K}{a^2} = \frac{8\pi G}{3}\rho \ . \tag{A.7}$$

If $K = 0$, the Hubble parameter determines the critical energy density $\rho_c \equiv 3H^2/8\pi G \approx 1.9 \times 10^{-24} h^2$ g cm^{-3}. This allows us to quantify the matter content of the Universe by the dimensionless parameter

$$\Omega \equiv \frac{\rho}{\rho_c} = 1 + \frac{K}{a^2 H^2} \; . \tag{A.8}$$

From observations Ω_0 is expected to lie in the range $0.2 < \Omega_0 \leq 1$. The theory of inflation predicts that $\Omega = 1$ [112, 124]. If the strong energy condition, $\rho + 3p > 0$, holds, $\Omega = 1$ is an unstable fix point, because aH is a monotonic decreasing function of time. From this point of view it is a miracle why we live in an epoch with $\Omega_0 = \mathcal{O}(1)$. This is the so-called flatness problem. Inflation solves this problem by violating the strong energy condition. A vacuum dominated epoch inflates the Universe until $\Omega = 1$, because aH is growing exponentially during inflation. By the same mechanism inflation allows that CMB photons from antipodal regions on the sky can have the same temperature, because they may be in causal contact. Without inflation this would be impossible (horizon problem). At the end of inflation the Universe is heated, i.e. the energy from the coherent motion of scalar fields goes into particle and entropy production. The Universe ends up to be radiation dominated with a temperature $T \gg 100$ GeV. This temperature follows because 'new physics' is needed to explain the genesis of the observed baryon asymmetry.

In the radiation dominated epochs the most important events are the electroweak transition, the QCD transition, and the era of nucleosynthesis. The energy density in the radiation dominated Universe reads $\rho = (\pi^2/30) g T^4$, see (1.2). Thus, while $g(T) = \text{const.}$, $T \propto 1/a$. In general, the conservation of entropy implies $\mathrm{d}(g(T) T^3 a^3) = 0$. Neutrinos do not interact with other matter below a temperature of ~ 1 MeV. This follows from the comparison of the neutrino interaction rate $\Gamma_\nu \sim G_\mathrm{F}^2 T^5$ and the Hubble rate $H \sim T^2/M_\mathrm{Pl}$. At $T \sim 0.2$ MeV e^+e^- pairs annihilate into photons. This increases the photon temperature T, but the neutrino temperature T_ν is unaffected. The conservation of entropy for the neutrinos and for the photons plus $e^\pm$ separately gives

$$T_\nu = \left(\frac{4}{11}\right)^{\frac{1}{3}} T \; . \tag{A.9}$$

The temperature of the CMB, which has been measured by COBE to be $T_0 = 2.728 \pm 0.002$ [129]. According to (A.9) todays neutrino temperature is 1.95 K and $g(T_0) = 2 + 21/4(4/11)^{4/3} \approx 3.363$.

The moment when the energy density in radiation and matter are equal, $\rho_\mathrm{RAD}(a_\mathrm{eq}) = \rho_\mathrm{MAT}(a_\mathrm{eq})$, is called equality. The scale factor at equality is

$$\frac{a_\mathrm{eq}}{a_0} \approx 4.15 \times 10^{-5} \Omega_\mathrm{MAT}^{-1} h^{-2} \tag{A.10}$$

and the comoving Hubble radius at equality reads

$$R_{\rm H}^{\rm eq}(a_0) \approx 13.7\Omega_{\rm MAT}^{-1}h^{-2}{\rm Mpc}\ . \tag{A.11}$$

After equality the Universe is matter dominated. The most important events are the start of structure formation at equality and the formation of atoms and decoupling of photons at redshifts $z_{\rm atom} \approx 1300$ and $z_{\rm dec} \approx 1100$ resp. The epoch of nonlinear structure formation starts at $z = \mathcal{O}(10)$. Some issues (linear perturbations) of structure formation are discussed in Appendix B.

Let me finally solve the time dependence of the scale factor taking matter and radiation into account. From Eq. (A.7) and $\rho_{\rm MAT}(a_{\rm eq}) = \rho_{\rm RAD}(a_{\rm eq}) = \rho(a_{\rm eq})/2$ we find

$$\frac{\dot a^2}{a_{\rm eq}^2} = \frac{4\pi G}{3}\rho(a_{\rm eq})\left[\frac{a_{\rm eq}}{a} + \left(\frac{a_{\rm eq}}{a}\right)^2\right]\ . \tag{A.12}$$

Let me introduce conformal time η via

$$d\eta \equiv \frac{dt}{a(t)} \tag{A.13}$$

and denote derivatives with respect to conformal time by $(\cdot)'$. Then Eq. (A.12) reads

$$\frac{(a')^2}{a_{\rm eq}^2} = \frac{4\pi G}{3}\rho(a_{\rm eq})a_{\rm eq}^2\left(\frac{a}{a_{\rm eq}} + 1\right)\ . \tag{A.14}$$

Integration of (A.14) with the initial condition $a(0) = 0$ gives

$$\frac{a}{a_{\rm eq}} = (\sqrt{2}-1)^2\left(\frac{\eta}{\eta_{\rm eq}}\right)^2 + 2(\sqrt{2}-1)\frac{\eta}{\eta_{\rm eq}}\ , \tag{A.15}$$

where $(\sqrt{2}-1)/\eta_{\rm eq} \equiv [(\pi G/3)\rho(a_{\rm eq})a_{\rm eq}^2]^{1/2}$. In the radiation dominated epoch $a \propto \eta \propto t^{1/2}$, in the matter dominated epoch $a \propto \eta^2 \propto t^{2/3}$.

Appendix B

Cosmological Perturbations

To describe the formation of structure (galaxies, clusters, voids, ...) we need to go beyond the isotropic, homogeneous models. The idea is that the large-scale structure of the Universe is seeded by quantum fluctuations during inflation.

Quantum fluctuations in the distribution of matter and of the space-time geometry become classical fluctuations during inflation and are frozen in until equality. At equality these small fluctuations start to grow on all scales. The most overdense regions evolve through the nonlinear action of gravity into the large-scale structure of the Universe. This picture has been confirmed by the observation of tiny anisotropies in the cosmic microwave background (CMB) with the COBE satellite and by redshift surveys as well as by numerical simulations.

The simplest model of structure formation (standard cold dark matter model) assumes a scale invariant Harrison-Zel'dovich spectrum for the primeval density fluctuations (inflation predicts such a spectrum) and it assumes that the dominant matter component of the Universe is cold dark matter (CDM) (baryons alone cannot explain the structures that are observed). The amplitude of the spectrum is normalized to the CMB anisotropies measured with COBE [60]. Although the standard CDM model cannot explain the observed galaxy two-point correlations (it overproduces structure on scales below ~ 10 Mpc), it may serve as a reference model and it is sufficient for a qualitative study of structure formation.

This appendix deals with linear cosmological perturbations. In the radiation dominated Universe perturbations are small enough to restrict the discussion to linear perturbations. The starting point are the Friedmann models (Appendix A). The metric and the variables that describe matter are perturbed around a Friedmann background. The perturbations are classified according to their transformation properties under spatial coordinate transformations into scalar, vector, and tensor perturbations. The physical meaning of this decomposition is that perturbations in energy density (scalar), rotational flows (vector), and gravitational waves (tensor) evolve independently. The mapping between the physical space-time and the Friedmann background is not unique. This freedom in choice of coordinates is called the gauge freedom of cosmological perturbations. Various gauges have been proposed in the literature to fix this freedom. In the scalar sector the most prominent gauges are the synchronous gauge (the observer uses coordinates that are adapted to her clock), the comoving gauge (the observer is comoving with matter), the zero shear gauge (the observers spatial hypersurfaces are free of shear), the uniform expansion gauge (the observed volume expansion agrees with the volume expansion of the background), and the uniform density gauge (the spatial hypersurfaces of the observer have constant energy density). Inflation does not seed rotational perturbations. Thus we expect that vector perturbations can be neglected on large scales. The tensor sector is free of gauge degrees of freedom.

Below I discuss the scalar and tensor perturbations in some detail. I follow Bardeen 1989 [56] and focus on the geometric properties of the constant-t (spatial) hypersurfaces (slices) Σ. I restrict the discussion to time-orthogonal slicings of space-time. A different point of view follows from the use of gauge-invariant description [130, 131, 57], however it turns out that the gauge-invariant quantities of Bardeen 1980 coincide with the zero shear slicing. I restrict the discussion to a spatially flat ($K = 0$) Friedmann background, because curvature is negligible in the radiation dominated Universe (see Appendix A).

B.1 Scalar Perturbations

For a time-orthogonal foliation of space-time the perturbed metric can be written as

$$ds^2 = -\,(1+2\alpha)\,dt^2 + a(t)^2\,[\delta_{ij}(1+2\varphi) + 2\partial_i\partial_j\gamma]\,dx^i dx^j \ , \tag{B.1}$$

with $\partial_i \equiv \partial/\partial x^i$. The perturbation of the lapse function is given by $\alpha(\mathbf{x}, t)$. Thus $1 + \alpha$ measures the lapse of physical time between the slices Σ_t and $\Sigma_{t+\mathrm{d}t}$. The intrinsic curvature of the spatial hypersurface Σ is generated by $\varphi(\mathbf{x}, t)$,

$$\mathcal{R}[\Sigma] = -4 \triangle \varphi \ . \tag{B.2}$$

The extrinsic curvature $K^i{}_j$ of Σ has 3 terms, the unperturbed term, the perturbation of the isotropic part, $\delta[\mathrm{tr}K^i{}_j(\Sigma)] \equiv \kappa$, and the anisotropic part ($\equiv$ shear of normals on Σ), which is generated by $\chi(\mathbf{x}, t)$,

$$K^i{}_j[\Sigma] = -H\delta^i{}_j + \frac{1}{3}\kappa\delta^i{}_j - (\partial^i\partial_j - \frac{1}{3}\triangle\,\delta^i{}_j)\chi \ , \tag{B.3}$$

where $\partial^i = a^{-2}\delta^{ij}\partial_i$. These geometric properties of Σ are computed from the metric perturbations as follows, $\chi = a^2\dot{\gamma}$, $\kappa = -3\left(\dot{\varphi} - H\alpha\right) - \triangle\chi$. Vanishing shear of the normal vector $\underline{n}(\Sigma)$ means $\chi = 0$ and vice versa, but note that χ (resp. γ) contributes both to the anisotropic part and to the isotropic part of $K^i{}_j$.

Here I focus on a slicing of space-time with unperturbed mean extrinsic curvature, $\delta[\mathrm{tr}K^i{}_j(\Sigma)] \equiv \kappa = 0$. This implies that fundamental observers, which are at rest on the slice Σ, $\underline{u}(\mathrm{obs}) = \underline{n}(\Sigma)$, have relative velocities, which in the mean over all directions follow the unperturbed Hubble flow. If the coordinate choice (gauge choice) is such that the time coordinate t is constant on the slices Σ, the gauge is fixed to be the Uniform Expansion Gauge (UEG) $\equiv$ Uniform Hubble Gauge (UHG) [56].

In the literature the most common gauges are the synchronous gauge, where the fundamental observers are moving inertially (i.e. $\alpha \equiv 0$), the longitudinal gauge ($\equiv$ zero shear gauge, $\chi \equiv 0$), where the fundamental observers expand isotropically, and the comoving gauge, where the fundamental observers sit in the fluid rest frame, $\underline{u}(\mathrm{obs}) = \underline{u}(\mathrm{matter})$. The uniform expansion gauge (UEG) is free of spurious gauge modes (in contrast to the synchronous gauge), it is nonsingular in the superhorizon limit and therefore easy to handle in numerical calculations (in contrast to zero-shear variables, as pointed out by Bardeen [56]), and it has the two basic fluid variables $\delta\rho$ and v_{peculiar} (in contrast to the comoving gauge).

As fundamental evolution equations in UEG for perfect fluids it is useful to take the energy-momentum conservation $\nabla_\mu T^\mu_\nu = 0$, i.e., the continuity equation and the 3-divergence of the Euler equation of general relativity. Each fluid separately must satisfy

$$\begin{aligned} \partial_t\epsilon &= -3H(\epsilon+\pi) - \triangle\psi - 3H(\rho+p)\alpha && \text{(B.4)} \\ \partial_t\psi &= -3H\psi - \pi - (\rho+p)\alpha\ , && \text{(B.5)} \end{aligned}$$

where $\epsilon \equiv \delta\rho = \delta T^0{}_0$, $\pi \equiv \delta p = 1/3\delta[\mathrm{tr}T^i{}_j]$, $\nabla_i\psi \equiv \delta T^0{}_i$ for each fluid separately. Note that $\nabla_i\psi \equiv S_i =$ momentum density (Poynting vector). The system of dynamical equations is closed by Einstein's $R^0{}_0$-equation,

$$(\triangle + 3\dot{H})\alpha = 4\pi G(\epsilon + 3\pi)\ , \tag{B.6}$$

where the sum over all fluids is taken on the right-hand side. In addition we need the Equation of state. For the background $p = p(\rho)$ for adiabatic expansion. The perturbed equation of state in general reads: $\pi = c_s^2\epsilon + \tau\delta S$, where c_s^2 is the isentropic sound speed and $\tau\delta S$ describes perturbations in the entropy per baryon. Perturbations with $\tau\delta S = 0$ are called adiabatic (isentropic) perturbations. Let us concentrate on the latter. Equations (B.4)

– (B.6) define the Cauchy problem for linear, scalar perturbations. The initial data (ϵ, ψ) can be chosen freely on $\Sigma_{\rm UE}$.

Einstein's ${R^0}_0$-equation in linear perturbation theory in UEG is an elliptic equation. Its Green function is a Yukawa potential with exponential cutoff at the Hubble radius, $\alpha \sim r^{-1}\exp(-\mu r)$, where $\mu^2 = -3\dot{H}$, instead of Newton's $1/r$-potential in the Poisson equation. ${R^0}_0$ gives the relative gravitational acceleration (geodesic deviation), averaged over all directions, of two test particles, which are moving nonrelativistically in the coordinate system at hand. In UEG $\delta {R^0}_0$ is determined by α, the perturbation of the lapse. In Newtonian physics the relative acceleration averaged over directions is given by $\Delta\Phi_{\rm Newton}$, i.e. ${R^0}_0$ and $\Delta\Phi_{\rm Newton}$ answer the same physics question. In UEG α plays the role of the gravitational potential. The basic equations have exactly the same structure as the Jeans equations: two first-order time-evolution equations for each fluid, Eqs. (B.4) and (B.5), supplemented by one elliptic equation, Eq. (B.6).

Out of the geometric quantities $(\kappa, \chi, \varphi, \alpha)$ only the lapse α appears in the equations needed to solve the dynamics in UEG. The spatial curvature φ and the shear of the fundamental observers χ are automatically absent from the above equations for perfect fluids, since these geometrical properties of Σ are irrelevant for the dynamical question at hand. One can compute φ and χ at any time from the energy and the momentum constraints, i.e. from the ${G^0}_0$ equation and the longitudinal contribution to the ${G^0}_i$ equation,

$$\triangle\varphi = -4\pi G\epsilon \tag{B.7}$$
$$\triangle\chi = -12\pi G\psi \; . \tag{B.8}$$

Since the evolution equations are linear, and the background is spatially homogeneous, each spatial Fourier mode with comoving wavelength $k \equiv k^{\rm phys}a$ evolves independently. It is convenient to rewrite equations (B.4) – (B.6) in the dimensionless variables $\delta \equiv \epsilon/\rho$ (density contrast) and $\hat{\psi} \equiv k_{\rm phys}\psi/\rho$. The variable $\hat{\psi}$ is related to the fluid velocity (peculiar velocity) $v_{\rm pec} = \frac{\rho}{\rho+p}|\hat{\psi}|$ and has the same order of magnitude as δ on subhorizon scales, $\lambda^{\rm phys} \ll R_{\rm H} = H^{-1}$. In UEG the system of evolution equations, written in terms of conformal time $()' \equiv \partial_\eta \equiv a\partial_t$, now reads

$$\frac{1}{\mathcal{H}}\delta' + 3(c_s^2 - w)\delta = \frac{k}{\mathcal{H}}\hat{\psi} - 3(1+w)\alpha \tag{B.9}$$
$$\frac{1}{\mathcal{H}}\hat{\psi}' + (1-3w)\hat{\psi} = -c_s^2\frac{k}{\mathcal{H}}\delta - (1+w)\frac{k}{\mathcal{H}}\alpha \tag{B.10}$$
$$\left[\left(\frac{k}{\mathcal{H}}\right)^2 + \frac{9}{2}(1+w)\right]\alpha = -\frac{3}{2}(1+3c_s^2)\delta \; , \tag{B.11}$$

with $\mathcal{H} \equiv (da/d\eta)/a$ and $w = p/\rho$. The Friedmann equation and the continuity equation for the background were used. The continuity and Euler equation refer to each fluid separately. In the $R^0{}_0$-equation $w = \sum_f p^{(f)}/\sum_f \rho^{(f)}$, $\delta = \sum_f \epsilon^{(f)}/\sum_f \rho^{(f)}$ and $c_s^2 = \partial \sum_f p^{(f)}/\partial \sum_f \rho^{(f)}$.

It is instructive to look at the superhorizon $\lambda^{\rm phys} \gg H^{-1}$ and at the subhorizon $\lambda^{\rm phys} \ll H^{-1}$ limit of equations (B.9) – (B.11) for general pressure and sound speed.

For superhorizon perturbations with arbitrary equation of state (e.g. QCD transition), we only have to keep the lowest order in $k/\mathcal{H}$ in the evolution equations. The Equations (B.9) – (B.11) for a one fluid model simplify to

$$\frac{1}{\mathcal{H}}\delta' - (1+3w)\delta = \frac{k}{\mathcal{H}}\hat{\psi} \tag{B.12}$$

$$\frac{1}{\mathcal{H}}\hat{\psi}' + (1-3w)\hat{\psi} = \frac{1}{3}\frac{k}{\mathcal{H}}\delta, \tag{B.13}$$

where the superhorizon limit of the Poisson equation $(1+w)\alpha = -\frac{1}{3}(1+3c_s^2)\delta$ was inserted. Note that the sound speed drops out in the superhorizon equations. For the growing mode the terms on the left hand side of the Euler equation add and $\left[\hat{\psi}/\delta\right]_{\rm grow} \propto k/\mathcal{H}$. Therefore, the right hand side of the continuity equation is negligible and the solution for the growing mode of the density contrast is

$$\delta \propto (k/\mathcal{H})^2 = (k_{\rm phys}/H)^2 \tag{B.14}$$

for superhorizon perturbations in the uniform expansion gauge. This result is independent of the thermodynamic behavior. It says that the evolution of the growing superhorizon mode, if expressed in terms of $\mathcal{H}$ (as opposed to expressing it in terms of t or a), is unaffected by a phase transition. Therefore the QCD-transition cannot affect superhorizon scales, and the spectrum of density perturbations stays flat for $\lambda^{\rm phys} \gg H^{-1}$. This result can also be formulated differently: using the energy-constraint (B.7) we find $\varphi = const$ for the dominant mode on superhorizon scales in UEG. This is the 'conservation law' [55, 58] for the quantity $\zeta \equiv \varphi + \frac{1}{3(1+w)}\delta$ for $w \neq -1$, since $\zeta \approx \varphi$ in the superhorizon limit.

For subhorizon analysis, $\lambda^{\rm phys} \ll H^{-1}$, with arbitrary equation of state, one can drop $\dot{H}$ in the general relativistic Poisson equation (B.6) since $|\dot{H}| = O(H^2) \ll k_{\rm phys}^2$. In the continuity equation (B.4) the time dilation term (last term) can be omitted since it follows from the Poisson equation that $\alpha = O(H^2/k_{\rm phys}^2)\delta \ll \delta$. In the subhorizon limit Eqs. (B.9) – (B.11) simplify to

$$\frac{1}{\mathcal{H}}\delta' + 3(c_s^2 - w)\delta = \frac{k}{\mathcal{H}}\hat{\psi} \tag{B.15}$$

$$\frac{1}{\mathcal{H}}\hat{\psi}' + (1-3w)\hat{\psi} = -c_s^2\frac{k}{\mathcal{H}}\delta - (1+w)\frac{k}{\mathcal{H}}\alpha \tag{B.16}$$

$$\left(\frac{k}{\mathcal{H}}\right)^2 \alpha = -\frac{3}{2}(1+3c_s^2)\delta \ . \tag{B.17}$$

In the case of the QCD transition, the transition time is short compared to the Hubble time $(t_+ - t_-) < t_{\rm H} = H^{-1}$ and therefore self-gravity of the dominant radiation fluid can be neglected in the Euler equation (B.16) for this component. On the other hand, CDM moves in the external gravitational potential provided by the radiation fluid, and is coupled to the radiation fluid via the gravity term in the Euler equation. Therefore we have to keep the gravity term in the CDM Euler equation.

For a purely radiation dominated universe $w = c_s^2 = \frac{1}{3}$, the exact solution to the equations (B.9) – (B.11) for the density contrast δ and the peculiar velocity $\hat{\psi}$ can be written in terms of spherical Bessel and Neumann functions [132],

$$\delta = xf(x) + \frac{3}{x^2+6}x^2\frac{d}{dx}f(x) \tag{B.18}$$

$$\hat{\psi} = \frac{1}{x^2+6}x^3\frac{d}{dx}f(x), \tag{B.19}$$

where $x \equiv k_{\rm phys}/H = k/\mathcal{H}$. For a radiation dominated universe $x = k\eta$, $f(x) \equiv \left[Aj_1(x/\sqrt{3}) + Bn_1(x/\sqrt{3})\right]/\sqrt{3}$. The normalization is chosen in such a way that the subhorizon modes, $\lambda^{\rm phys} \ll H^{-1}$, of δ and $\sqrt{3}\hat{\psi}$ are acoustic oscillations with constant amplitude $\sqrt{A^2+B^2}$. The initial conditions for the growing mode in the radiation dominated superhorizon regime are given by

$$\delta = A\frac{1}{6}x^2 \tag{B.20}$$

$$\hat{\psi} = A\frac{1}{54}x^3 \tag{B.21}$$

for $x \to 0$.

B.2 Tensor perturbations

The line element of tensor perturbations (gravitational waves) is given by

$$\mathrm{d}s^2 = -\mathrm{d}t^2 + a^2(\delta_{ij} + h_{ij})\mathrm{d}x^i\mathrm{d}x^j \ . \tag{B.22}$$

h_{ij} is a transverse, traceless tensor with two possible polarizations. The linearized equation of motion reads

$$\partial_t^2 h_{ij} + 3H\partial_t h_{ij} - \triangle h_{ij} = 0 \ . \tag{B.23}$$

As for scalar perturbations it is useful to work in Fourier space and to use conformal time. For each polarization the amplitude satisfies

$$h'' + 2\mathcal{H}h' - k^2 h = 0 \ , \tag{B.24}$$

which can be solved by introducing the new variable $\mu \equiv h/a$. The equation of motion for μ is a simple harmonic oscillator

$$\mu'' + \left(\frac{a''}{a} - k^2\right) = 0 \ . \tag{B.25}$$

For superhorizon tensor perturbations $a''/a \gg k^2$ and the dominant mode is $\mu = a$, thus $h = const$. For subhorizon perturbations $a''/a \ll k^2$ and $\mu \propto \sin(k\eta + \phi_k)$, thus h decays with $1/a$, according to the covariant conservation of energy of a gravitational wave ($\rho_{\mathrm{g}} \propto \omega^2 h^2 \propto 1/a^4$). Note that this behavior is independent from the equation of state.

Bibliography

[1] E. V. Shuryak, Phys. Rep. **61**, 71 (1980); D. Gross, R. Pisarski, and L. Yaffe, Rev. Mod. Phys. **53**, 43 (1981); F. Wilczek, e-print astro-ph/9806395 (1998).

[2] K. Olive, Nucl. Phys. B **190**, 483 (1981); E. Suhonen, Phys. Lett. **119B**, 81 (1982); S. A. Bonometto and M. Sakelariadou, Astrophys. J. **282**, 370 (1984).

[3] C. J. Hogan, Phys. Lett. **133B**, 172 (1983).

[4] T. DeGrand and K. Kajantie, Phys. Lett. **147B**, 273 (1984).

[5] E. Witten, Phys. Rev. D **30**, 272 (1984).

[6] J. H. Applegate and C. J. Hogan, Phys. Rev. D **31**, 3037 (1985); **34**, 1938 (1986) (Erratum).

[7] M. Gyulassy et al., Nucl. Phys. B **237**, 477 (1984).

[8] H. Kurki-Suonio, Nucl. Phys. **B255**, 231 (1985).

[9] K. Kajantie and H. Kurki-Suonio, Phys. Rev. D **34**, 1719 (1986).

[10] Y. Iwasaki et al., Phys. Rev. D **46**, 4657 (1992); **49**, 3540 (1994); B. Grossmann and M. L. Laursen, Nucl. Phys. B **408**, 637 (1993); B. Beinlich, F. Karsch, and A. Peikert, Phys. Lett. B **390**, 268 (1997).

[11] G. M. Fuller, G. J. Mathews, and C. R. Alcock, Phys. Rev. D **37**, 1380 (1988); B. S. Meyer et al., Phys. Rev. D **43**, 1079 (1991).

[12] J. Ignatius et al., Phys. Rev. D **49**, 3854 (1994); **50**, 3738 (1994).

[13] M. B. Christiansen and J. Madsen, Phys. Rev. D **53**, 5446 (1996).

[14] J. Ignatius and D. J. Schwarz, in preparation (1998).

[15] J. H. Applegate, C. J. Hogan, and R. J. Scherrer, Phys. Rev. D **35**, 1151 (1987); G. M. Fuller, G. J. Mathews, and C. R. Alcock, Phys. Rev. D **37**, 1380 (1988); H. Kurki-Suonio, Phys. Rev. D **37**, 2104 (1988); R. A. Malaney and G. J. Mathews, Phys. Rep. **229**, 145 (1993).

[16] In-Saeng Suh and G. J. Mathews, e-print astro-ph/9805179 (1998).

[17] K. Kainulainen, H. Kurki-Suonio, and E. Sihvola, e-print astro-ph/9807098 (1998).

[18] R. V. Wagoner, W. A. Fowler, and F. Hoyle, Astrophys. J. **148**, 3 (1967); D. N. Schramm and R. V. Wagoner, Ann. Rev. Nucl. Part. Sci. **27**, 37 (1977); A. M. Boesgaard and G. Steigman, Ann. Rev. Astron. Astrophys. **23**, 319 (1985); T. P. Walker et al., Astrophys. J. **376**, 51 (1991); M. S. Smith, L. H. Kawano, and R. A. Malaney, Astrophys. J. Supp. **85**, 219 (1993); C. J. Copi, D. N. Schramm, and M. S. Turner, Science **267**, **267**, 192 (1995); Astrophys. J. **455**, L95 (1995); K. A. Olive and D. N. Schramm, in C. Caso et al., Eur. Phys. J. **C3**, 1 (1998), available on the PDG WWW pages (URL: `http://pdg.lbl.gov/`).

[19] K. Jedamzik et al., Astrophys. J. **422**, 423 (1994).

[20] C. J. Hogan, Phys. Rev. Lett. **51**, 1488 (1983).

[21] B. Cheng and A. Olinto, Phys. Rev. D **50**, 2743 (1994).

[22] C. Schmid, D. J. Schwarz, and P. Widerin, Hel. Phys. Acta **69**, 198 (1996).

[23] C. Schmid, D. J. Schwarz, and P. Widerin, Phys. Rev. Lett. **78**, 791 (1997).

[24] C. Schmid, D. J. Schwarz, and P. Widerin, Phys. Rev. D **59**, 043517 (1999).

[25] M. Crawford and D. N. Schramm, Nature **298**, 538 (1982).

[26] L. J. Hall and S. D. H. Hsu, Phys. Rev. Lett. **64**, 2848 (1989); E. D. Carlson et al., Phys. Rev. Lett. **65**, 2225 (1990).

[27] K. Jedamzik, Phys. Rev. D **55**, R5871 (1997).

[28] D. J. Schwarz, Mod. Phys. Lett. A **34**, 2771 (1998).

[29] R. Brandenberger, I. Halperin, A. Zhitnitsky, e-print hep-ph/9808471 (1998).

[30] H. Reeves, Phys. Rep. **201**, 335 (1991).

[31] S. A. Bonometto and O. Pantano, Phys. Rep. **228**, 172 (1993).

[32] R. A. Malaney and G. J. Mathews, Phys. Rep. **229**, 145 (1993).

[33] D. J. Schwarz, Nucl. Phys. A **642**, 332c (1998).

[34] G. Boyd et al., Phys. Rev. Lett. **75**, 4169 (1995); Nucl. Phys. **B469**, 419 (1996).

[35] C. Bernard et al., Phys. Rev. D **54**, 4585 (1996).

[36] A. Chodos et al., Phys. Rev. D **9**, 3471 (1974); T. De Grand et al., ibid. **12**, 2060 (1975); T. D. Lee, *Particle Physics and Introduction to Field Theory* (Harwood Academic Publishers, Chur, 1981).

[37] For recent reviews see K. Kanaya, Nucl. Phys. B (Proc. Suppl.) **47**, 144 (1996); E. Laermann, Nucl. Phys. B (Proc. Suppl.) **63**, 141 (1998).

[38] E. Farhi and R. L. Jaffe, Phys. Rev. D **30**, 2379 (1984).

[39] R. Balian and C. Bloch, Ann. Phys. (N.Y.) **60**, 401 (1970); ibid **64**, 27 (1971); ibid **84**, 559 (1974) (Erratum); M. S. Berger and R. L. Jaffe, Phys. Rev. C **35**, 213 (1987); ibid **44**, 566 (1991) (Erratum); J. Madsen, Phys. Rev. D **50**, 3328 (1994).

[40] MILC Collaboration, Phys. Rev. D **55**, 6861 (1997).

[41] R. Pisarski and F. Wilczek, Phys. Rev. D **29**, 338 (1984); F. Wilczek, Int. J. Mod. Phys. A **7**, 3911 (1992); K. Rajagopal and F. Wilczek, Nucl. Phys. **B399**, 395 (1993).

[42] Y. Iwasaki et al., Z. Phys. C **71**, 343 (1996); Nucl. Phys. B (Proc. Suppl.) **47**, 515 (1996).

[43] F. R. Brown et al., Phys. Rev. Lett. **20**, 2491 (1990).

[44] J. Engels et al., Phys. Lett. B **396**, 210 (1996).

[45] M. Hackel et al., Phys. Rev. D **46**, 5648 (1992).

[46] A. Bodmer, Phys. Rev. D **4**, 1601 (1971).

[47] The E864 collaboration: T. A. Armstrong et al., Nucl. Phys. A **625**, 494 (1997) and references therein.

[48] C. Alcock and A. Olinto, Annu. Rev. Nucl. Part. Sci. **38**, 161 (1988); *Strange Quark Matter in Physics and Astrophysics*, eds. J. Madsen and P. Haensel, Nucl. Phys. B (Proc. Suppl.) **24B** (1991); C. Greiner and J. Schaffner-Bielich, e-print nucl-th/9801062 (1998); J. Madsen, e-print astro-ph/9809032 (1998).

[49] J. Madsen and K. Riisager, Phys. Lett. B **158**, 208 (1985).

[50] K. Sumiyoshi et al., Phys. Rev. D **42**, 3963 (1990).

[51] C. Alcock and E. Farhi, Phys. Rev. D **32**, 1273 (1985); J. Madsen, H. Heiselberg, and K. Riisager, Phys. Rev. D **34**, 2947 (1986).

[52] K. Sumiyoshi and T. Kajino, Nucl. Phys. B (Proc. Suppl.) **24**, 80 (1991); P. Bhattacharjee et al., Phys. Rev. D **48**, 4630 (1993).

[53] This mechanism for enhanced baryon penetration through the phase interface was pointed out to me by M. Hofmann.

[54] V. Mukhanov and G. Chibisov, Pis'ma Zh. Eksp. Teor. Fiz. **33**, 549 (1981) [JETP Lett. **33**, 532 (1981)]; A. Starobinsky, Phys. Lett. B **117**, 175 (1982); A. Guth and S.-Y. Pi, Phys. Rev. Lett. **49**, 1110 (1982); S. Hawking, Phys. Lett. B **115**, 295 (1982).

[55] J. M. Bardeen, P. J. Steinhardt, and M. S. Turner, Phys. Rev. D **28**, 679 (1983).

[56] J. M. Bardeen, in *Cosmology and Particle Physics*, ed. A. Zee (Gordon and Breach, New York, 1989).

[57] V. F. Mukhanov, H. A. Feldman, and R. H. Brandenberger, Phys. Rep. **215**, 203 (1992).

[58] J. Martin and D. J. Schwarz, Phys. Rev. D **57**, 3302 (1998).

[59] G. F. Smoot et al., Astrophys. J. **396**, L1 (1992).

[60] C. L. Bennett et al, Astrophys. J. **464**, L1 (1996).

[61] E. R. Harrison, Phys. Rev. D **1**, 2726 (1970); Ya. B. Zel'dovich, Mon. Not. R. astr. Soc. **160**, 1P (1972).

[62] S. Weinberg, Astrophys. J. **168**, 175 (1971).

[63] P. Sikivie, Phys. Rev. Lett. **51**, 1415 (1983); C. Hagmann et al., Phys. Rev. Lett. **80**, 2043 (1998).

[64] A. Gould, Astrophys. J. **386**, L5 (1992); A. Ulmer and J. Goodman, ibid **442**, 67 (1995); G. F. Marani, et al., e-print astro-ph/9810391 (1998).

[65] K. Jedamzik, V. Katalinic, and A. V. Olinto, Phys. Rev. D **57**, 3264 (1998).

[66] G. Sigl, A. V. Olinto, and K. Jedamzik, Phys. Rev. D **55**, 4582 (1997).

[67] A. Kosovsky, M. S. Turner, and R. Watkins, Phys. Rev. Lett. **69**, 2026 (1992); Phys. Rev. D **45**, 4514 (1992); A. Kosovsky and M. S. Turner, Phys. Rev. D **47**, 4372 (1993).

[68] C. J. Hogan, Mon. Not. R. astr. Soc. **218**, 629 (1986).

[69] M. Kamionkowski, A. Kosovsky, and M. S. Turner, Phys. Rev. D **49**, 2837 (1994).

[70] B. J. Carr and J. E. Lidsey, Phys. Rev. D **48**, 543 (1993); B. J. Carr, J. Gilbert, and J. Lidsey, Phys. Rev. D **50**, 4853 (1994).

[71] K. Jedamzik, e-print astro-ph/9805147 (1998).

[72] MACHO Collaboration, Astrophys. J. **486**, 697 (1997); EROS Collaboration, Astron. Astrophys. **324**, L69 (1997).

[73] C.Y. Cardall and G. M. Fuller, e-print astro-ph/9801103 (1998).

[74] C. Schmid and P. Widerin, e-print astro-ph/9808142 (1998).

[75] A. A. Starobinskii, Pis'ma Zh. Eksp. Teor. Fiz. **30**, 719 (1979) [JETP Lett. **30**, 682 (1979)].

[76] M. V. Sazhin, Astron. Zh. **55**, 65 (1978) [Sov. Astron. **22**, 36 (1978)]; S. Detweiler, Astrophys. J. **234**, 1100 (1979).

[77] V. M. Kaspi, J. H. Taylor, and M. F. Ryba, Astrophys. J. **428**, 713 (1994); S. E. Thorsett and R. J. Dewey, Phys. Rev. D **53**, 3468 (1996); M. P. McHugh et al., Phys. Rev. D **54**, 5993 (1996).

[78] J. P. Blaizot and J. Y. Ollitrault, Phys. Rev. D **36**, 916 (1987).

[79] V. V. Dixit and J. Lodenquai, Phys. Lett. B **153**, 240 (1985).

[80] S. Weinberg, *Gravitation and Cosmology* (John Wiley & Sons, New York, 1972).

[81] G. Jungman, M. Kamionkowski, and K. Griest, Phys. Rep. **267**, 195 (1996).

[82] For reviews see: H. P. Nilles, Phys. Rep. **110**, 1 (1984); H. E. Haber and G. L. Kane, Phys. Rep. **104**, 181 (1985).

[83] J. Ellis et al., Phys. Lett. B **413**, 355 (1997); Phys. Rev. D **58**, 095002 (1998).

[84] K. Griest, Phys. Rev. D **38**, 2357 (1988); **39**, 3802 (1989) (Erratum).

[85] S. Hofmann and D. J. Schwarz, in preparation (1998).

[86] D. L. Tubbs and D. N. Schramm, Astrophys. J. **201**, 467 (1975).

[87] J. Ellis, in: *Cosmology and Large Scale Structure*, Les Houches, session LX, eds. R. Schaeffer et al. (Elsevier Sci., Amsterdam, 1996) pp. 825.

[88] J. E. Kim, Phys. Rep. **150**, 1 (1987); M. S. Turner, Phys. Rep. **197**, 67 (1990); G. G. Raffelt, Phys. Rep. **198**, 1 (1990); e-print astro-ph/9707268 (1997); P. Sikivie, e-print hep-ph/9611339 (1996).

[89] D. Gross, R. Pisarski, L. Yaffe, Rev. Mod. Phys. **53**, 43 (1981); M. S. Turner, Phys. Rev. D **33**, 889 (1986).

[90] C. J. Hogan and M. J. Rees, Phys. Lett. **B205**, 228 (1988); E. Kolb and I. I. Tkachev, Phys. Rev. Lett. **71**, 3051 (1993); Phys. Rev. D **49**, 5040 (1994); Astrophys. J. **460**, L25 (1996).

[91] B. J. Carr and S. W. Hawking, Mon. Not. R. astr. Soc. **168**, 399 (1974).

[92] D. K. Nadezhin, I. D. Novikov, and A. G. Polnarev, Astron. Zh. **55**, 216 (1978) [Sov. Astron. **22**, 129 (1978)]; G. V. Bicknell and R. N. Henriksen, Astrophys. J. **232**, 670 (1979).

[93] L. Randall, M. Soljačić, and A. H. Guth, Nucl. Phys. B **472**, 377 (1996); e-print hep-ph/9601296 (1996); J. Garcia-Bellido, A. Linde, and D. Wands, Phys. Rev.D **54**, 6040 (1996).

[94] J. S. Bullock and J. R. Primack, Phys. Rev. D **55**, 7423 (1997).

[95] L. D. Landau, E. M. Lifschitz, and L. P. Pitajewski, Lehrbuch der theoretischen Physik, vol. V, 7. ed., Berlin 1987.

[96] L. P. Csernai and J. I. Kapusta, Phys. Rev. D **46**, 1379 (1992).

[97] K. Kajantie, Phys. Lett. B **285**, 331 (1992).

[98] H. Kurki-Suonio and M. Laine, Phys. Rev. D **54**, 7163 (1996), and references therein.

[99] D. Stauffer, Phys. Rep. **54**, 1 (1979).

[100] H. Kurki-Suonio, Phys. Rev. D **37**, 2104 (1988).

[101] L. Rezzolla and J. C. Miller, Phys. Rev. D **53**, 5411 (1996); L. Rezzolla, Phys. Rev. D **54**, 6072 (1996).

[102] J. H. Applegate, C. J. Hogan, and R. J. Scherrer, Phys. Rev. D **35**, 1151 (1987).

[103] B. Banerjee and S. M. Chitre, Phys. Lett. B **258**, 247 (1991); **260**, 462 (1991) (Erratum).

[104] A. Heckler and C. J. Hogan, Phys. Rev. D **47**, 4256 (1993).

[105] K. Jedamzik and G. M. Fuller, Astrophys. J. **423**, 33 (1994).

[106] S. Burles et al., e-print astro-ph/9901157 (1999).

[107] C. R. Alcock, G. M. Fuller, and G. J. Mathews, Astrophys. J. **320**, 439 (1987).

[108] K. Jedamzik, G. M. Fuller, and G. J. Mathews, Astrophys. J. **423**, 50 (1994).

[109] P. Mészáros, Astron. Astrophys. **37**, 225 (1974).

[110] L. F. Abbott and D. D. Harrari, Nucl. Phys. B **264**, 487 (1986); B. Allen, Phys. Rev. D **37**, 2078 (1988); E. D. Stewart and D. H. Lyth, Phys. Lett. **B** 302, 171 (1993).

[111] L. M. Krauss, Nature **313**, 32 (1985).

[112] E. W. Kolb and M. S. Turner, *The Early Universe* (Addison-Wesley, Redwood City, 1990).

[113] A. Vilenkin, Phys. Lett. **107B**, 47 (1981); A. Vilenkin and E. P. S. Shellard, Cosmic Strings and Other Topological Defects (Cambridge University Press, Cambridge, 1994) pp. 306.

[114] R. R. Caldwell and B. Allen, Phys. Rev. D **45**, 3447 (1992).

[115] D. P. Bennett, Phys. Rev. D **34**, 3592 (1986); Phys. Rev. D **34**, 3932 (1986). R. R. Caldwell, R. A. Battye, and E. P. S. Shellard, Phys. Rev. D **54**, 7146 (1996).

[116] FUSE (The Far Ultraviolet Spectroscopic Explorer), URL: `http://fuse.pha.jhu.edu/`.

[117] MAP (Microwave Anisotropy Probe),
URL: `http://map.gsfc.nasa.gov/`
and PLANCK,
URL: `http://astro.estec.esa.nl/SA-general/Projects/Planck/`.

[118] H. I. Kim, B.-H. Lee, and C. H. Lee, e-print astro-ph/9901286 (1999).

[119] G. F. Marani et al., e-print astro-ph/9810391 (1998).

[120] Reviews on the generation and detection of stochastic gravitational waves can be found in: K. S. Thorne, in *300 Years of Gravitation* (eds. S. Hawking and W. Israel, Cambridge University Press, Cambridge, 1987) pp. 330; B. Allen, Les Houches Lecture Notes Sept. 1995, preprint gr-qc/9604033.

[121] V. A. Rubakov, M. V. Sazhin and A. V. Veryaskin, Phys. Lett. **115B**, 189 (1982); R. Fabbri and M. D. Pollock, ibid. **125B**, 445 (1983); L. F. Abbott and M. B. Wise, Nucl. Phys. B **244**, 541 (1984); A. A. Starobinskii, Pis'ma Astron. Zh. **11**, 323 (1985) [Sov. Astron. Lett. **11**, 133 (1985)]; M. S. Turner, M. White, and J. E. Lidsey, Phys. Rev. D **48**, 4613 (1993).

[122] Axion search at LLNL,
URL: `http://www-phys.llnl.gov/N_Div/Axion/axion.html`.

[123] Y. B. Zeldovich and I. D. Novikov, *Relativistic Astrophysics Vol. 2: The Structure and Evolution of the Universe*, (The University of Chicago Press, Chicago, 1983).

[124] A. Linde, *Particle Physics and iInflationary Cosmology* (Harwood Academic Publishers, Amsterdam, 1990).

[125] P. J. E. Peebles, *Principles of Physical Cosmology* (Princeton University Press, Princeton, 1993).

[126] T. Padmanabhan, *Structure Formation in the Universe* (Cambridge University Press, Cambridge, 1993).

[127] W. Thirring, *Klassische Feldtheorie, Lehrbuch der Mathematischen Physik, Band 2* (Springer, Wien, 1990).

[128] S. Perlmutter et al., Nature **391**, 51 (1998); A. G. Reiss et al, e-print astro-ph/9805201 (1998).

[129] D. J. Fixsen et al., Astrophys. J. **473**, 576 (1996).

[130] J. M. Bardeen, Phys. Rev. D **22**, 1882 (1980).

[131] H. Kodama and M. Sasaki, Prog. Theor. Phys. Suppl. **78**, 1 (1984).

[132] J. Hwang, Astroph. J. **415**, 486 (1993).